2014

Microrheology of soft matter and living cells in equilibrium and non-equilibrium systems

Ming-Tzo Wei
Lehigh University

Microrheology of soft matter and living cells in equilibrium and non-equilibrium systems

by

Ming-Tzo Wei

Presented to the Graduate and Research Committee
of Lehigh University
in Candidacy for the Degree of
Doctor of Philosophy

in

Bioengineering Program

Lehigh University
September 2014

Approved and recommended for acceptance as a dissertation in partial fulfillment of the requirements for the degree of Doctor of Philosophy.

Student: Ming-Tzo Wei

Dissertation Title: Microrheology of soft matter and living cells in equilibrium and non-equilibrium systems

_____

Date

_____

H. Daniel Ou-Yang, Dissertation Director, Chair

_____

Accepted Date

Committee Members:

_____

Dimitrios Vavylonis

_____

Sabrina Jedlicka

_____

Xiaohui (Frank) Zhang

Acknowledgments

This dissertation could not have been completed without the constant guidance and unwavering support of my advisor Dr. H. Daniel Ou-Yang. I would also like to thank my committee members, Dr. Dimitrios Vavylonis, Dr. Sabrina Jedlicka, and Dr. Xiaohui Zhang, for their valuable time, expertise and suggestions. I would like to express my gratitude to Dr. Susan Perry, Dr. Berengere Abou, Dr. Miriam Rafailovich, and Dr. Joel Cohen for letting me ask outrageous questions.

In addition, I would like to thank my colleagues who helped me complete this work. I would like to thank Wei Nie, Yingjie Yu, Colleen T. Curley, and Matthew Dragovich for their experimental support. I would also like to thank Yi Hu, Jingyu Wang, Jinxin Fu, Joseph Junio, Jacob Mazza, and Marko Chavez for valuable discussions and creative ideas.

Finally, I would like to thank my friends and family for their continuous support. In particular, I am grateful to my wife Yi-Hsuan Yeh for her patience and encouragement. Without her support, I would not have had the courage to finish this work.

Contents

Abstract

Myosin-generated stresses are responsible for non-equilibrium mechanical behavior of synthesized cytoskeletal networks *in vitro*. In particular, it is found that myosin stresses can modify the network elasticity. For living cells, it has been suggested that internally generated stress might help cells sense and mimic the stiffness of their environments. However, cellular mechanical responses to intracellular stress are not well understood.

To address these questions, we studied microrheology inside living cells by comparing their mechanical properties to those expected by a statistical analysis of non-thermal fluctuations. We used an experimental method that combines optical tweezers-based active microrheology with particle-tracking passive microrheology. First, we calibrated the trapping force in the linear restoring-force regime with oscillatory optical tweezers. Then, we used optical tweezers to test the response functions against the fluctuation-dissipation theorem in equilibrium systems (i.e., polymer solutions or colloidal crystal gels) and in non-equilibrium systems (i.e., living cells).

In living cells, we employed cellular microrheology using an internal probe as well as an externally attached particle. Whereas extracellular probes attached to the cytoskeleton provide a measure of global cell mechanical properties, intracellular probes provide direct measurements of intracellular mechanical properties. We used an engulfed micro-particle as a probe to study local intracellular stress and stiffness. The relationship between fluctuations in stress and in cell elasticity for living cells under different internal tensions reveals a strong non-linearity between cell elasticity and intracellular stress, which follows a master curve. Our results show that the motors induce an internal tension that forces the network into a non-equilibrium and non-linear state.

These aspects provide a better understanding of the noise in a non-equilibrium system. The relationship between the different sources of noise in living cells helps reveal the inner workings of the highly dynamic cytoskeleton network. Studies of intracellular stress and mechanical properties

promote our current understanding of how cells sense and respond to their mechanical environment. Such knowledge could lead to new designs in biomaterials and advance our understanding of diseases related to cellular mechanotransduction. Our studies in active systems contribute to our knowledge of fundamental non-equilibrium statistical physics in biological systems.

1. Introduction

Soft matter physics is a subfield of condensed matter physics comprising a variety of physical states. Most soft-matter systems have a multitude of fluctuating energy barriers of comparable height [1], which can cause matter to develop complex viscoelasticity, phase transitions, or self-assembly behavior [2]. An open question in soft matter physics is how to understand the properties of these complex phenomena. In this thesis, we use rheology to study the physical properties of soft matter (i.e., polymers, colloid solutions, living cells) in both equilibrium and non-equilibrium systems. In this chapter, an overview of soft matter is introduced in *Section* 1.1. Then, rheology and cellular microrheology are described in *Sections* 1.2 and 1.3. Finally, the techniques of cellular microrheology are described in *Section* 1.4.

1.1 Introduction to Soft Matter

Soft matter is a convenient term for states of materials [1, 2]. In 1991, Pierre-Gilles de Gennes received the Nobel Prize for discovering, from simple thermodynamics, the order parameter to study in complex soft-matter systems such as liquid crystals and polymers [3]. Many of these materials have specific physicochemical properties including micro- or nano- size scales, a large number of internal degrees of freedom, weak interactions between structural elements, and structural bond energies comparable to thermal energy. These properties lead to large thermal fluctuations [4]. The fluctuations in a system at equilibrium are strictly dictated by how the system dissipates energy. In a mechanical system in thermal equilibrium, fluctuations in the local density tell us about the viscoelasticity of the material. However, in a non-equilibrium system, fluctuations may not follow the same rule. In this thesis, we investigate the physical properties in both equilibrium systems (i.e., polymer solutions or colloidal crystal solutions) and non-equilibrium systems (i.e., living cells).

One specific class of soft matter - polymer - can be found from natural materials like wood or silk, as well as from synthetic plastics, fiber, or gels, which have many applications. To form a polymer, a monomer species must link to other monomers by either step-growth or chain polymerization [5]. Polymer solutions have a complex phase behavior making them more viscous than a water solution. In the solid state, polymers are difficult to crystallize due to the large entropy associated with straightening out every polymer chain [6]. Depending on the time-scale of the observation, polymers can become glassy or viscoelastic [5]. Polymeric behavior depends on the interactions between polymer molecules. These interactions are affected by their concentration. In a dilute solution, the molecules are well separated and do not interact with each other. Each molecule can be considered an isolated coil. When the concentration is increased, coils start to overlap; at this point, the concentration of polymer segments in the bulk solution is equal to the average concentration of segments in the individual coils. Polymer chains in dilute, overlap concentration, and semi-dilute solutions are sketched in Figure 1.1.

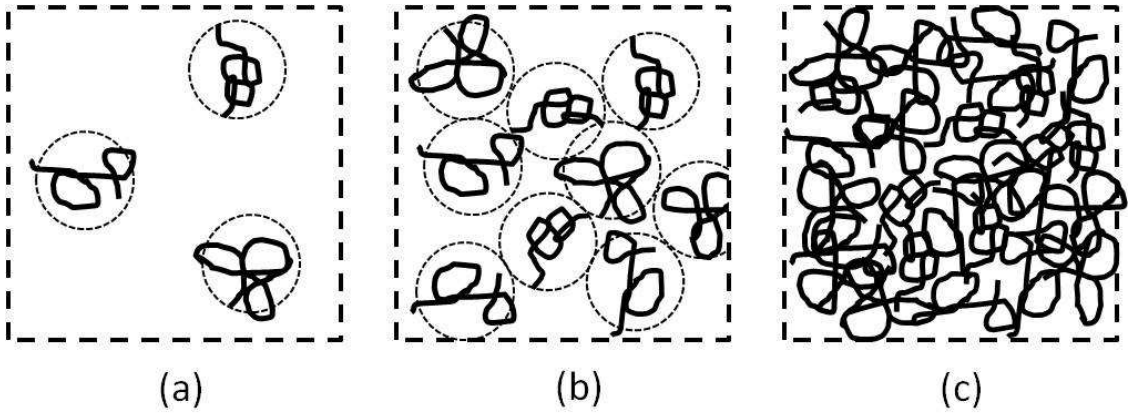

Figure 1.1 Schematic representation of (a) dilute, (b) overlap concentration and (c) semi-dilute polymer solutions.

Colloids are another specific class of soft matter. The world around us is full of colloids such as smoke, mist, and rocks; even our body and foods contain colloidal particles. For industrial applications, synthetic paints, foams, and pastes must be prepared using materials containing

colloids. Study of the inter-particle interactions is a central issue in the technology of preparation and processing of colloid dispersions and in creating colloid stability. A typical colloid with dimension in the range of 1 nm to 1 μm has a large surface-to-volume ratio, which is important for surface chemistry. In colloidal particle solutions, the balance of attractive and repulsive forces controls the stability of the dispersion; under certain conditions, they can attract each other and aggregate, termed flocculation [7]. Charges at the surface of a colloid particle attract counterions that form a layer called the electric double layer [8]. The double layer includes two regimes. First, the surface charges attract ions that adsorb and bind tightly to the surface, forming the Stern layer. The second layer is composed of attracted ions that organize more diffusely due to random thermal motions. The distribution and concentration of charged species can be described by the Poisson-Boltzmann equation. In the study of inter-particle interactions, the velocity of a charged colloid particle induced by an electric field can be measured by electrophoresis. In addition, the viscoelastic properties of a colloidal-particle solution can be used to study the structural and dynamical complexity of a colloidal system through rheological approaches.

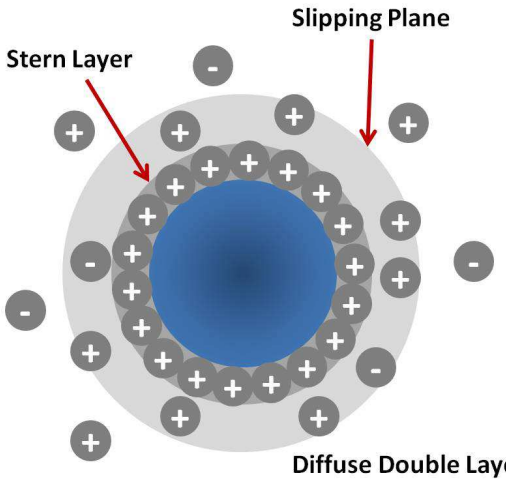

Figure 1.2 Diagram showing the ionic concentration around a charged colloidal particle.

Compared to polymer materials or colloid solutions, biological soft materials are more complex. Biological soft matter is sensitive to temperature, pH, and salt concentration. Unlike the

equilibrium systems mentioned previously, living biological materials (i.e., cell, bacterial, or virus) are maintained far from equilibrium due to an input of ATP energy. The study of such non-equilibrium system is introduced in *Chapter* 4.

The typical experimental methods to study the physical properties of soft matter materials are:

(1) Microscopy methods: optical microscopy can be used to examine the macro-aggregates formed by polymers or to view colloidal particles around 1 μm in size. Polarized optical microscopy is useful for identifying birefringent structures formed by liquid crystals. Electron microscopy provides structural information to sub nanometer resolution and is used to image dry materials.

(2) Scattering methods: static light scattering can provide information on particle size and shape by analysis of diffraction from point scatters for Rayleigh or Mie scattering. Dynamic light scattering is used to study the diffusion of polymer or colloidal solutions. X-ray and neutron scattering can be used to probe features with sub nanometer resolution due to the smaller wavelength.

(3) Spectroscopic methods: nuclear magnetic resonance is a method to probe the motions of nuclei on molecules when they come into resonance with an oscillating magnetic field. Nuclear magnetic resonance spin relaxation measurements have also provided information on the local dynamics of segments of a polymer chain. Infrared and Raman spectroscopy are used to probe vibrational or rotational motions of molecules, providing information about specific bonds.

(4) Rheology methods: rheology, which will be introduced in more detail in *Section* 1.2, is the study of mechanical responses to a dynamic stress or strain. In this thesis, we focus on using rheology to study the physical properties of soft matter including polymers, colloidal solutions, and biological soft matter.

1.2 Introduction to Rheology

Rheology is the study of the deformation of matter in response to an applied force [9, 10]. In a broad sense, the term rheology ("rheo" means "to flow") refers both to studies of the deformation, as well as to the flow of materials under the influence of applied forces. Rheological behavior encompasses macroscopic phenomena including flow of viscous liquids, mechanical properties of elastic solids, and viscoelasticity. In classical terms, the mechanical properties of elastic solids can be described by Hooke's law, which states that an applied stress is proportional to the resultant strain but is independent of the rate of strain. For liquids, the corresponding statement is known as Newton's law, where the stress is independent of the strain but proportional to the rate of strain. Simple solids store energy and provide a spring-like, elastic, response, whereas simple liquids dissipate energy through viscous flow. In many cases, a material may exhibit the characteristics of both a liquid and a solid. Rheological measurements reveal both the elastic property (capability to store mechanical energy) and viscous property (characteristic dissipation of energy, often in the form of heat) both of which generally depend on the time scale [11]. The system is then said to be in a viscoelastic state.

Rheology has applications in geophysics, materials science, and physiology. In geophysics, viscoelastic properties of both solid-earth materials and the flow of lava can be measured by their small yield stress at either short or long time scales [11]. In materials science, rheology is used to study several important industrial products including cement, paint, and chocolate. A detailed understanding of the complex viscoelastic properties under applied stress provides important knowledge to maintain the stability of the product and to control variations. In physiology, rheology is used to study body fluids which have complex viscoelastic properties. Hemorheology, the study of blood flow, mechanical properties of blood cells, and viscosity of plasma, is an important sub-branch of microrheology with a long history with critical biomedical applications [12, 13].

One way to characterize a rheological response is to study complex mechanical properties including stored and dissipative mechanical energy. The shear modulus (*G*) is one of the mechanical properties determined by the measurement of strain (deformation per length) is response to stress (force per unit area). There are several different moduli that can be defined by the direction of the applied forces. Young's modulus (*E*) is the extension of a material under tension, and the bulk modulus (K) is the deformation under a compression. The shear modulus and bulk modulus of homogeneous isotropic linear elastic materials are related to Poisson's ratio, υ, which is the negative ratio of transverse to axial strain. An incompressible material that deforms elastically at small strains would have a Poisson's ratio of 0.5.

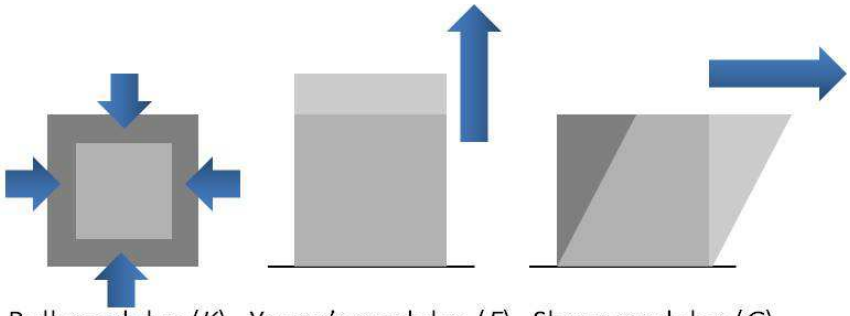

	K	E	G
K		$E/3(1-2\nu)$	$2G(1+\nu)/3(1-2\nu)$
E	$3K(1-2\nu)$		$2G(1+\nu)$
G	$3K(1-2\nu)/2(1+\nu)$	$E/2(1+\nu)$	

Figure 1.3 Schematics showing the direction of the applied stress in several common measurements of mechanical properties including the bulk modulus (*K*), Young's modulus (*E*), and shear modulus (*G*). The chart shows the relations among the 3 moduli terms of Poisson's ratio.

Compared to these rheological studies for the measurement of bulk-average viscoelastic properties, cellular rheology calls for the development of microrheology [14-17] to reduce the sample volume. Applying microrheology in cellular environments provides useful information on the molecular and structural dynamics in living cells and on the physical behavior of cellular cytoskeletal networks. These aspects of the cell will be discussed in more detail in the next section.

1.3 Introduction to Cellular Microrheology

Living cells are highly dynamic and inhomogeneous. A variety of motor proteins, meander along transporting cargo across the cells and generate forces to maintain the cell's mechanical integrity using the three-dimensional network as a scaffold. There is abundant evidence relating the cells' mechanical properties to the cells' functions [18-26]. However, owing to the complexity of living cells, a comprehensive understanding of the relationship between the mechanical properties and the biological functions is lacking. Many aspects of cellular physiology rely on the ability to control mechanical forces in order to maintain cell shape. The dynamic, mechanical cellular behavior is determined by networks of filamentous proteins known as cytoskeleton.

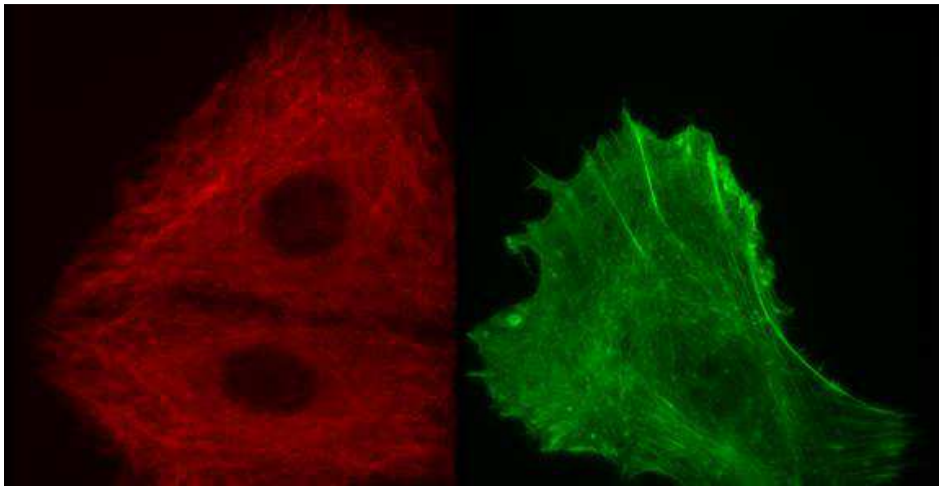

Figure 1.4 Fluorescent images of (left) microtubule filaments and (right) actin filaments in fibroblast cells.

The cytoskeleton, a network of protein filaments that supports the shape and motion of a living cell, contains three main cytoskeletal filaments: actin filaments, intermediate filaments, and microtubules. (1) Actin filaments form by polymerization of globular actin (G-actin) subunits into a twisted filamentous actin (F-actin). ATP-actin can bind to one end (the barbed end) for filament growth, called polymerization; depolymerization occurs at the other end (the pointed end). Actin

bundle filaments, termed "stress fibers", generate contractile forces due to myosin-motor activity controlled by the Rho family of small GTP-binding proteins. (2) Intermediate filaments have an average diameter of 10 nanometers and organize the internal three-dimensional structure of the cell without the requirement of GTP and ATP hydrolysis. They play a role in anchoring organelles and serve as structural components of cell-cell and cell-matrix junctions. (3) Microtubules, highly dynamical structures exhibiting polymerization and depolymerization, are commonly organized by the centrosome.

The dynamic proteins in these cytoskeletal networks can be imaged, to reveal their structure [27]. An understanding of the biophysical properties of living cells is still lacking due to a lack of studies of the mechanical behaviors of the dynamic cytoskeleton. Mechanically exploring their interior noninvasively has been a major challenge. Studying cellular mechanical behavior requires the development of quantitative experimental methods and physical models such as cellular microrheology, which will be described in the next section.

1.4 Overview of Cellular Microrheology Techniques

Microrheology of living cells can be used to gain insight into the inhomogeneous structure and dynamics of the cytoskeleton [16, 28-30]. As a living polymer network, the cytoskeleton is constantly polymerizing and depolymerizing, depending on the biological functions of cells [31]. It has been shown that the cytoskeleton is directly connected to the nucleus, and that external shear stress stimuli [32] can lead to cytoskeletal reorganization as well as to modulations of gene expression [21]. It is also well known that the differentiation of stem cells depends on the attachment of the cell to a substrate [33-38]. Like many mechanical systems, the stress-strain relationship of biological cells also depends on the mechanical integrity of the cells and the extracellular matrix around the cells. Knowledge of the role of cellular mechanical forces or cellular stresses would provide a better understanding of the complex system of cellular signaling pathways [21]. More details will be discussed in *Chapter 4*.

In this Section, we detail a variety of cellular microrheology techniques. Microrheology can be broadly classified as either passive or active; the former involves measurement of the passive motions of probes due to thermal or Brownian fluctuations [39-42], and latter involves measurement of the dynamic responses of the probes to active forces [43, 44].

In the passive approach, the Brownian motion of probed particles embedded in the sample medium are tracked and analyzed to deduce the viscoelastic property of the sample [43-47]. In an equilibrium system where only thermal forces act on a probed particle, the motion of the particle is the random walk caused by thermal fluctuations constrained by the viscoelasticity of the surrounding material. The embedded particles must be much larger than any structural size of the material, and the measurements of tracking particle motions must be faster than the macroscopic stress relaxation time. The accuracy of passive microrheology depends on accurate tracking of the motions of probe particles as a function of time. For these studies, target cells can be deeply

embedded in a three-dimensional matrix [15, 48, 49], a condition similar to cells in their physiological environment and difficult to probe by other methods.

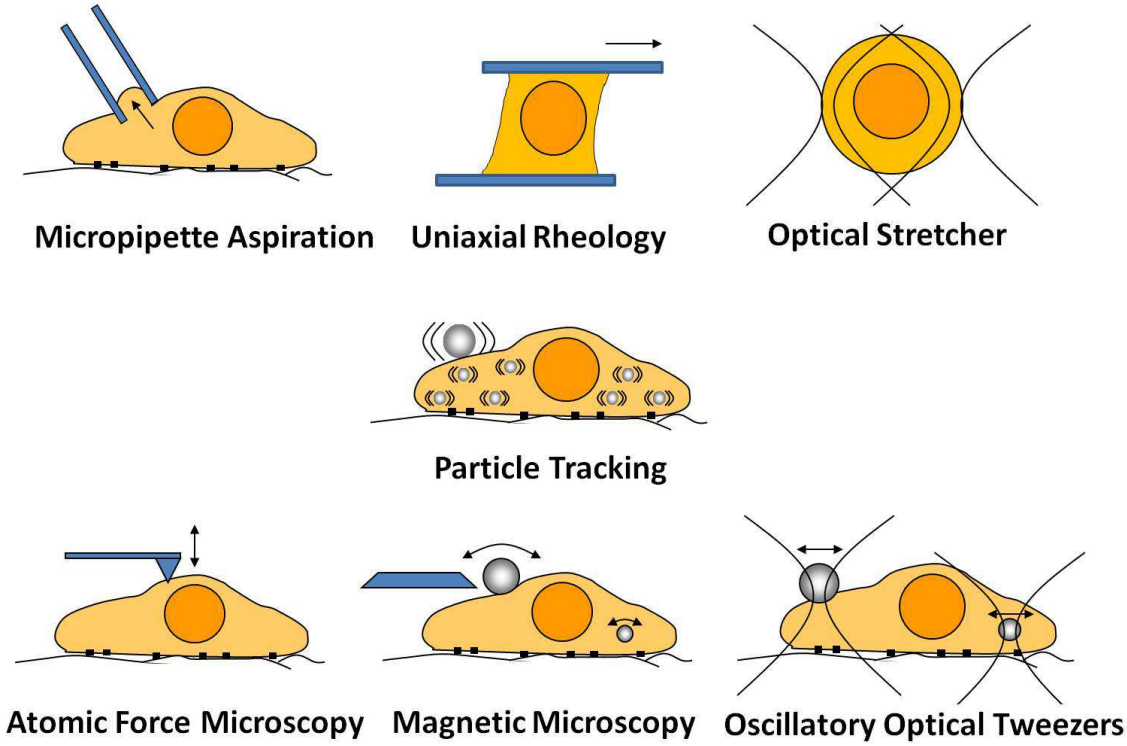

Figure 1.5 A schematic diagram of different microrheology platforms including active and passive approaches.

In the active approach, external forces would be applied to the cell, measure its dynamic mechanical response, and calculate the viscoelastic property [21, 50-53]. There are several methods typically used in the active approach.

(1) Micropipette aspiration: a cell is aspirated into a micropipette by applying suction pressure (0.1–10 kPa). The aspiration length of the cell inside the micropipette is imaged and recorded as a function of time [54-58]. This method can measure the elastic and viscous properties of living cells. However, quantification of the mechanical properties depends strongly on different theoretical models; so the most recent application of micropipette aspiration is simply to capture or hold cells.

(2) Uniaxial rheology: invented by Thoumine and Ott [59], this method consists of two parallel microplates that support cell adhesion and spreading. A whole cell is stretched between two plates. The micro-plate is used as a nN-scale force transducer. Measureable forces range from 1 nN to 1 μN, and several manipulation modes are possible, including compression, traction, aspiration and adhesive rupture. This method can provide a force strong enough to induce significant deformations of an entire cell.

(3) Optical stretcher: consisting of either two counter-propagating laser beams [60-63] or dual-single strongly focused laser beams [64-66], this method has been used for noninvasive and non-mechanical-contact trapping and stretching of biological cells in suspension to measure their viscoelastic properties. However, this approach is limited by the various approximations and assumptions involved in the theoretical modeling used to calculate the optical stretching force [67].

(4) Atomic force microscopy (AFM): this technique can be used to measure the “stiffness map” of the cell surface. The key component of AFM is a sharp tip mounted on a cantilever which scans over the sample surface. It has sub-nanometer resolution to probe global and local nano-mechanical properties of cells [68, 69].

(5) Magnetic cytometry: this method can be used to measure cell-membrane or intracellular viscoelasticity by applying oscillatory forces to magnetic particles [70, 71]. The viscoelasticity can be probed using magnetic tweezers or magnetic twisting. The particle movement is due to its induced magnetic dipole with the magnetic field gradient. The corresponding displacement of the magnetic particle is used to measure local cellular mechanical properties.

(6) Optical tweezers: this technique [72, 73] can generate an oscillatory optical force on a probed particle, either attached on the cell membrane or embedded in the cytoplasm to probe viscoelasticity [45, 46, 74-76]. The experimental data from optical tweezers can only be used to study viscoelastic responses at low force in the linear regime. This regime will be discussed in

Section 2.2.3. An oscillatory optical tweezers-based active microrheological approach is the major method used in this research.

The subsequent chapters are arranged as follows. In *Chapter* 2, we begin with an overview of the basic principles of oscillatory optical tweezers-based microrheology. Then, we illustrate applications of this technique to determine the micro-mechanical properties of equilibrium systems (i.e., polymer and colloidal crystal solutions) in *Chapter* 3, and non-equilibrium systems (i.e., living cells) in *Chapter* 4. We end by summarizing recent progress and future prospects in *Chapter* 5.

2. Materials and Methods

2.1 Sample Preparation

2.1.1 Preparation of Polymer Solutions

Poly(ethylene oxide) (PEO), also known as poly(ethylene glycol) (PEG), is a synthetic polyether. These polymers are amphiphilic and soluble in water as well as in many organic solvents. The micromechanical properties of an aqueous solution of PEO polymer are measured as described in *Sections 3.1* and *3.3*. Samples of polyethylene oxide (Sigma, #181986, glass-transition temperature *Tg* = -67℃, molecular weight *MW* = 100 kg/mol) with linear formula $(-CH_2CH_2O-)_n$. are seeded with a small amount (volume fraction~ 10^{-5}) of particles as a microrheology probe. As discussed in the previous section, the semi-dilute regime, above the concentration where individual polymer chains start to overlap, is bigger than 0.5 wt%. For a 20 wt% solution of 100 kg/mol PEO in water, the average mesh size of the polymer network is around 8 nm, which is much smaller than the size of the micron-sized particle used in our study.

2.1.2 Preparation of Colloidal Liposome Solutions

Liposomes are formed from a thin lipid bi-layer composed of cationic, anionic, or neutral lipids. The lipids are first dissolved in chloroform ($CHCl_3$) and then mixed in the desired ratio. The lipid solution would be clear to assure a homogeneous mixture. Then, the mixed lipid solution is added to a round-bottom flask and the chloroform is removed by rotary evaporation. By placing the flask on a vacuum pump overnight, a thin lipid film forms on the walls of the flask and is thoroughly dried. The dry lipid film can be removed from the walls by adding de-ionized water and shaking. Charged liposomes produce a viscous gel, which produces a stable, multi-lamellar liposome suspension. Then, the multi-lamellar liposomes can be farther processed by an extrusion, which makes homogeneously-sized unilamellar liposomes. Extrusion through polycarbonate filters with 100 nm

pores yields colloidal liposomes with a mean diameter of 105 nm as shown in Figure 2.1(a). The particle charge of liposomes is determined by the ratio between a charged lipid (POPG; $C_{42}H_{82}NO_8P$, *MW* = 771.0, Avanti) and neutral lipid (POPC; $C_{40}H_{76}NaO_{10}P$, *MW* = 760.1, Avanti). Zeta potentials of the charged liposomes in de-ionized water are shown in Figure 2.1(b).

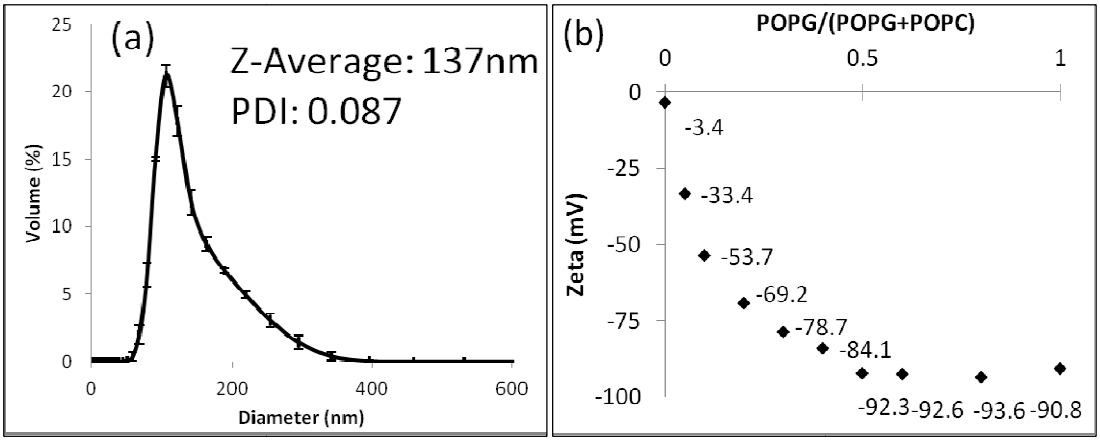

Figure 2.1 (a) Particle size and (b) zeta potential of charged liposomes are measured by dynamic light scattering (Malvern Nano Zetasizer).

2.1.3 Preparation of HeLa Cells

Several HeLa cell lines that stably express GFP fusion proteins have been engineered. This includes GFP-fusion markers for crucial cytoskeletal components such as tubulin [77], myosin regulatory light chain (MRLC) [78], EB1 [77], IC74-mfGFP (marker for dynein) [79] (see Figure 2.2). HeLa cells (human cervical epithelial adenocarcinoma cells) expressing MRLC-GFP [78] are used in our study. HeLa cells are cultured in Dulbecco's modified eagle medium (DMEM; 500 mL, Invitrogen #11960-044) supplemented with high glucose (4.5%), 10% fetal bovine serum (50 mL, Invitrogen #10082-147, heat activated at 56℃ for 30 minutes), 1% penicillin/streptomycin (5 mL, Invitrogen #15140-122), 7.5% sodium bicarbonate (5 mL, Sigma #S8761), 200 mM glutamine (6 mL, Invitrogen #25030-081), and 1% G418 solution (50 μL G418/ 5 mL media, Invitrogen #10131-035). The cell line was generously provided by Dr. Keiju Kamijo at the National Institutes

of Health. Cells are seeded onto polyacrylamide (PA) substrates coated with collagen type I (0.2 mg/ml) on 22 x 22 mm cover-slips ($6x10^4$ cells/cover slip). Different PA substrates, having varying elastic moduli, are prepared [80, 81]. Details of the preparation of PA thick films will be described in the next section. Cells are grown under standard culture conditions (37°C, 5% CO_2, in a humidified environment).

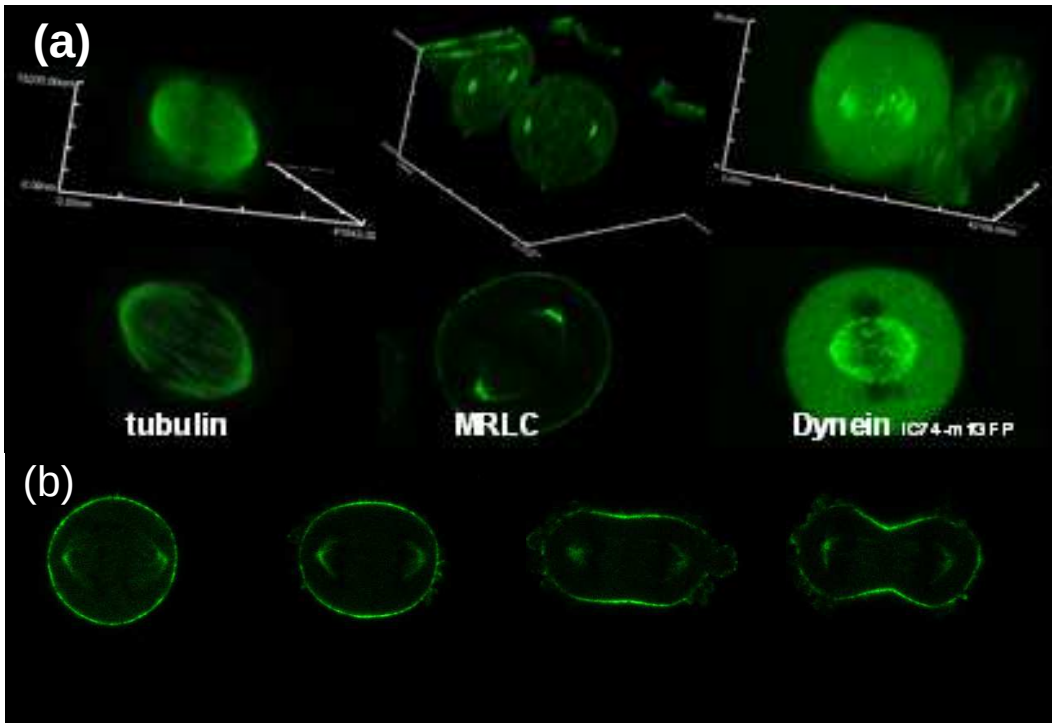

Figure 2.2 (a) 3D images of dividing cells expressing tubulin fused to GFP, myosin regulatory light chain fused to GFP (MRLC-GFP), and dynein labeled by IC74-mfGFP. (b) Images of dividing cells expressing MRLC-GFP. Single confocal slices are obtained at 900 sec intervals. The images show increasing concentration of myosin into an equatorial region during anaphase and cytokinesis.

2.1.4 Preparation of Polyacrylamide Thick Films

Using protocols described by Yeung *et al.* [80], polyacrylamide thick films are generated on functionalized 22 mm x 22 mm cover-slips which are flamed, coated with 0.1N-NaOH and air dried.

Cover-slips are incubated in 30 μL 0.5% silane (3-aminopropyltrimethyoxysilane, Acros Organics, #31251000) for 5 minutes. After extensive rinsing, cover-slips are incubated in 70% glutaraldehyde (Alfa Aesar, #10149118) in PBS for 30 minutes. After rinsing, cover-slips are dried and stored for future use.

Next, polyacrylamide ($(-CH_2CHCONH_2-)_n$) gels of various stiffness are fabricated on the surface of the activated cover-slips. Differences in stiffness are achieved by varying the amounts of acrylamide (*MW* = 71.08; Acros Organics, #164855000) and bis-acrylamide (*MW* = 154.2; Promega, #0000037459) in the gel solution according to Table 2.1 and Figure 2.3. 1 mL of solution is degassed for 30 minutes under house vacuum. 0.5 μL of TEMED (J.T.Baker, #0000033235) and 5 μL of 10% ammonium persulfate (*FW* = 228.2 Acros, #401165000) are added to initiate polymerization and mixed thoroughly. A volume of 20 μL of the polyacrylamide mixture is immediately pipetted onto the surface of a glass slide and the activated cover-slip is carefully placed on top. A Rain-X coated 18 mm circular cover glass is placed on top of the gel solution, and the polyacrylamide is allowed to polymerize for 25-60 minutes. After polymerization, the circular cover glass is removed.

Table 2.1 Expected modulus of elasticity after polymerization of relative Acrylamide and Bis-Acrylamide concentrations.

Young's Modulus (kPa)	1.05	3.15	5	16.7	60
Acrylamide (%)	3	5	5.5	10	10
Bis-Acrylamide (%)	0.1	0.1	0.1	0.15	0.5
40% Acrylamide (mL)	75	125	137.5	250	250
2% Bis-Acrylamide (mL)	50	50	75	75	250
0.5M HEPES pH4.22(mL)	100	100	100	100	100
TEMED (mL)	0.5	0.5	0.5	0.5	0.5
ddH_2O (mL)	618.9	725	541.4	575	243.9

The heterobifunctional cross-linker sulfo-SANPAH (Thermo Scientific #OK194189) is used to crosslink extracellular matrix molecules onto the gel. 0.5 mg sulfo-SANPAH is diluted in 1 mL

HEPES (50 mM and pH = 8) and 5 µL DMSO immediately before coupling. Then, 100 µL of the sulfo-SANPAH solution is pipetted on the surface. Treatment consisted of applying sulfo-SANPAH cross-linker solutions and incubating under ultraviolet light for 15 minutes. After several rinses with 50 mM HEPES pH 8, a 0.2 mg/ml collagen type I (Rat Tail High Concentration 9.87 mg/mL; BD, #354249) solution is placed on the gels. Substrates are incubated overnight to sterilize before cell seeding.

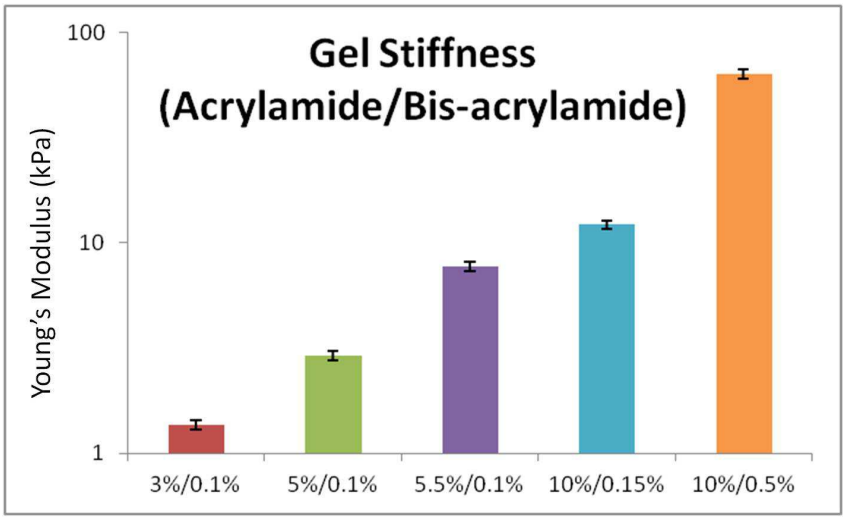

Figure 2.3 Mechanical properties of polyacrylamide substrates. Young's modulus of polyacrylamide gels with various acrylamide/ bis-acrylamide ratios is measured by atomic force microscopy (AFM).

The thickness of each sample as measured by vertical slicing of acquired volumetric confocal images is around 100 µm. Atomic force microscopy (AFM) is used to measure the stiffness of the polymer substrate. Control of the relative positions between an AFM cantilever and the substrates is achieved using a piezoelectric translator (P-841; PhysikInstrumente, Waldbronn, Germany). Vertical motion of the AFM in the range 1 nm to 1 µm can yield a vertical force in the range 10 pN to 10 nN. The AFM forces are monitored by use of a quadrant photodiode to sense changes in the reflection angle of a laser beam reflected off the top the cantilever. Force constants of the

cantilevers (MLCT-UC; Bruker, CA) are calibrated by analysis of their thermal fluctuations according to the method of Hutter and Bechhoefer [82]. The sensitivity of the laser point motion within the photodiode is calibrated by scanning the glass slide on which the gels are plated, then measuring the resulting slope of the indentation scan in units of (m/V). Knowledge of these parameters yields a force from the voltage output of the photodiode.

2.2 Optical Components and Configurations

Optical tweezers [83] use a highly focused laser beam to form a stable trap that can confine a micron or nanosized particle in three-dimensional space. The tweezers thus enable non-invasive manipulation, without any mechanical contact, of microscopic probe particles embedded in a sample. Since its first demonstration in 1986 by Ashkin *et al.* [72], single-beam optical tweezers have been used to manipulate microscopic objects such as colloidal particles [84], bio-molecules [85, 86], and biological cells [74, 87-89]. Optical tweezers have also been used as pico-Newton force transducers to measure the strength of molecular bonds [90] and to determine the transmission of forces in the microscopic environments of complex fluids [91-94]. Combining the ability to manipulate micro-particles with force measurements, optical tweezers have been used to study the micromechanical properties of soft materials [95, 96] such as colloidal crystals [97-100], liquid crystals [101-103], carbon nanotube suspensions [104], actin-coated lipid vesicles [105-107], living cells [108-113], cytoskeletal networks [114-117], DNA networks [49, 118], polymer solutions [46, 119, 120], collagen gels [121, 122], human erythrocyte membranes [67, 123-126], and even individual strands of DNA molecules [86, 127]. In this section, we introduce the oscillatory optical tweezer system and describe calibration of the trapping force in the linear restoring-force regime. Then we discuss two-particle optical interactions in *Section* 2.2.4. With proper calibration, the optical tweezers can be used as a convenient micro-rheometer, which will be discussed in *Chapter* 3 and *Chapter* 4.

2.2.1 Oscillatory Optical Tweezers Setup

We construct our oscillatory optical tweezer system (as shown in Figure 2.4) with two lasers: a high-power laser (λ = 1064 nm) to trap and oscillate particles, and a low-power laser (λ = 980 nm) to track trapped particle displacement. The tracking laser intensity is attenuated so that its power is lower than that of the trapping laser by two orders of magnitude in order to prevent disturbance of optical trapping effects. Both beams are expanded and collimated to fully fill the back aperture

of a high-focusing microscope objective (100X). The oscillatory PZT-driven mirror shifts the incident angle of the beam (without a position shift). Through optical conjugation, adjustment of the distance between the two lens as a beam expander (BE) causes a change of the incident angle of the beam at the back aperture of the microscope objective. This produces a lateral translation of the focal spot without laterally shifting the beam outside the back aperture of a microscope objective.

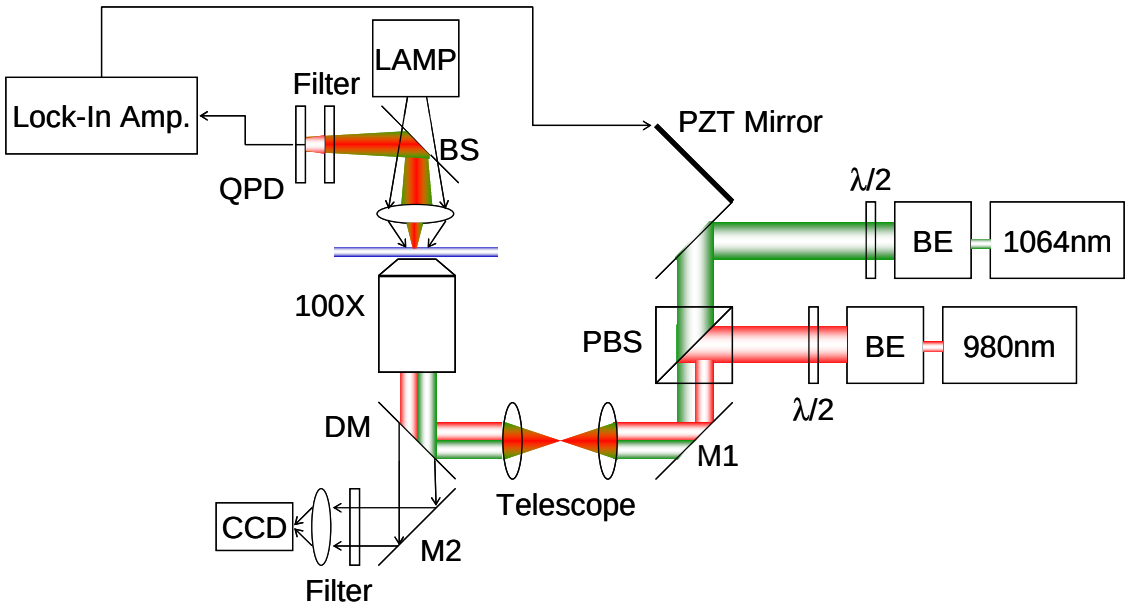

Figure 2.4 A schematic diagram of the experimental setup; BE: beam expander; PZT Mirror: mirror mounted on a PZT (piezo-electric stage); PBS: polarizing beam splitter; M: mirror; DM: dichroic mirror; BS: beam splitter; QPD: quadrant photodiode; CCD: charge-coupled device.

Since the trapping and detection beams are collinear and parfocal, any movements of the particle can be deduced from the diffraction of the detection beam relative to that of the trapping beam. Light from the tracking beam diffracted by the particle is collected by the condenser and projected onto a quadrant photodiode (QPD, S7479, Hamamatsu) in the transverse sample plane. For accurate detecting, the voltage output of the detector is limited to a linear function of the displacement of the trapped particle. Our present particle tracking system provides spatial

resolution in the sub-nanometer range. To analyze the voltage from the detector, we use a lock-in amplifier referenced to the sinusoidal signal that drives the PZT-driven mirror. This provides great sensitivity to determining of the displacement amplitude and phase shift of the trapped particle. Wide-field images of the trapped particle are captured by a CCD camera for optical alignment, image observation, and analysis. In addition, scanning of the trapping beam is accomplished by oscillating (along the x-axis) the mirror mounted on the PZT stage as is illustrated in Figure 2.5.

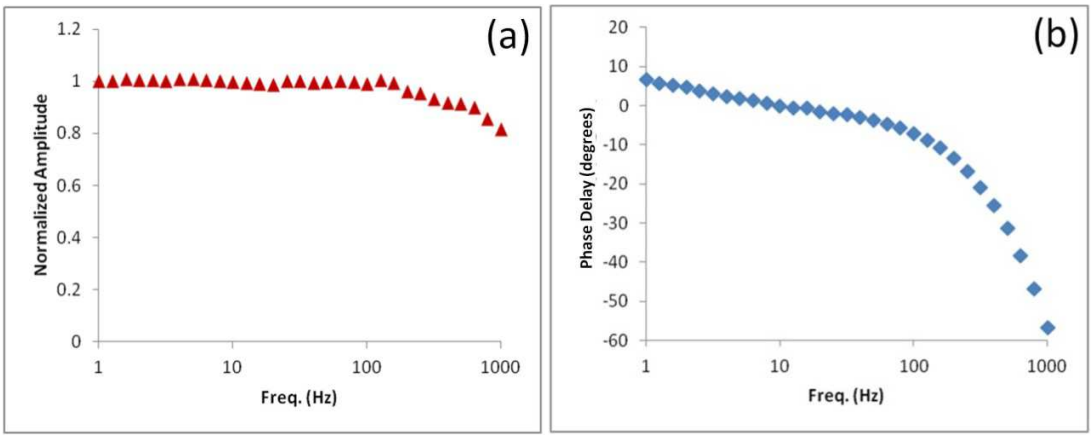

Figure 2.5 (a) Normalized amplitude and (b) phase delay of the mirror-mounted PZT stage as a function of the oscillation frequency from 1Hz to 1000Hz.

2.2.2 Calibration of Optical-Tweezers Force Constant

With proper calibration [128-137], the optical tweezers can be used as a convenient force transducer. Measurements of the optical forces on a particle trapped by optical tweezers can be calibrated by several different approaches. In the fluid-drag approach, a trapped particle is dragged along a direction perpendicular to the optical axis with a viscous force gradually increased until the particle escapes from the optical trap [128, 133, 138]. In the thermal-fluctuation approach, the force constant can be deduced either by analyzing the spatial distribution of the Brownian motion of an individual particle in the optical tweezers [139-143] or by analyzing the power spectrum of the thermal fluctuations [129, 144]. In the forced-harmonic-oscillator approach, the

force constant can be calculated from the frequency-dependent amplitude and phase of a particle that is harmonically driven by oscillatory optical tweezers in a liquid with known viscosity [145, 146]. In this section, we describe the forced-harmonic-oscillator method.

The motion of a particle, trapped and oscillated by the oscillatory optical tweezers in a viscous medium, is determined by force imparted by the optical tweezers and the viscous drag force experienced by the particle. We can describe the optical trapping force by Hooke's law, with an optical force constant "k_{OT}", in the linear restoring force regime. Here, the optical force is proportional to the displacement when the displacement is sufficiently smaller than the optical force-regime, which will be described in the next section [147]. Figure 2.6 shows the forces on a particle of radius "*a*", in an oscillatory optical tweezers in a simple viscous liquid. In the linear restoring-force regime, the oscillatory optical tweezers can be modeled as a quadratic potential well, oscillating with constant amplitude "*A*". For a simple viscous liquid, the drag force is the Stokes drag $F_{drag} = 6\pi\eta a\dot{x}$, where $\dot{x}$ is the velocity of the particle and η is the shear viscosity of the liquid.

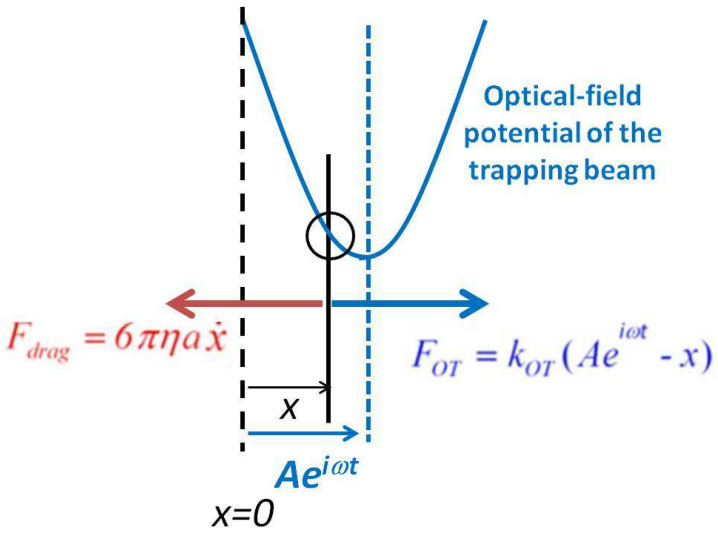

Figure 2.6 Forces on a particle trapped by an oscillatory optical tweezers.

The force exerted on the particle by the optical tweezers is the force constant multiplied by the distance from the center of the particle to the center of the trap. A second, stationary laser beam focused by a low numerical aperture, with optical intensity much weaker than that of the trapping beam, is used to track the position of the particle. The equation of motion of the particle is

$$m\ddot{x}(\omega,t) = -6\pi\eta a\dot{x}(\omega,t) + k_{OT}(Ae^{i\omega t} - x(\omega,t)) \tag{2.1-a}$$

where *m* is the mass of the particle, *x* is the displacement of the particle from the center of the tracking beam, and *A* is the amplitude of the oscillatory optical tweezers with angular frequency ω. Since the Reynolds number of the particle motion is low, $6\pi\eta a\dot{x} >> m\ddot{x}$, one can ignore the first term, $m\ddot{x}$, and Equation 2.1-a can be simplified to Equation 2.1-b for a micron-sized particle with oscillating frequencies in the range of ω = 1～6000 rad/s as discussed below.

$$6\pi\eta a\dot{x}(\omega,t) + k_{OT}x(\omega,t) = k_{OT}Ae^{i\omega t} \tag{2.1-b}$$

A steady-state solution of Equation 2.1-b can be written in the form $x(\omega,t) = D(\omega)e^{i(\omega t-\delta(\omega))}$, where the displacement amplitude "*D*" and the relative phase "δ" can be obtained experimentally by the use of a lock-in amplifier. The amplitude $D(\omega)$ of the displacement of the particle is given by

$$D(\omega) = \frac{Ak_{OT}}{\sqrt{{k_{OT}}^2 + (6\pi\eta a\omega)^2}} \tag{2.2-a}$$

and the phase shift $\delta(\omega)$ is given by

$$\delta(\omega) = \tan^{-1}\left(\frac{6\pi\eta a\omega}{k_{OT}}\right) \tag{2.2-b}$$

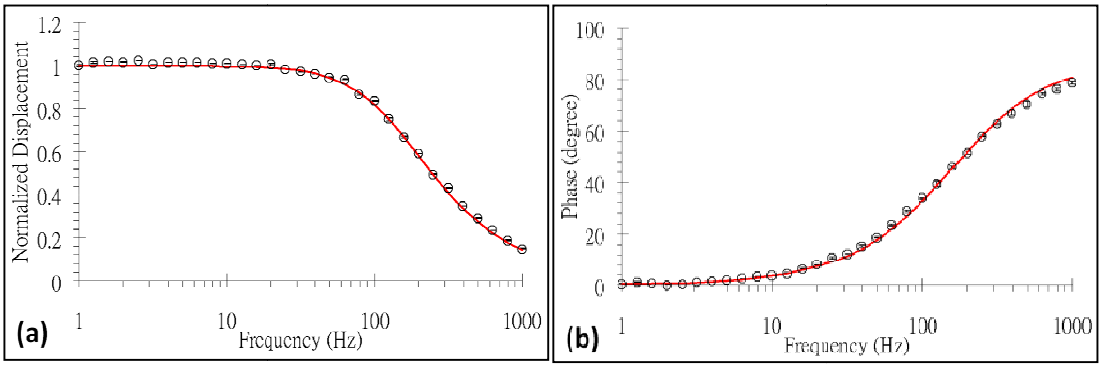

Figure 2.7 (a) The normalized amplitude and (b) the relative phase as a function of the oscillation frequency of a 1.5 μm diameter polystyrene particle in de-ionized water in an oscillatory optical tweezers. The open circles represent experimental data and the solid lines are fitted with the optical force constant k_{OT} as the only fitting parameter in Equations 2.2-a and 2.2-b.

The amplitude of the displacement has two distinct regimes as shown in Figure 2.7. At low frequencies, the amplitude of the particle's displacement takes on the form $D(\omega)= A$. In this regime, the elastic force of the trap dominates the motion of the particle. At high frequencies, the viscous damping force dominates the motion of the particle, and the amplitude of the particle's displacement takes the form $D(\omega)=Ak_{OT}/6\pi\eta a\omega$. Over the entire angular frequency range, the tangent of the phase is a linear function of angular frequency, given by $\tan\delta(\omega) = 6\pi\eta a\omega / k_{OT}$.

The optical force constant (k_{OT}) is determined by Equations 2.2-a and 2.2-b [109, 147, 148] where the viscosity η of water is taken to be 0.9548 mPa sec at 22℃. Figures 2.7(a) and 2.7(b), respectively, depict the angular frequency-dependent amplitude $D(\omega)$ and phase shift $\delta(\omega)$ of an oscillating polystyrene particle (diameter = 1.5 μm) in de-ionized water. The open circles represent the experimental data and the solid lines are the fits with the optical force constant k_{OT} as the only fitting parameter in Equation 2.2. The force constant k_{OT} determined from the best fit is 15.65±0.52 pN/μm from the amplitude data and 14.70±0.42 pN/μm from the phase data at laser trapping power of 6 mW.

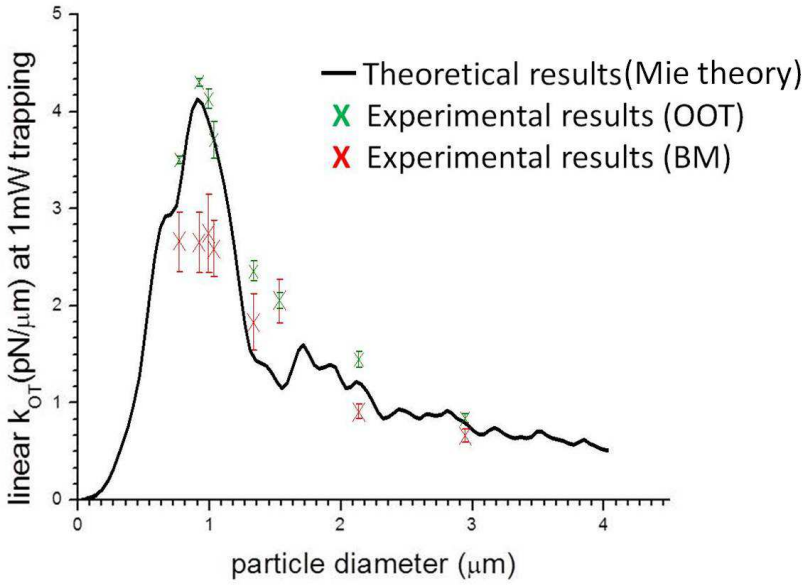

Figure 2.8 Experimental and theoretical results for k_{OT} *vs.* particle size at 1 mW laser power. Green crosses: measured by oscillatory optical tweezers, OOT; red crosses: measured by tracking particle Brownian motion, BM; black solid line: generalized Mie theory. Means and standard deviations are obtained by repeating each experiment 10 times under identical experimental conditions.

Optical forces on colloidal particles have been calculated using mainly three different models: (a) the ray optics model [130, 149], which is a good approximation for the particle radius "*a*" when it is bigger than optical wavelength "λ"; (b) the electromagnetic field model [150, 151], a good approximation for the particle radius when $a < \lambda$; and (c) generalized Mie theory, which is applicable when the particle size is comparable to the wavelength of the trapping laser [131, 152, 153]. In the linear restoring force regime, the optical force constants (per mW of optical trapping power) as a function of particle size, obtained from the generalized Mie theory (Figure 2.8, the black solid line) are in good agreement with the experimental data measured by oscillatory optical tweezers approach (Figure 2.8, green crosses). When the particle diameter approaches the trapping-laser wavelength ($\lambda \sim$ 800 nm in water), the transverse linear optical spring constant

reaches a maximum, which agrees with the theoretical result. This is also consistent with the experimental results [142, 143] obtained by tracking the Brownian motion of a trapped particle (the red crosses) as shown in Figure 2.8.

2.2.3 Transverse Force Profiles associated with an Individual Particle

For the design of optical trapping-based force transducers, the transverse force profile (especially in the linear restoring-force regime) associated with a particle in an optical trap needs to be determined. A pair of overlapping optical traps with unmatched strength has been used in experiments where the stronger trap served as a linear force transducer to map the force profile of the weaker trap [147]. Several techniques (such as a flow system [128-133], a double-stranded DNA tether [134], or an additional laser beam [135-137]) have been used to measure the maximum transverse trapping force of the optical tweezers. Use of an additional laser beam as a force sensor serves several purposes. First, it acts as an optical cage to prevent the trapped particle from escaping along the axial direction [133]. Second, it eliminates the need for an additional vehicle such as a double-stranded DNA linkage [134] or a fluidic flow system [128-133].

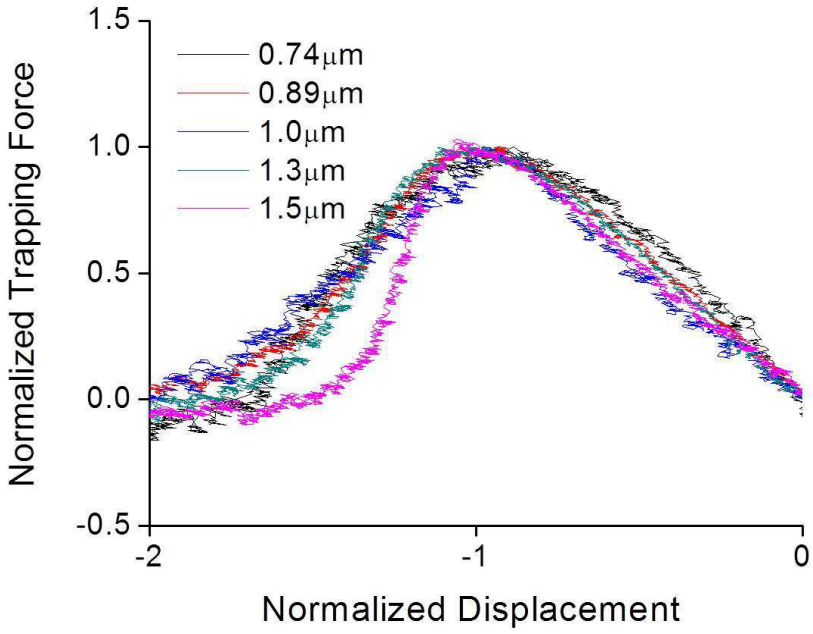

Figure 2.9 Experimental results showing the normalized trapping force as a function of the normalized particle displacement for different polystyrene particle sizes.

Experimental data for the trapping forces (normalized by the corresponding maximum trapping force) as a function of the particle displacements (normalized by the positions of the maximum trapping forces) are shown in Figure 2.9 for different polystyrene particle diameters. For particle sizes smaller than or comparable to the trapping laser wavelength, the normalized trapping force profiles closely follow the gradient of the Gaussian profile, which is expected from paraxial theory [151].

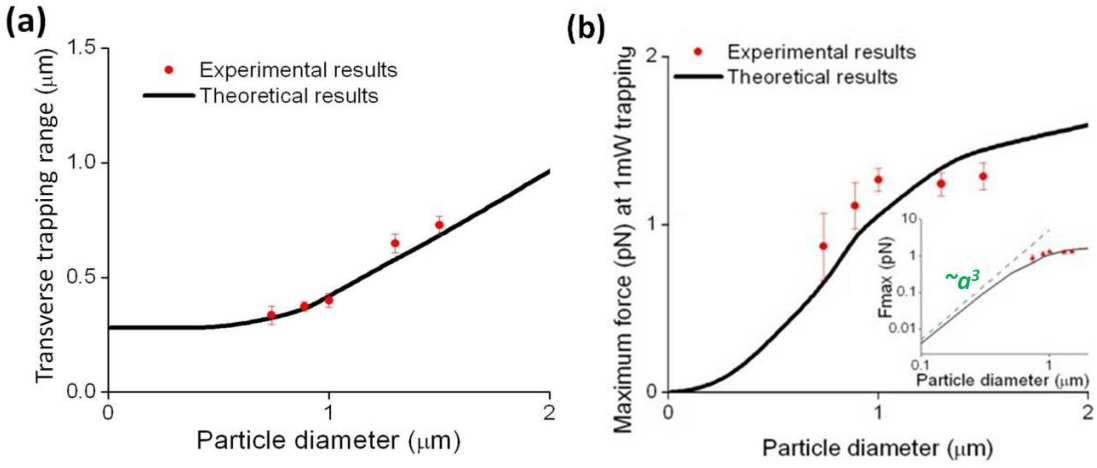

Figure 2.10 (a) The transverse trapping range (TTR) as a function of particle diameter; (b) the maximum trapping force as a function of particle diameter: experimental (red dots) and theoretical (black line: generalized Mie theory corrected for spherical aberration). The inset in (b) shows the maximum trapping force versus particle diameter on a log-log plot, where the green dashed line shows an a^3 dependence.

As the particle size increases, the normalized force profiles deviate from the gradient of the Gaussian profile in the region outside the transverse trapping range (TTR), which is defined as the radial distance from the center of the trap to the position where the trapping force is maximum. In general, TTR depends on the particle size as shown in Figure 2.10(a). For particles with radius smaller than the beam-waist radius (~ 0.3 μm in our experiments), the particle “sees” or “senses” the beam waist; hence, the TTR is mainly dictated by the beam-waist radius and is independent of

the particle size. For particles with radius comparable to or larger than the beam-waist radius, the TTR increases approximately linearly with the particle radius as a result of convolution of the trapping-beam intensity profile and the particle volume.

The maximum transverse optical trapping force as a function of particle diameter is shown in Figure 2.10(b). The theoretical result shows that for small particles (i.e., for particle sizes much smaller than the trapping wavelength, i.e., 1064 nm in our experiment), the maximum transverse optical force is approximately proportional to particle volume as expected from the dipole theory [151] (see inset in Figure 2.10(b)). For Mie particles where the particle size is comparable to the trapping beam wavelength, the maximum trapping force is a weak function of the particle size [147].

2.2.4 Optical Interaction between Two Colloidal Particles

The gradient optical force, which we discussed in the earlier section, can trap and manipulate a small particle. However, in the presence of multiple particles, the gradient force does not tell the entire story. There is an additional optical interaction which couples the particles [154]. This optical interaction between two colloidal particles was first demonstrated experimentally by Burns *et al.* in 1989 [155, 156], who recognized it to be caused by an optical gradient force in a periodic potential resulting from interference of the incident light with light scattered by the particles. Illuminated by coherent light, dielectric particles can self-assemble into an array with periodicity equal to the wavelength of the light [154-156]. Lateral optical binding [157-162] has raised much interest from both fundamental and technical points of view partly because of its potential for applications such as photonic crystals. Here, we studied the optical binding force between two colloidal particles and measured the XX, YY and XY forces (shown Figure 2.11) as a function of distance between a pair of dielectric Mie particles. We compared the experimental results with numerical simulation using generalized Mie theory.

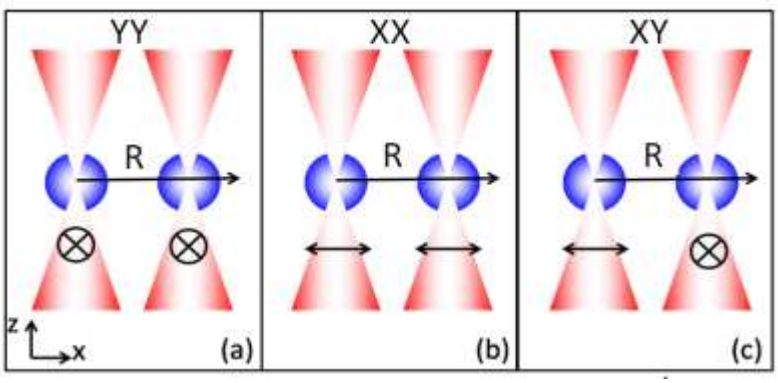

Figure 2.11 Experimental configurations. In (a)-(c), the trapping beams are red, and the particles are blue. The polarization directions are indicated in black. In (a) and (b), the polarizations of the incident beams are, respectively, perpendicular (YY configuration) and parallel (XX configuration) to the X-separation vector of the two particles. In (c), the polarizations of the two beams are orthogonal (XY configuration).

Two pairs of optical tweezers produced by a single laser are found to satisfy the requirements for the experiments. Two 1.5 μm diameter polystyrene particles are positioned in two coherent and independent optical traps, each formed by focusing an IR laser (40 mW, λ = 1064 nm) with a microscope objective lens (Olympus, PlanFluo, 100X, N.A.=1.3). One of the traps blinks by use of an optical chopper at 31 Hz. The position of the blinking trap is movable in the direction perpendicular to the laser beam by use of a motor-controlled lens. The other trap, non-blinking, is stationary. A second laser (λ = 980 nm), much weaker than the trapping laser, is used to track the position of the particle in the stationary trap.

Using optical tweezers as a force sensor with known optical spring constants [109, 142, 143, 145, 146], we measured forces between the two particles from the magnitude and phase (relative to that of the blinking light) of the particle displacement as a function of the distance between the particles. We determine the optical force by subtracting the hydrodynamic coupling [92, 163]. But not all the optical forces on the particles are due to optical binding. When two optical tweezers are near each other they exert forces on both particles, and the strength of the optical cross-talk increases with decreasing particle separation. Since two overlapping coherent optical fields interfere, the particles experience an additional force due to the interfering field. We can measure the force due to cross-talk by measuring the force on the particle in the stationary trap when the blinking tweezer has no trapped particle. The pure binding force is found by subtracting the optical cross-talk force from the total optical force.

Figure 2.12 shows both the measured and calculated binding forces [141, 153, 164-170] for the YY (Figure 2.12(a)) and XX (Figure 2.12(b)) configurations *vs.* the center-to-center separation between two 1.5 μm-diameter polystyrene spheres. The theoretical calculation shows that the spatial periodicity of the binding force for both YY and XX configurations must be equal to the laser wavelength in the medium. To demonstrate that the spatial oscillation of the binding force is caused by a phase delay, we measure the force as a function of the relative phase between the two trapping beams at fixed relative positions. The force *vs.* relative phase for the YY configuration

is shown in Figure 2.12(c). Black, red, and blue correspond to particle separations of 3.0, 3.6, and 4.2 μm, respectively; the data show that the optical binding force at a fixed particle separation varies sinusoidally with the relative phase shift and that the magnitude of the force decreases with separation, as expected.

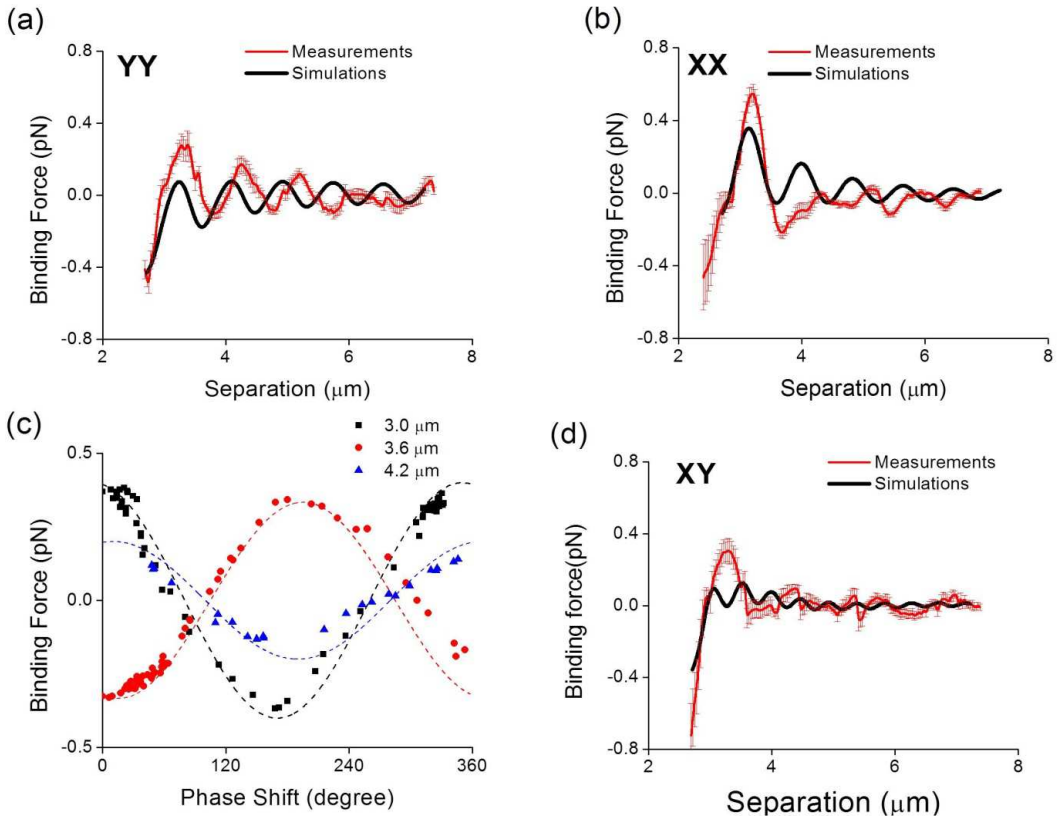

Figure 2.12 Experimental measurements (red line) and simulations (black line) of the binding force for different polarization configurations (YY (a), XX (b) and XY(d)) as a function of the particle center-to-center separation. (c) Binding forces for the YY configuration as a function of relative phase between the two optical traps. The dotted lines are guides to the eye that illustrate the sinusoidal nature of the curves.

While the magnitude of the XY binding force (Figure 2.12(d)) is smaller than the XX and YY binding forces by a factor of two, the XY binding force shows characteristics different from those of

XX and YY: the spatial periodicity of the XY binding force is half the wavelength, and the force at a fixed particle separation is independent of the relative phase of the two beams. The optical force in the XY configuration is caused by another mechanism, i.e., interference of the *E*-field of the trapping beam with light scattered first from the particle in the trap to the neighbor particle, then re-scattered back to the original particle. Since this twice-scattered wave travels a distance 2*R*, the phase delay between the incident and the twice-scattered wave is *2Rk* (*R* is the particle separation and *k* is the wave number of the laser beam in water), which gives the optical force a spatial oscillation of period ½ wavelength.

For *E*-fields polarized in the directions perpendicular (YY) and parallel (XX) to the direction between the particles, the binding forces are long-range (~1/R) and oscillatory in space with multiple points of stability. For particles of size comparable to the optical wavelength, the magnitude of the binding force is comparable to the intrinsic (Coulomb and van der Waals) interactions between the colloidal particles. Interplay of the two types of colloidal forces can affect the ensemble behavior of particles in an optical field.

A new binding force was discovered for the crossed (XY) laser polarization configuration. Termed “self-binding”, the new binding force differs from “mutual-binding” [155, 156] in the following senses: (1) it is caused by double scattering of light from both particles, thus is a second order effect; it is observable only because the stronger first-order mutual-binding is forbidden by parity for the XY configuration, (2) the spatial periodicity of the stability points is half the wavelength. In self-binding, the partner particle serves only as a back-scatterer. Hence, the partner can be of any shape, making self-binding potentially responsible for the phenomenon that particles, when illuminated by light, are attracted to a nearby solid wall [171]. This effect of optical interactions between two trapped colloidal particles should be considered in the use of two-particle active microrheology for studying the mechanical properties of two probe particles. This will be discussed in *Section* 3.3.

In conclusion, with each experiment serving for proper calibration, we found (1) the transverse linear optical spring constant (k_{OT}) reaches a maximum when the particle diameter approaches the trapping laser wavelength; (2) the trapping linear range increases approximately linearly with the particle radius for particles with radius larger than the beam waist-radius; (3) maximum trapping force is approximately proportional to particle volume for particle sizes much smaller than the trapping wavelength; however, the maximum trapping force is a weak function of the particle size when the particle size is comparable to the trapping-beam wavelength; (4) optical binding forces generate a sub-picoNewton optical gradient force in a periodic potential created by interference of the incident light and the light scattered by the particles. Using oscillatory optical tweezers-based microrheology, we will use a micron-sized probe (~the trapping laser wavelength) to create a stronger optical force for local measurement. In addition, using two-particle active microrheology, we will use two laser beams with crossed laser polarization to minimize optical binding effects.

3. Microrheology of Polymer and Colloidal-Crystal Solutions

In this chapter, we consider the mechanical properties of polymer and colloidal-crystal solutions measured by oscillatory optical tweezers. This approach allows us to measure the storage and the loss moduli (*G'* and *G"*). We consider single-particle active microrheology of a homogeneous polymer and colloidal-crystal solutions in *Sections 3.1* and *3.2*, respectively. The results are consistent with the corresponding bulk mechanical properties measured by a conventional-rheometer and micromechanical properties obtained from passive microrheology [172]. However, the experimental results of single-particle microrheology of inhomogeneous soft materials differ from the corresponding macroscopic mechanical properties. In *Section* 3.3, we consider the application of two-particle active microrheology to study the effects of microscopic heterogeneous mechanical properties of a polymer solution between two probe particles.

3.1 Response Function for an Oscillating Particle in a Viscoelastic Medium

To relate the motion of a single particle to the mechanical properties of the material surrounding the particle, the complex response function is extended to deduce the viscoelasticity of the material. The complex response function, $\alpha^*(\omega)$, is the ratio of the displacement of a particle to the external forces on the particle. $\alpha^*(\omega) = x(\omega) / F(\omega)$ where $x(\omega)$ is the angular frequency dependent displacement of the particle and $F(\omega)$ is the external force on the particle. The response function from Equation 3.1, ignoring the inertia of the particle, can be expressed as

$$\alpha^*(\omega) = \frac{x(\omega)}{F(\omega)} = \frac{1}{i\omega 6\pi a\eta + k_{OT}} \tag{3.1}$$

A single spherical particle trapped by optical tweezers in a viscous medium can be modeled by a viscoelastic medium with an *effective complex shear modulus*, $G^*_{eff}(\omega) = 1/6\pi a\alpha^*(\omega)$. Conventionally, the viscoelasticity of a complex fluid is characterized in terms of the complex

shear modulus [173] $G^*(\omega) = i\omega\eta^*(\omega) = G'(\omega) + iG''(\omega)$, where $\eta^*(\omega)$ is the complex viscosity and $G'(\omega)$ and $G''(\omega)$ are the storage (or elastic) modulus and the loss (or viscous) modulus, respectively. Using these nomenclatures, the relationship between $G^*_{eff}(\omega)$ and $G^*(\omega)$ can be expressed as

$$G^*_{eff}(\omega) = \frac{1}{6\pi a\alpha^*(\omega)} = \frac{k_{OT}}{6\pi a} + i\omega\eta^*(\omega) = \frac{k_{OT}}{6\pi a} + G^*(\omega) = \frac{k_{OT}}{6\pi a} + G'(\omega) + iG''(\omega) \tag{3.2}$$

where the first term on the right side of Equation 3.2 represents the contribution from the elasticity of optical tweezers, and the other terms represent the viscoelasticity of the material surrounding the probe particle.

When a particle in a fluid is subjected to an oscillating force, the effective complex shear modulus can be deduced from the angular frequency-dependent in-phase and out-of-phase motion relative to the oscillating force as follows:

$$G^*_{eff}(\omega) = \frac{1}{6\pi a\alpha^*(\omega)} = \frac{F}{6\pi a x(\omega)} = \frac{Ak_{OT}}{6\pi a x(\omega)} = \frac{Ak_{OT}}{6\pi a D(\omega)}\left(cos\delta(\omega) + i\ sin\delta(\omega)\right) \tag{3.3}$$

From Equation 3.4, the storage and loss moduli, $G'(\omega)$ and $G''(\omega)$, of the material surrounding the probe particle can be determined from the phase shift "δ" and amplitude "D" of the particle (in response to the oscillatory optical tweezers) by the following relationships:

$$G^*(\omega) = \frac{k_{OT}}{6\pi a}\left(\frac{A}{x(\omega)} - 1\right) = G'(\omega) + iG''(\omega) \tag{3.4-a}$$

$$G'(\omega) = \frac{k_{OT}}{6\pi a}\left(\frac{A\cos\delta(\omega)}{D(\omega)} - 1\right) \quad and \quad G''(\omega) = \frac{k_{OT}}{6\pi a}\left(\frac{A\sin\delta(\omega)}{D(\omega)}\right) \tag{3.4-b}$$

Here we present, as a specific example, the application of oscillatory optical tweezers to study the micromechanical properties of an aqueous solution of polyethylene oxide (PEO; *MW* = 100 kg/mol). The results are in agreement with the bulk mechanical properties [174]. For a 20 wt% solution of PEO in water, the average mesh size of the polymer network is much smaller than the size of the probe particle (1.5 μm diameter polystyrene sphere). Although PEO has been shown to adsorb onto the surface of a polystyrene particle, adsorption is not an issue because the thickness of the adsorbed polymer has been determined to be approximately 24 nm [175].

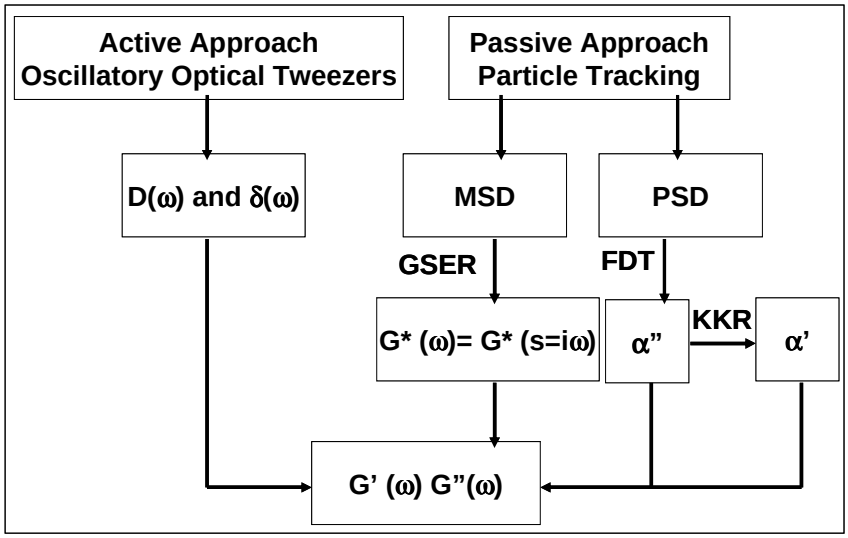

Figure 3.1 Flowchart explaining the ways of obtaining the frequency-dependant elastic and viscous moduli by active and passive measurements of the motions of a probing particle. MSD: mean square displacement; PSD: power spectral density; GSER: generalized Stokes-Einstein relation; FDT: fluctuation-dissipation theorem; KKR: Kramers-Kronig relations.

The flowchart of approaches for obtaining the elastic and viscous moduli is shown in Figure 3.1. Below we compare the mechanical properties of a 20 wt% solution of PEO in water as measured by the oscillatory-optical-tweezers active microrheological approach *vs.* those obtained by the particle-tracking passive microrheological approach (without optical tweezers). In the active approach, the complex shear modulus can be measured directly as described by Equation 3.5; in

the passive approach, the complex shear modulus can be determined by tracking the Brownian motion and using the fluctuation-dissipation theorem (FDT) [176, 177] or the generalized Stokes-Einstein relation (GSER) [178].

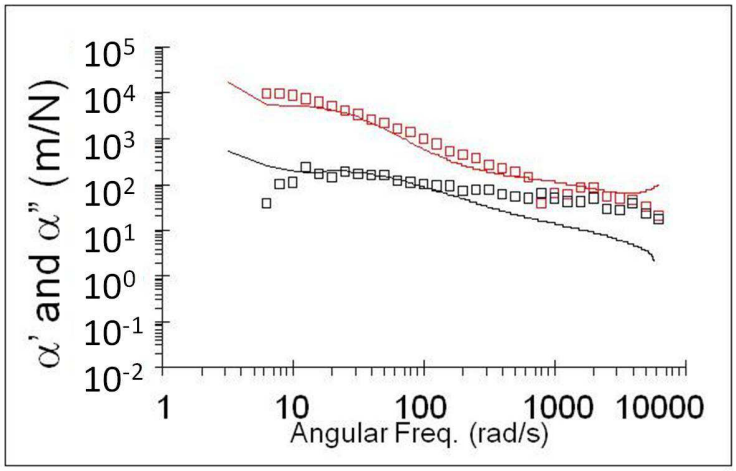

Figure 3.2 Experimental results of real part (α', shown in black) and the imaginary part (α'', shown in red) of the complex response function as a function of frequency obtained by the active oscillatory optical tweezers approach (□) and the passive particle tracking approach (solid lines) according to the Kramers-Kronig relation (KKR).

According to the fluctuation-dissipation theorem (FDT), the imaginary part of the complex response function $\alpha''(\omega)$ can be written as:

$$\alpha''(\omega) = \frac{\omega}{2k_B T} C(\omega) \tag{3.5}$$

where $C(\omega)$ is the power spectral density analyzed from particle displacement fluctuations, k_B is the Boltzmann constant, and T is the absolute temperature. The imaginary part of the complex response function $\alpha''(\omega)$ deduced from Equation 3.5, agrees with the corresponding results

obtained by the active approach in this equilibrium system. According to the Kramers-Kronig relation (KKR), the real part of the compliance function $\alpha'(\omega)$ can be expressed as:

$$\alpha'(\omega) = \frac{2}{\pi} P \int_0^\infty \frac{\xi \alpha''(\xi)}{\xi^2 - \omega^2} d\xi = \frac{2}{\pi} \int_0^\infty \cos(\omega t)\, dt \int_0^\infty \alpha''(\xi) \sin(\xi t) d\xi \tag{3.6}$$

The reciprocal of $\alpha^*(\omega)$ is the complex shear modulus $G^*(\omega) = G'(\omega) + iG''(\omega)$, where $G'(\omega)$ and $G''(\omega)$ are given by

$$G'(\omega) = \frac{1}{6\pi a} \frac{\alpha'(\omega)}{\alpha'(\omega)^2 + \alpha''(\omega)^2} \tag{3.7-a}$$

$$G''(\omega) = \frac{1}{6\pi a} \frac{-\alpha''(\omega)}{\alpha'(\omega)^2 + \alpha''(\omega)^2} \tag{3.7-b}$$

The loss modulus $G''(\omega)$ obtained by the active and the passive approaches agree well. However, the storage modulus $G'(\omega)$ measured by the active approach and the passive approach do not agree in both the high and low frequency regimes because the lower and the upper bounds of the frequency range of the integral in Equation 3.7 are replaced by finite values (6 rad/s and 6000 rad/s, respectively).

In Figure 3.3, the results indicate that the micro-rheological properties of semi-dilute PEO solutions agree with the bulk mechanical properties [174] within the frequency range 6 rad/s to 100 rad/s accessible by both techniques [148]. For angular frequencies in the range of 100 rad/s to 6000 rad/s, a comparison can be made between the micromechanical properties determined by the oscillatory optical tweezers and by dynamic light scattering [174]. The results in Figure 3.3 indicate that the polymer solution has liquid-like behavior ($G'' > G'$) in the lower frequency regime and solid-like behavior ($G' > G''$) in the higher frequency regime.

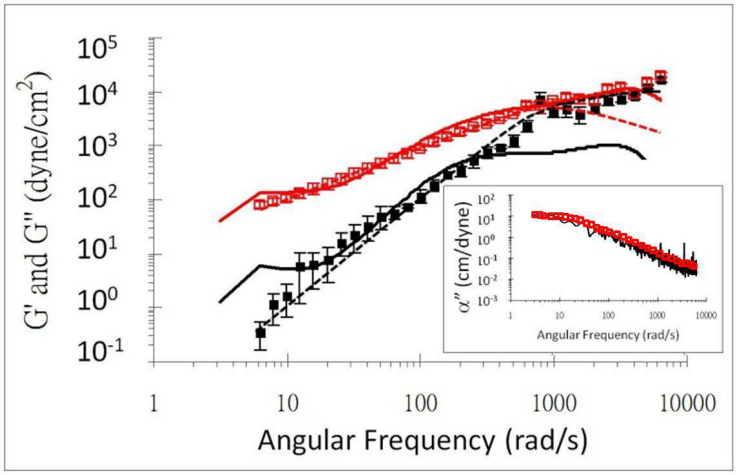

Figure 3.3 The experimental results of storage modulus *G'* (solid symbols) and loss modulus *G''* (open symbols) as a function of frequency obtained by active oscillatory optical tweezers (□) and passive particle tracking (solid lines). The dotted lines represent *G'* and *G''* based on the Maxwell model. The inset shows the imaginary part of the compliance function measured by passive particle tracking (without optical tweezers; solid line), and by active oscillatory optical tweezers (squares).

The experimental results of the mechanical properties as a function of frequency can be fitted to the Maxwell model. The Maxwell element contains a spring and a dashpot (viscosity) in series. Spring and dashpot are subjected to the same stress($\sigma = \sigma_S = \sigma_D$); the deformation of spring and dashpot are additive ($\gamma = \gamma_S + \gamma_D$). The dashpot causes the deformation to be time-dependent. Differentiation of the tensile deformation with respect to time delivers the rate equation, $\dot{\gamma} = \dot{\gamma}_s + \dot{\gamma}_D$. Here it is convenient to express the stress as $\sigma = \sigma_0 \exp(\mathrm{i}\,\omega \mathrm{t})$; $\dot{\sigma} = \mathrm{i}\,\omega\sigma_0 \exp(\mathrm{i}\,\omega \mathrm{t}) = \mathrm{i}\,\omega\sigma$ and the strain response by the phase lag δ via $\gamma = \gamma_0 \exp(\mathrm{i}\,\omega \mathrm{t} + \delta)$; $\dot{\gamma} = \mathrm{i}\,\omega\gamma_0 \exp(\mathrm{i}\,\omega \mathrm{t} + \delta) = \mathrm{i}\,\omega\gamma$. Then, we substitute the complex stress (σ) and strain (γ) into the constitutive equation for a Maxwell fluid: $\dot{\gamma} = \dot{\gamma}_s + \dot{\gamma}_D = \dot{\sigma}/G + \sigma/\eta$. We can rewrite $i\omega\gamma = i\omega\sigma/G + \sigma/\eta$ and then rearrange as $\gamma/G\sigma = 1 + G/i\omega\eta = 1 + 1/i\omega\tau$

with characteristic decay time τ given by the ratio of the viscosity to shear modulus. In a Maxwell model, this expression describes the variation of the complex modulus with frequency and separates the real and imaginary components:

$$G^* = G' + iG'' = G^*_\infty \left(\frac{\tau^2\omega^2 + i\tau\omega}{1+\tau^2\omega^2} \right) \tag{3.8}$$

with two adjustable parameters τ and G^*_∞, where G^*_∞ is the plateau modulus and τ is the relaxation time of the system. The relaxation time occurs at the crossover frequency between the storage and loss moduli. According to the theory of rubber elasticity [179], $G^*_\infty = \nu k_B T$, where ν is the number of elastically active chains in the network per unit volume. The rheology is well described by the Maxwell model [180, 181], with fitted parameters G^*_∞ = 10578 dyne/cm^2 and τ = 1 ms (the dotted lines in Figure 3.3).

The results indicate that the mechanical properties of semi-dilute PEO solutions compare well with the bulk mechanical properties and microrheological properties measured by passive particle tracking. The results thus provide a measure of confidence with regard to the oscillatory optical tweezers technique.

3.2 Electro-mechanical Coupling in Colloidal-Crystalline Suspensions of Charged Liposome

In this section, we investigate colloidal interactions by using single-particle active microrheology. Colloidal crystals, a highly ordered array of colloidal particles, have been extensively studied. The behaviors of colloidal crystals reveal insights into mechanisms of self-assembly and phase transitions, which might be applied from colloidal studies to systems of atoms. Phase transitions have been studied by topological transformations. In order to study the details of particle interactions, such as electrostatic or hydrodynamic, individual micron spheres in colloidal suspensions are large enough for their motions to be tracked by video microscopy. For nano-sized colloidal particles, it is difficult to observe individual particles due to the optical-imaging diffraction limit. To study interaction, the macroscopic viscoelastic properties of colloidal suspensions can be measured by light scattering or rheology. However, studies of charge-dependent interactions between charged colloidal particles are missing due to a lack of control of charge on colloidal particles.

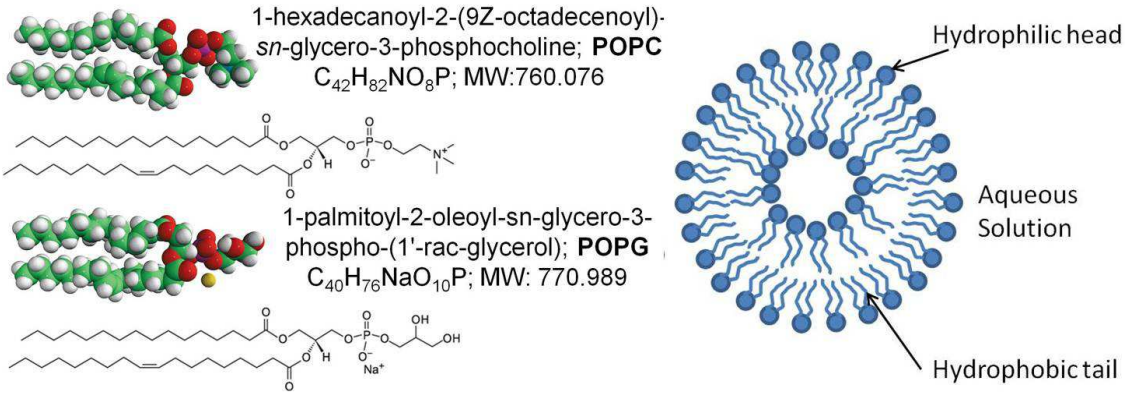

Figure 3.4 The structure of POPC, POPG and a liposome. (From: http://avantilipids.com)

Here, we use charged 100 nm-sized liposomes in aqueous suspension to study mutual electrostatic repulsions. The ratio between charged lipid (POPG; $C_{42}H_{82}NO_8P$, *MW* = 771.0, Avanti) and neutral lipid (POPC; $C_{40}H_{76}NaO_{10}P$, *MW* = 760.1, Avanti) of liposomes can control the particle charge as shown in Figure 3.4. There are approximately 90,000 lipids per a 100 nm-sized liposome including both leaflets.

When the mean distance between liposomes is less than Debye screening length, the suspension self-organizes into a highly ordered array, forming a crystal structure. Mutual repulsions between liposomes in de-ionized water produce an electrostatically-stabilized gel as shown in Figure 3.5. The rigidity of the gel is related to the liposome charge, size, concentration, and the ionic strength of the solution. In principle, it is possible to determine the liposome charge by measurement of the mechanical properties (i.e. bulk modulus, shear modulus, or osmotic pressure) of colloidal-crystal solutions.

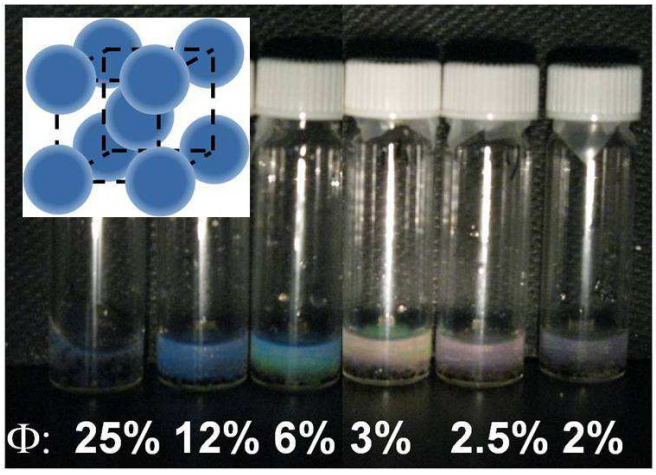

Figure 3.5 Backscattering of charged liposome solution when illuminated by white light (POPG:POPC = 20:80) with varying volume fraction (Φ).

To measure the shear modulus *G'* of the gel in de-ionized water as a function of the intrinsic liposome charge at various ratios between POPG and POPC, we trap and oscillate a polystyrene

probed particle (1.5 μm diameter) in the colloidal-crystal solution and, using a lock-in amplifier, measure the amplitude and phase of the probed particle's displacement. Figure 3.6 shows the shear modulus of a colloidal-crystal solution having 12.5% volume fraction charged liposomes, (POPG:POPC = 10:90) in de-ionized water as a function of frequency. The result, as shown in Figure 3.6, indicates the gel has solid-like behavior ($G' > G''$) in the frequency regime (1~1000Hz) and stabilizes its structure to maintains its stiffness for 24 hours.

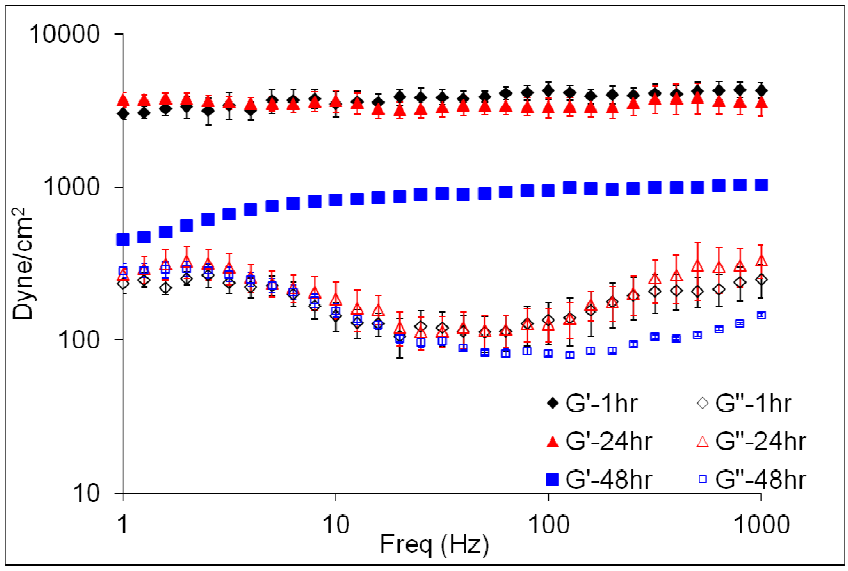

Figure 3.6 Mechanical properties of a charged liposome (POPG:POPC=10:90) suspension having 12.5% volume fraction liposomes as a function of frequency measured by oscillatory optical tweezers microrheology.

The shear modulus is proportional to the second derivative of the interaction potential energy with respect to the direction of shear. The interaction potential can be modeled as a screened Coulomb potential in the Debye-Hückel approximation with an effective liposome charge Z^*. We use the following expression for the shear modulus of a body-centered cubic (bcc) colloidal-crystal [182]:

$$G' = \frac{4}{9} cV(\mathrm{d})(\kappa \mathrm{d})^2 \tag{3.9}$$

where *c* is the colloidal particle number density, *d* is the nearest-neighbor inter-particle distance, *V(d)* is the potential energy of two charged particles separated by distance *d*, and *κ* is the inverse Debye screening length.

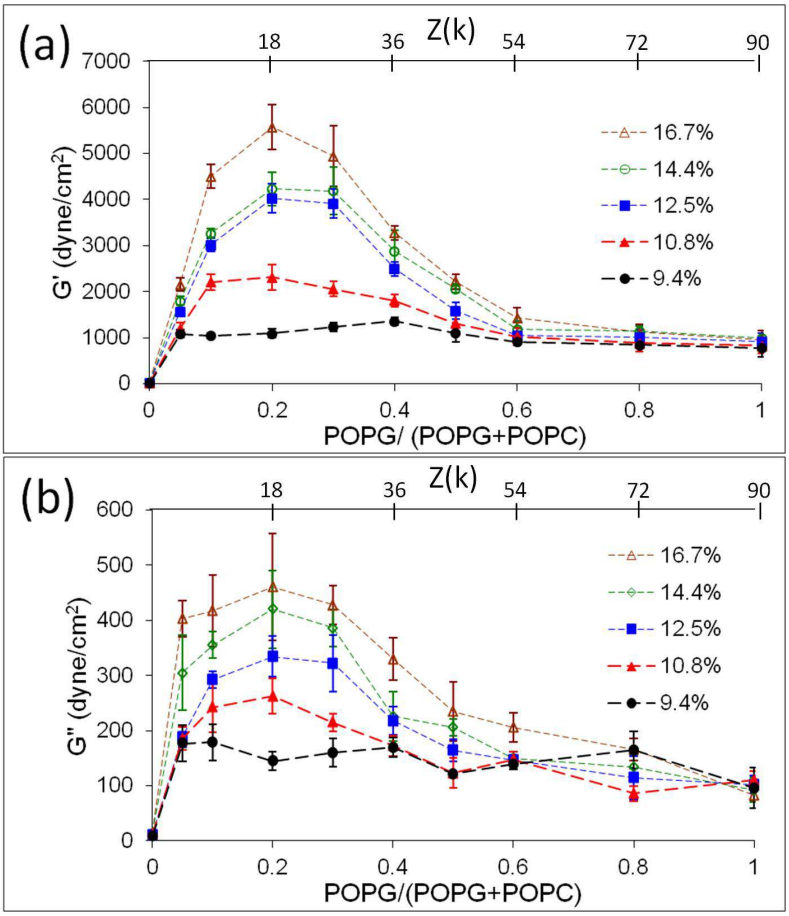

Figure 3.7 100 nm liposomes composed of negatively-charged POPG and neutral-charged POPC at various ratios in de-ionized water. Experimental data show that (a) elastic and (b) viscous moduli of the suspensions at varying liposome concentrations depend on the charge of the colloidal particles. The means and the standard errors are obtained by repeating each condition 5 times.

For point charges, the Debye-Hückel screened Coulomb potential energy between two particles in a de-ionized solution is:

$$\mathrm{V(d)} = \frac{\left(Z^{*}e\right)^{2}}{\varepsilon d}\exp(-\kappa \mathrm{d}) \tag{3.10}$$

where ε is the dielectric constant of the water solution and Z^* is the effective charge per particle. Here, κ is the inverse Debye screening length, $\kappa = \sqrt{4\pi\lambda_B Z^* c}$, where $\lambda_B = e^2/\varepsilon k_B T$ is the Bjerrum length.

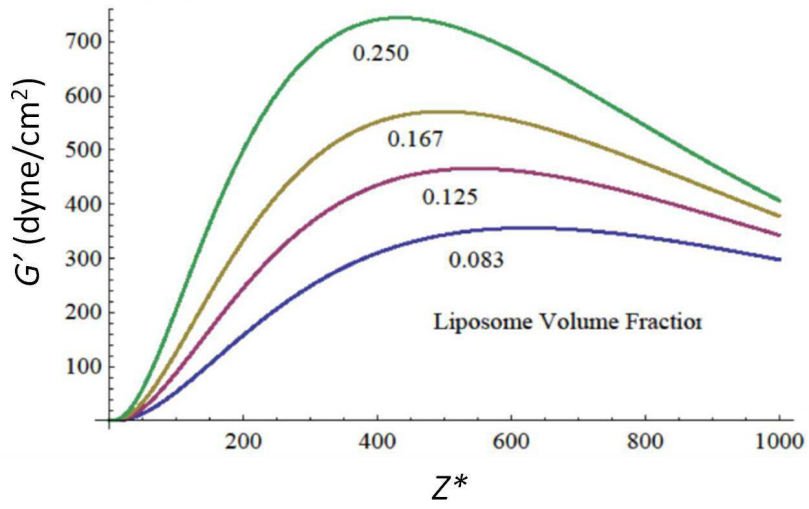

Figure 3.8 Theoretical results of shear moduli of 100 nm liposomes composed of negatively-charged POPG and neutral-charged POPC at various in de-ionized water.

The magnitudes of our experimental *G'* values are 10 times higher than those calculated with a screened Coulomb potential for point charges. The experimental *G'* as a function of the liposome intrinsic charge *Z* is maximal at *Z* = 20,000~30,000, while the simple theory using a screened Coulomb potential gives a *G'* maximum at *Z** = 300~400. The relation of *Z* to *Z** yields information on interfacial phenomena. However, the Debye-Hückel screened Coulomb potential energy, Equation 3.10, does not include finite-size sphere-sphere repulsions, which should be corrected in

the theoretical calculations. Our microrheological study provides new information to understand the potential energy between two charged particles in equilibrium systems.

3.3 Response Tensor for Coupled-Oscillation of Two Particles in a Viscoelastic Medium

Single-particle microrheology can be extended to two-particle microrheology to investigate mechanical inhomogeneities in soft materials at length scales comparable to the distance between the probes. Two-particle microrheology particularly contributes to understanding of the mechanical properties of biological materials [115, 183]. Here, we present the micromechanical properties of a 20 wt% polyethylene oxide solution (*MW* = 100 kg/mol) surrounding a single probe particle as well as between two particles.

Much like the single-particle case, the formalism used to describe the hydrodynamic coupling between two particles in a simple viscous liquid can be extended to deduce the viscoelasticity of the medium. Consider a viscoelastic fluid in which two identical particles are held by two optical tweezers in two separated quadratic potential wells. Under the condition that one of optical tweezers is oscillatory and the other is stationary, the equations of motion of the particles (x_1 and x_2) are given by (neglecting the inertia of the particles) [91, 92]:

$$x_1(\omega,t) = \alpha^*_{11}(\omega)\left[k_{OT1}\left(Ae^{i\omega t} - x_1(\omega,t)\right)\right] + \alpha^*_{12}(\omega)(-k_{OT2}x_2(\omega,t)) \tag{3.11-a}$$

$$x_2(\omega,t) = \alpha^*_{21}(\omega)\left[k_{OT1}\left(Ae^{i\omega t} - x_1(\omega,t)\right)\right] + \alpha^*_{22}(\omega)(-k_{OT2}x_2(\omega,t)) \tag{3.11-b}$$

where A is the amplitude of the oscillatory optical tweezers with angular frequency ω, and k_{OT} is the force constant of the optical trap. To allow for possible inhomogeneity in the fluid, we introduce $\alpha^*_{11}(\omega) = 1/(6\pi a G^*_{11})$, $\alpha^*_{12}(\omega) = 1/(4\pi R G^*_{12})$, $\alpha^*_{21}(\omega) = 1/(4\pi R G^*_{21})$, and $\alpha^*_{22}(\omega) = 1/(6\pi a G^*_{22})$.

Here R is the distance between the particles at the initial position, G^*_{11} is the local complex shear modulus of fluid surrounding the particle in the oscillatory trap, G^*_{12} and G^*_{21} are the

non-local complex shear moduli of the fluid between the two particles, and G^*_{22} is the local complex shear modulus of fluid surrounding the particle in the stationary trap as shown in Figure 3.9. By symmetry, $G^*_{12} = G^*_{21}$, and $\alpha^*_{12} = \alpha^*_{21}$. Viscoelasticity is taken into account by requiring that the viscosity is complex and is a function of frequency. For simplicity, in what follows, the force constants of the two optical traps are equal; i.e., $k_{OT1} = k_{OT2} = k_{OT}$. Here, to avoid optical binding forces acting on the trapped particles, we use dual optical tweezers with the crossed (XY) laser polarization. When the separation distance is greater than 4 μm, the self-binding force can be ignored because the energy of self-binding (< 0.1 pN at 40mW trapping power) is comparable with thermal energy (k_BT) as shown in Figure 2.12.

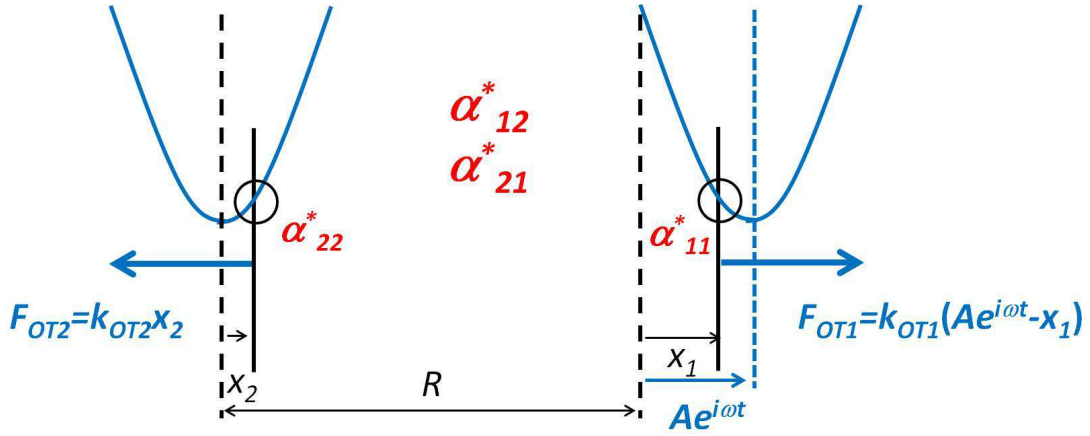

Figure 3.9 Schematic diagram of two particles in a viscoelastic liquid with complex response function; each particle is in one of two separate quadratic potential wells a distance *R* apart.

The purpose of measuring the correlated motions of two particles arises from the fact that these motions can be used to determine the *non-local* mechanical properties, $G^*_{12}(\omega)$, between the two probe particles. While the local mechanical properties, $G^*_{11}(\omega)$ and $G^*_{22}(\omega)$, can be determined by measuring the motion of a single probe particle, the non-local properties are expected to vary as a function of the distance between the two particles in an inhomogeneous viscoelastic medium [184, 185]. Thus, by varying the distance between the two particles and measuring the correlated

motions, we can actively measure the average mechanical properties between the two particles to probe different length scales of the inhomogeneity.

To solve Equation 3.11 for the local and non-local mechanical properties, we assume that the distance between the particles is large enough ($R > a$) such that the particle in the stationary trap does not affect the motion of the particle in the oscillatory trap, except for coupling through the intervening medium as prescribed by $G^*_{12}(\omega)$. This weak-coupling approximation is justified by the assumption that the amplitude of the oscillation of the particle in the stationary trap is expected to be so small that its feedback to the other particle is a high order effect that can be neglected. Thus, the last term on the right side of Equation 3.11-a can be ignored, and the local complex shear moduli become

$$G^*_{11}(\omega) = \frac{k_{OT}}{6\pi a}\left(\frac{A}{x_1(\omega)} - 1\right) \tag{3.12}$$

The above expressions for the local mechanical properties around each probe particle are identical to the corresponding expressions for the storage and loss moduli given in the previous section. The non-local complex modulus is given by

$$G_{12}{}^*(\omega) = \frac{k_{OT}}{4\pi R}\left[\frac{A}{x_2(\omega)} + \frac{x_1(\omega)}{x_2(\omega)}\left(\frac{x_1(\omega)}{A} - 2\right)\right] \tag{3.13}$$

where $x_1(\omega) = D_1(\omega)e^{-i\delta_1(\omega)}$ and $x_2(\omega) = D_2(\omega)e^{-i\delta_2(\omega)}$ are the displacements of the particles in the oscillatory optical tweezers and the stationary optical tweezers, respectively. The mechanical properties of the medium between the two particles can thus be determined by measuring the motion of the particles $x_1(\omega)$ and $x_2(\omega)$. Explicitly, the non-local storage and loss moduli are given by

$$G'_{12}(\omega) = \frac{k_{OT}}{4\pi R}\left[\frac{A\cos\delta_2(\omega)}{D_2(\omega)} + \frac{D_1^{\,2}(\omega)\cos(\delta_2(\omega)-2\delta_1(\omega))}{AD_2(\omega)} - \frac{2D_1(\omega)\cos(\delta_2(\omega)-\delta_1(\omega))}{D_2(\omega)}\right] \quad \text{(3.14-a)}$$

$$G''_{12}(\omega) = \frac{k_{OT}}{4\pi R}\left[\frac{A\sin\delta_2(\omega)}{D_2(\omega)} + \frac{D_1^{\,2}(\omega)\sin(\delta_2(\omega)-2\delta_1(\omega))}{AD_2(\omega)} - \frac{2D_1(\omega)\sin(\delta_2(\omega)-\delta_1(\omega))}{D_2(\omega)}\right] \quad \text{(3.14-b)}$$

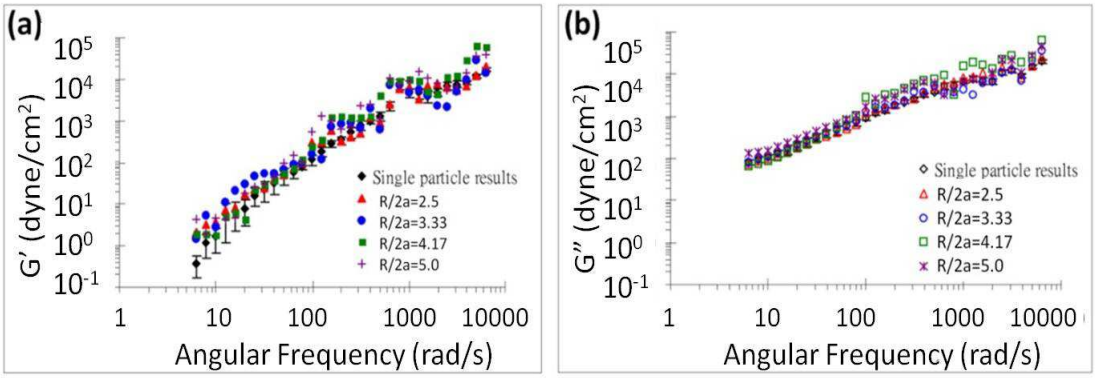

Figure 3.10 A comparison between (a) the local storage modulus and the non-local storage modulus; (b) the local loss modulus and the non-local storage modulus, at several particle distances for a 20 wt% solution of PEO. In the legends, "*R*" is the distance between the two probe particles and "*a*" is the particle radius.

As noted earlier, the PEO solution is homogeneous on length scales comparable to the size (1.5 μm diameter) of the probe particle, meaning that the local mechanical properties of the medium surrounding the probe particle are comparable to the bulk mechanical properties. Figure 3.10 shows the non-local storage modulus and loss modulus at several length scales (i.e., the distance between two particles). The non-local mechanical properties probed by the two-particle microrheological approach agree reasonably well with the results obtained by single particle microrheology.

In conclusion, since the two-particle microrheology technique allows the distance between two particles to be varied systematically, the non-local micro-mechanical properties of the medium

between two probe particles can be compared to the local micro-mechanical properties surrounding a probe particle. Using these methods, we can measure the mechanical properties both of polymer solutions and of colloidal-crystal solutions. For systems in mechanical equilibrium, an agreement is achieved in the measurement of the imaginary part of the response function $\alpha''(\omega)$ by active (single- and two- particle) and passive approaches. Study of microrheology in non-equilibrium systems will be discussed in *Chapter 4*. This technique will present useful information regarding microscopic inhomogeneous structures in soft materials to be acquired in the future.

4. Microrheology of Living Cells

The ability to measure mechanical properties at the sub-cellular level is important for the study of mechanotransduction [186]. In this chapter, we describe the method of oscillatory optical tweezers-based active microrheology. We have introduced the different microrheology approaches in *Section* 1.4. Here, we show comparative studies of extracellular/ intracellular and active/ passive microrheology in *Sections* 4.1 and 4.2, respectively. In *Section* 4.3, we combine active and passive microrheology to study microrheology in living cells in non-equilibrium states and with non-linear mechanical responses.

4.1 Comparative Study of Extracellular and Intracellular Microrheology

The mechanical properties of living cells, characterized by the frequency dependence of the storage and loss moduli (*G'* and *G"*), were reported by Fabry *et al.*, [187] who used magnetic tweezers to manipulate ferromagnetic particles attached to the cell membrane. The frequency dependence of the storage modulus (*G'*) was found to follow a weak power-law behavior and was characterized as a soft glassy material. In addition, Hoffman *et al.* [16, 17, 188] utilized laser-tracking microrheology to demonstrate that the complex shear modulus (*G**) also follows a weak power-law dependence with frequency. The question is whether the cell mechanical properties measured by a probe located outside the cell faithfully reflect the intracellular mechanical properties. Due to a lack of consistency between various existing measurements of the mechanical properties of cells and the intrinsic inhomogeneity of the cell interior, it is difficult to compare results obtained by different experiments on different cells. To address such questions, we conduct experiments that measure cell mechanical properties using probes either located on the outer surface of the plasma membrane or embedded inside the cell, as shown in Figure 4.1 [109, 110].

Specifically, we measure the storage and loss components of the complex shear modulus, $G^*(\omega)=G'(\omega)+iG(\omega)''$, of alveolar epithelial cells using a oscillatory optical tweezers-based microrheometer [145, 146]. In this technique, $G^*(\omega)$ is obtained by trapping and oscillating a 1.5 μm silica particle that is linked to the cytoskeleton through attachment with integrin receptors in the plasma membrane. Results obtained by this technique are compared with results obtained by optical tweezers forced oscillation of a micron endogenous intracellular organelle.

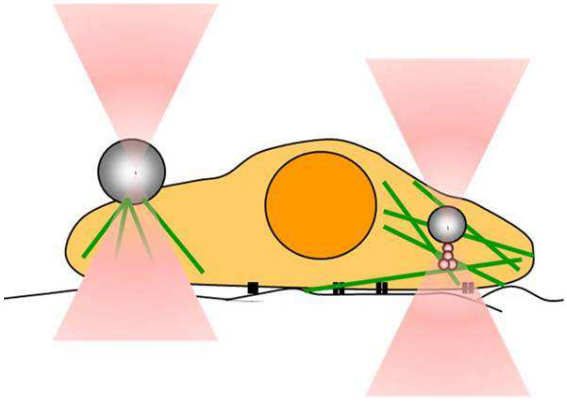

Figure. 4.1 Sketch of an oscillatory optical-tweezers-based microrheometer with an extracellular antibody-coated particle (left circle) or an intracellular granular structure (lamellar body, right circle).

For these studies, human lung epithelial type II cell (CCL-185 from American Type Culture Collection) is cultured in Ham's F12K cell culture and is grown under standard culture conditions (37°C, 5% CO2 and 95% air) as shown in Figure 4.2. Protein-A coated 1.5 μm silica particles (G. KISKER GbR, Germany) are treated with the anti-integrin α_V antibody (Sigma, Monoclonal Anti-integrin α_V antibody produced in mouse, I3783, CD51) by incubation at 50 μg per 1 mg of particles in 1x phosphate buffered saline (PBS) solution [189]. The particles are incubated overnight with cells seeded on a cover-slip. Unbound particles are washed away with phosphate buffered saline (PBS). This process allows the particles to adhere to the plasma membrane through integrin-antibody linkages, as is illustrated in Figure 4.2 (below), where the contact area

between the cell membrane and the particle is characterized by the particle radius "*a*" and the half-angle, "θ" .

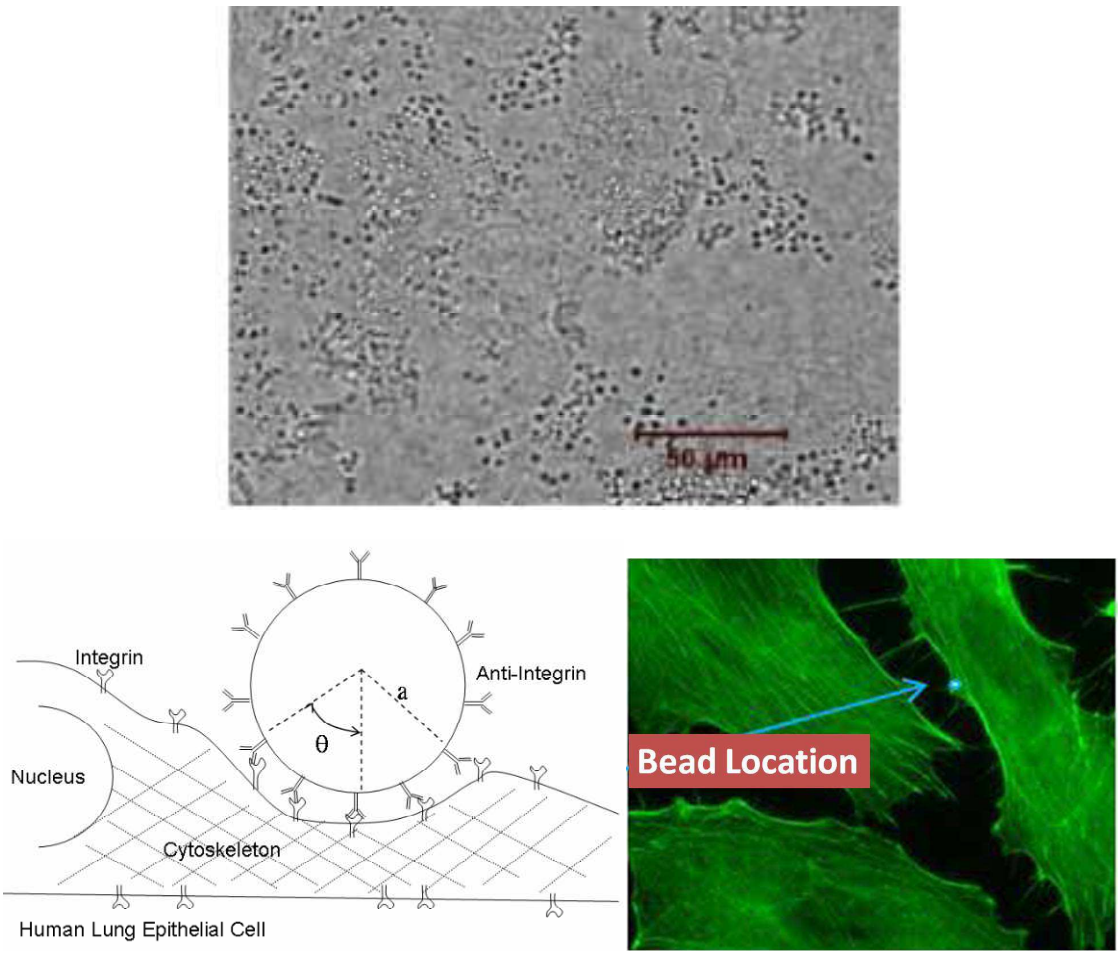

Figure 4.2 (Top) A bright-field image of lamellar bodies that exist abundantly in alveolar epithelial type II cells. (Below) A schematic diagram of integrin antibody coated particles attaching to the plasma membrane (particle size not to scale). Also shown is a fluorescent image of actin cytoskeleton (phalloidin) with bead location outlined in blue.

To apply an extracellular probe, we trap an anti-integrin α_V-conjugated silica particle (diameter = 1.5 μm) externally attached to the plasma membrane of the lung epithelial cell and oscillated by the trapping beam with an amplitude of 100 nm. We determine the viscoelasticity of the cell from

the amplitude (D) and the phase shift (δ) of the oscillating particle by modifying the approach developed for a particle embedded in a homogeneous and isotropic medium (see Equation 4.1) with an approach reported by Laurent *et al.* [190], which accounts for a system in which the particle under a static force is located at the interface of an aqueous medium and a viscoelastic medium. In this case, the storage modulus $G'(\omega)$ and the loss modulus $G''(\omega)$ of the viscoelastic medium are given by:

$$G'(\omega) = \frac{k_{OT}}{4\pi a}\left(\frac{3}{2\sin\theta} + \frac{\cos\theta}{\sin^3\theta}\right)\left(\frac{A\cos\delta(\omega)}{D(\omega)} - 1\right) \tag{4.1-a}$$

$$G''(\omega) = \frac{3k_{OT}}{16\pi a \sin\theta}\left(\frac{A\sin\delta(\omega)}{D(\omega)}\right) \tag{4.1-b}$$

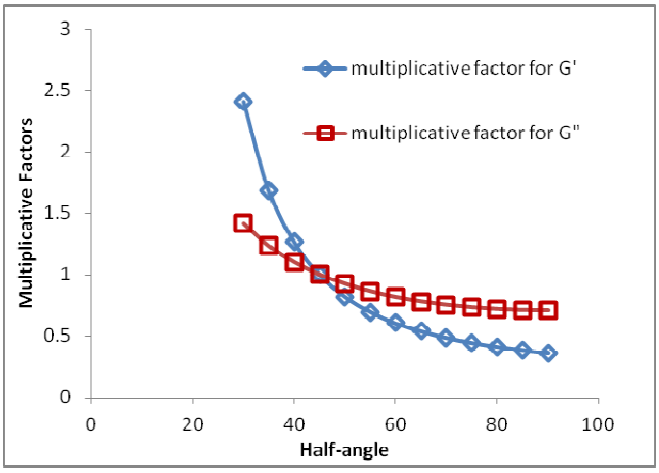

Figure 4.3 A constant multiplicative factor to the values of G' and G'' using different values of half-angle in the range of 30 - 90 degrees.

Due to the lack of an accurate measurement for the subtending half-angle θ, we assume $\theta = \pi/4$ in all of our calculations. Note that the choice of θ only influences the magnitude of G' and G'' and does not influence power-law fits (as shown in Figure 4.4). Estimates of G' and G'' using different values of θ yield a constant multiplicative factor to their values. For θ in the range of 30 -

90 degrees, the multiplicative factors are 2.4 – 0.36 for *G′* and 1.4 - 0.71 for *G″*, respectively, as shown in Figure 4.3.

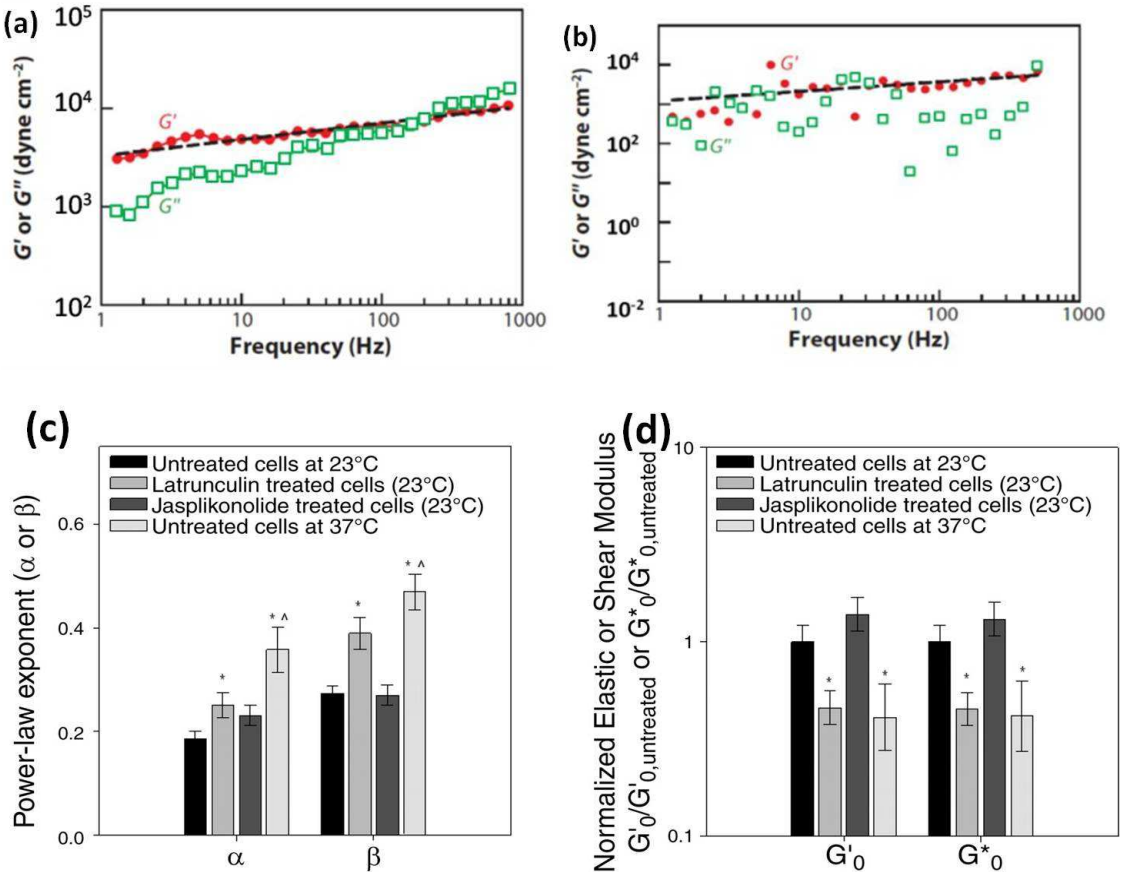

Figure 4.4 The storage modulus *G′* (solid symbols) and the loss modulus *G″* (open symbols) of cells, as a function of frequency, probed with (a) an anti-integrin conjugated silica particle attached to the plasma membrane, (b) an intracellular organelle. In both (a) and (b), the dashed line represents a power-law fit to *G′*. (c) The effect of latrunculin treatment, jasplakinolide treatment, and 37°C temperature on average power-law exponents. (d) Effect of latrunculin treatment, jasplakinolide treatment, and 37°C temperature on normalized elastic and shear moduli. Data are means ± SE. *Significant difference compared with untreated cells at 23°C ($P < 0.05$). ^Significant difference compared with latrunculin-treated cells ($P < 0.05$).

Because the multiplicative factor is significantly larger when θ is smaller than 30 degrees, we avoid trapping any particles that are loosely bound to the cell surface, namely, particles that visibly move synchronously with the oscillatory trap at low oscillatory frequencies. The experimental measurements of cellular mechanical properties show for epithelial cells treated with Latrunculin A (which depolymerizes actin) are softer than cells treated with Jasplakinolide (which stabilizes actin filaments) [110], as shown in Figure 4.4 (c) and (d). The results show that the oscillatory optical-tweezer technique provides a promising approach for probing the mechanical behavior of living cells.

For intracellular probing, we use optical tweezers to trap and oscillate an internal granule (probably a lamellar body which exists abundantly in alveolar epithelial type II cells). Figure 4.2 shows a bright-field image of these lamellar bodies. To further characterize these lamellar bodies, we calculate that the intracellular granules used in this study (i.e. lamellar bodies) are spherical, have a uniform spatial distribution, and are ~2 μm in diameter.

Intracellular *G′* and *G″* are determined from the experimentally measured particle displacement magnitude (*D*) and phase shift (δ) using Equation 4.2.

$$G'(\omega) = \frac{k_{OT}}{6\pi a}\left(\frac{A\cos\delta(\omega)}{D(\omega)} - 1\right) \tag{4.2-a}$$

$$G''(\omega) = \frac{k_{OT}}{6\pi a}\left(\frac{A\sin\delta(\omega)}{D(\omega)}\right) \tag{4.2-b}$$

where k_{OT} is the spring constant of optical tweezers, "*a*" is the radius of the particle, "*A*" is the amplitude of oscillatory optical tweezers. However, these organelles have different optical properties from those of the artificial particles (silica or polystyrene), so the k_{OT} used for calculating *G** must be different due to the refractive- index-dependent gradient optical force. We re-scale k_{OT} by taking the ratio of the estimated optical contrast of the organelles (composed of 80%

proteins/lipids (n~1.5) and 20% water (n=1.33)) in cytoplasmic fluids (80% water and 20% proteins) to the optical contrast of a silica particle (n=1.45) in water. The re-scaling reduced k_{OT} to approximately 61% of the value for a 1.5 μm silica particle in water. We do not consider scaling of k_{OT} due to the particle size difference between the lamellar bodies and the silica particle because the gradient force is a weak function of particle size for particles larger than the trapping wavelength as shown in Figure 2.8.

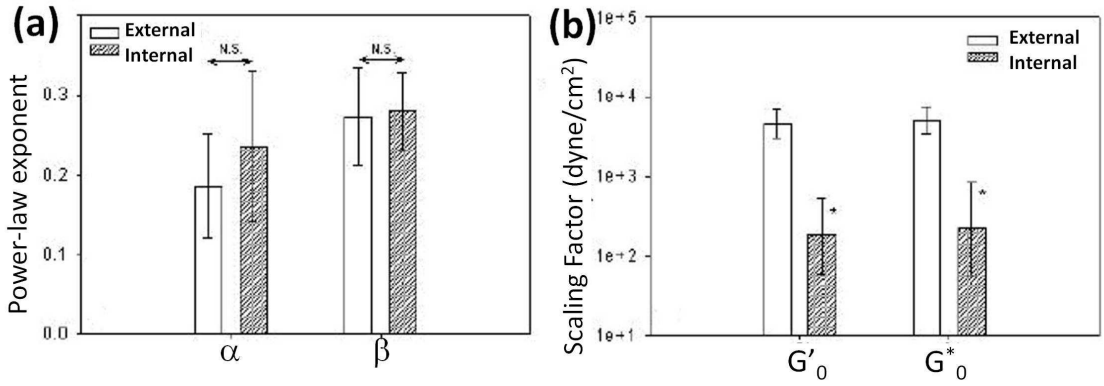

Figure 4.5 (a) Power-law exponents of *G'* and *G** for extracellular and intracellular data. Error bars represent standard deviations and the means are not statistically different. (b) Magnitudes of pre-factor G'_0 and G^*_0 for extracellular and intracellular data.

To compare external and internal measurements, we plot the mean values of the power-law exponents ($G'=G'_0(\omega/\omega_0)^{\alpha}$ and $|G^*|=G^*_0(\omega/\omega_0)^{\beta}$.) and the scaling pre-factors (G'_0 and G^*_0) in Figure 4.5 (a) and (b). These tests indicate that the mean values of both G'_0 and G^*_0 measured by trapping intrinsic intracellular granules are significantly lower than those measured by trapping a particle externally attached to the cytoskeleton. Although both external and internal measurements yield comparable power-law relationships, the internal storage and shear moduli are lower than the moduli measured using externally bound particles. Note that uncertainties in θ cannot count for such large differences between the intra- and extracellular measurements. The larger moduli measured with the external particles could be influenced by extensional stiffness or other

mechanical properties of the plasma membrane. To investigate the role of membrane mechanics, future measurements should utilize acLDL-coated particles, which bind to low-density lipoprotein receptors (since these receptors are not linked to the cytoskeleton) [191]. Although using an intracellular organelle as a probe provides a direct measurement of intracellular local mechanical properties, determination of the optical force constant, k_{OT}, of the optical tweezers requires knowledge of the indices of refraction of the probe and the surrounding material, which leads to uncertainty in the measured mechanical properties.

In conclusion, we use oscillatory optical tweezers to determine the intracellular viscoelasticity of human lung epithelial cells by forced oscillation of an anti-integrin α_V-conjugated silica particle externally attached to the plasma membrane and of an endogenous intracellular granule. The two methods give comparable results. We have demonstrated that the optical-force oscillation of external probes attached to the cytoskeleton can provide reliable measurements of “whole-cell mechanics”. However, in comparison, the intracellular oscillation of endogenous organelles is more useful in investigating intracellular heterogeneity and temporal fluctuations. We will focus on the intracellular measurements in the following sections.

4.2 Comparative Study of Active and Passive Cellular Microrheology

In the previous section, we discussed measurements of cell mechanical properties using probes located exterior to the plasma membrane and using probes embedded inside the cell. The intracellular measurement can be useful in studying intracellular temporal fluctuations for investigating the non-equilibrium state inside living cells. It is well known that cells generate and react to forces through a non-equilibrium network of cytoskeleton and motor proteins [192, 193]. The mechanical properties of active cytoskeletal-network systems may be dependent on intracellular tension created by active motors [59, 115, 194-200]. Motor activity is an example of how non-equilibrium systems [201] may be created in living cells [113, 202]. Non-equilibrium mechanical behavior has been observed with an *in vitro* model system consisting of an actin network with embedded myosin motors [114], and has also been observed in living cells [112, 113].

In this section, by using a combination of active and passive microrheological approaches, we test the response functions obtained by active and passive microrheology by use of the fluctuation-dissipation theorem. Cell microrheology is examined using both active [109, 119, 187] and passive [16, 17, 185] approaches. By use of the fluctuation-dissipation theorem (FDT) to compare the results of active and passive microrheology, intracellular mechanical properties and non-thermal fluctuating forces can be measured in non-equilibrium systems [115]. For the active microrheology (AMR) measurements, optical tweezers are used to trap and oscillate an engulfed particle (1 μm polystyrene particle) inside a living HeLa cell. When a force (F) acts on the particle, the deformation of the surrounding medium can be used to yield the linear response of the particle via $u=\alpha^* F$, where u is the position of the particle and α^* is the complex response function. For a simple incompressible and homogeneous elastic medium, the response function is related to the shear modulus G^* of the medium via $\alpha^* = 1 / (6\pi G^* a)$, where "a" is the radius of the probe particle. The mechanical properties can be characterized by the complex viscoelastic modulus $G^*=G'+iG''$.

We directly determine *G′* and *G″* from the experimentally measured particle displacement magnitude and phase [109].

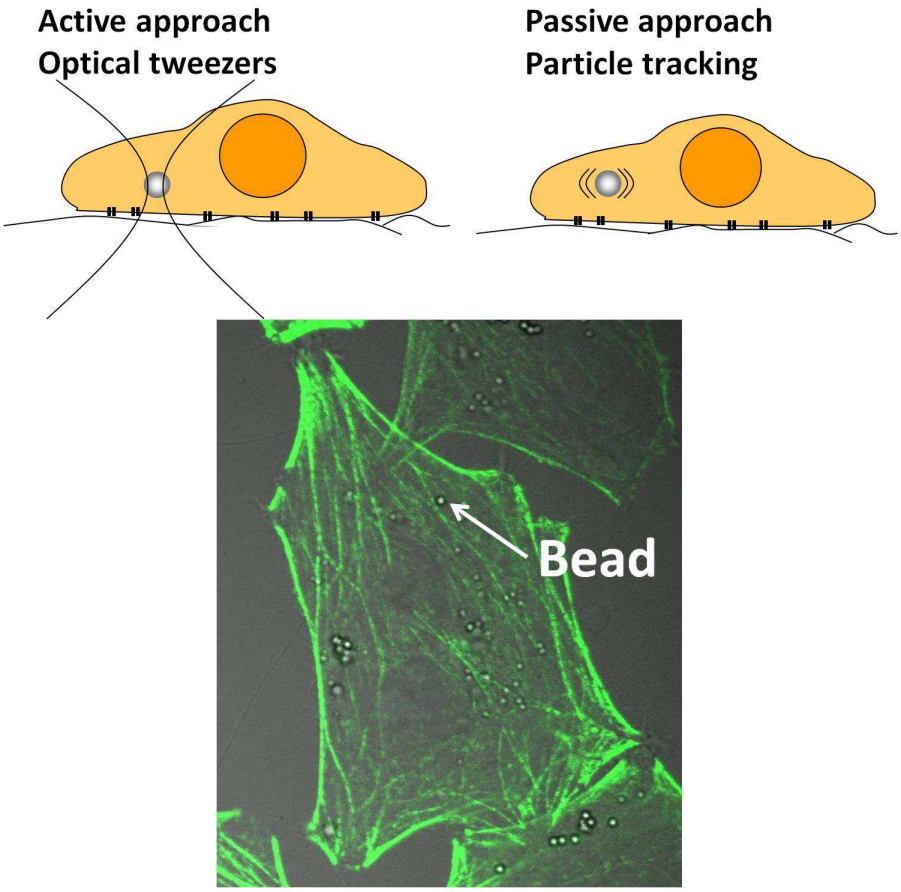

Figure 4.6 Sketch of the two cellular microrheology techniques. The left figure shows the active approach based on oscillatory optical tweezers, in which an intracellular particle is trapped. The right figure shows the passive approach where a CCD camera is used to track fluctuations in the particle position.

Using passive microrheology (PMR) measurements, the fluctuations of a 1 μm polystyrene particle entrapped in HeLa cells were recorded by a fast CCD camera. Fluctuations of the particle position can be observed by particle tracking analysis with 10 nm resolution. In a typical run, the particle is followed for 300 seconds with signal acquisition at 500 frames/second. Since a living

cell might be a non-equilibrium mechanical system [112, 113], the fluctuations of a probed particle measured by PMR would include both thermal fluctuations as well as non-thermal fluctuations due to dynamic non-thermal forces.

To distinguish thermal from non-thermal fluctuations of an engulfed micro-particle in a living cell, we compare the particle's fluctuations obtained by active and passive microrheology. The thermal fluctuation spectrum ($C_{thermal}$) of a probe particle is found using AMR measurement of the imaginary part of the response function (α'') [109]. In an equilibrium system, only thermal forces act on the probe, and the power spectral density of the displacement fluctuations is directly related to the mechanical response of the material by the fluctuation-dissipation theorem:

$$C_{thermal}(\omega) = \frac{2k_B T}{\omega}\alpha''(\omega) \tag{4.3}$$

where $C_{thermal}(\omega)$ is the power spectral density in an equilibrium system, α'' is the imaginary part of the response function (α^*), k_B is the Boltzmann constant, and T is the absolute temperature.

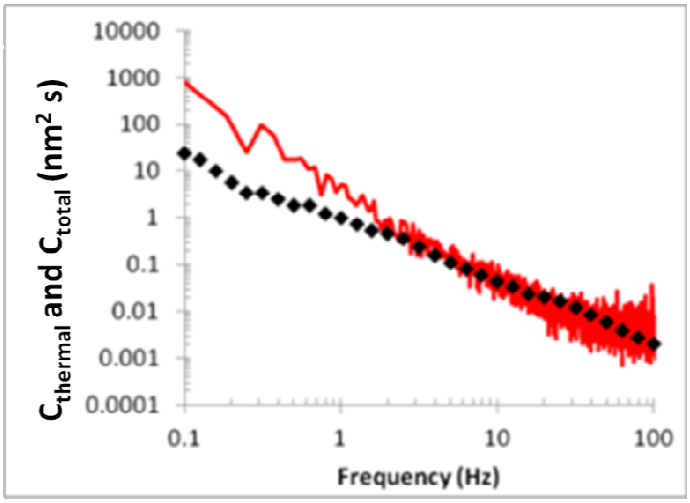

Figure 4.7 Estimated value of the thermal fluctuations ($C_{thermal}$) by active microrheology (black dots) and the power spectrum (C_{total}) measured by passive microrheology (red lines) .

The thermal fluctuations ($C_{thermal}$) determined by active microrheology (diamonds) and the total fluctuation power spectrum (C_{total}) measured by passive microrheology (red lines) are shown in Figure 4.7. At lower frequencies, the fluctuations measured by PMR (C_{total}) have a larger magnitude than the fluctuations estimated by AMR ($C_{thermal}$). This result implies that molecular motors might induce additional low-frequency non-thermal fluctuations of a probed particle. We will further discuss the molecular motors' functions in *Section* 4.3.

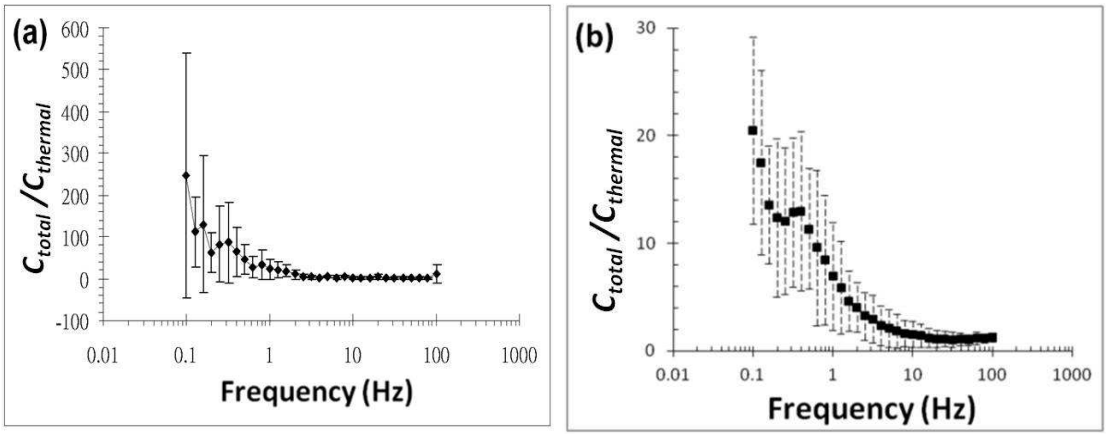

Figure 4.8 Experimental results of ratio between the total fluctuations (C_{total}) measured by passive microrheology and thermal fluctuations ($C_{thermal}$) estimated by active microrheology as a function of frequency by probing with (a) an endosome in human lung epithelial type II cells, and (b) an engulfed micro-particle in HeLa cells.

The ratio between the power spectrum of total fluctuations (C_{total}) measured by passive microrheology and thermal fluctuations ($C_{thermal}$) estimated by active microrheology is shown in Figure 4.8. The measurements using an endosome [203] and an engulfed micron-sized polystyrene particle as a probe [204] are shown in Figure 4.8 (a) and (b), respectively. This ratio was defined in previous studies as the ratio of the "*effective temperature*" (T_{eff}, = $C_{total}/C_{thermal}$ = $C_{total}\omega/2k_BT\alpha''$) of the system to the bath temperature [112, 113]. At frequencies lower than 10 Hz, the ratio obtained via an engulfed micro-particle is much lower than the corresponding values obtained via an endosome [29], presumably due to the different non-thermal fluctuations induced

by different molecular motors (i.e., actin motors vs. microtubule motors). At frequencies higher than 10 Hz, the results from AMR and PMR measurements are comparable. Such results indicate that the frequency limit of the non-equilibrium dynamics is caused by molecular motors.

To determine the intracellular non-thermal fluctuating forces, we combine active and passive microrheology to determine the non-thermal fluctuations. We determine the thermal fluctuation spectrum ($C_{thermal}$) of a probe particle using AMR measurement of the imaginary part of the response function (α'') [109]. Using the fluctuation-dissipation theorem (Equation 4.3), the estimated fluctuations can be determined ($2k_BT\alpha''/\omega$). The non-thermal force spectrum ($\langle f^2 \rangle$) [115] can be defined as the difference between the total fluctuation spectrum (C_{total}) measured by PMR and the thermal spectrum ($2k_BT\alpha''/\omega$) estimated by AMR.

$$\left\langle f^2 \right\rangle \alpha^{*2} = C_{total} - C_{thermal} = C_{total} - \frac{2k_BT\alpha''}{\omega} \tag{4.4}$$

Table 4.1 A comparison of the measurements of cellular "effective temperature" ($T_{eff} = C_{total}\omega / 2k_BT\alpha''$) and cellular non-thermal forces ($\langle f^2 \rangle$).

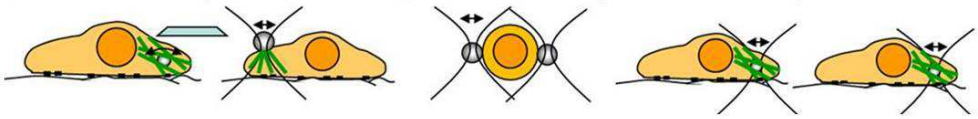

At 1Hz	Intracellular magnetic bead	Extracellular silica bead	Extracellular two beads	Intracellular organelle	Intercellular polystyrene bead
T_{eff}	100	15	2	23	7
$\langle f^2 \rangle$	7.3pN^2	10pN^2	0.1pN^2	100pN^2	3.1pN^2
Ref.	Wilhelm 2008	Gallet et al. 2009	Mizuno et al. 2009	Wei et al. 2010	Wei et al. 2014

The cellular non-thermal forces using either a probed particle attached to a cellular cortex [112, 183] or a probed particle bound inside a cell [113] can be studied by both local and non-local microrheology [113]. Comparing with previous reports [112, 113, 183] as shown in Table 4.1, the

measurements using an engulfed particle (1 μm-diameter polystyrene) as a probe show that the intracellular force is smaller than the tension on the cellular cortex. This result indicates that intracellular motors might be weaker or less active than motors on the cellular cortex. In the previous study by Wilhelm [113], the cellular non-thermal forces were found to be dependent on the probe size. They used active magnetic-particle rotational microrheology to measure intracellular non-thermal forces of 0.4, 2.7, and 5.7 pN for 0.3, 1, and 2.8 μm particles, respectively. They suggested that the smaller particles have fewer interactions with the networks, whereas bigger particles are more likely to encounter cytoskeleton filaments and undergo active transport. Using the non-local, two-particle microrheology technique, which was introduced in our *Section 3.3,* might provide more information about the inhomogeneous intracellular mechanical properties reported by Mizuno *et al* [183] as shown in Table 4.1. However, the experimental approach is limited to measure a suspended biological cells. We will use a single-particle active microrheology technique in the following sections.

In conclusion, to study non-equilibrium microrheology in living cells, we use the endogenous lamellar bodies and engulfed 1 μm polystyrene particles within the cell as probes to measure the intracellular compliance of living cells. Using the fluctuation-dissipation theorem, we compare the measurements by passive and active microrheology. The differences obtained from the results of those measurements can be parameterized by an "*effective temperature*" over the frequency range 0.1 – 100 Hz. The differences between active and passive approaches observed by using endogenous lamellar bodies are larger than those observed using an artificial particle as a probe. This difference can be caused by either different molecular motors generating different non-thermal forces or uncertainties in calibration of the oscillatory optical force due to the unknown lamellar bodies' refractive index, which was discussed in *Section* 4.1. In order to avoid the uncertainties associated with using a lamellar body as a probe, we will use engulfed 1 μm polystyrene particles to study the intracellular mechanics in response to substrate rigidity in the next section.

4.3 Nonlinear Intracellular Elastic Response to Intracellular Stress Depends on Substrate Rigidity

Living cells with mechanical integrity maintained by molecular motors in a cytoskeleton network are intrinsically non-equilibrium and mechanically non-linear, forming a coupled dynamic mechanical system. The dynamic mechanical interactions affect cellular functions such as cell spreading and stiffness [23, 205, 206] and stem-cell differentiation [33, 207]. It has been suggested that these cellular responses might be regulated by cellular traction stress arising from molecular motors [24, 33, 34]. This internally generated contractile stress might help cells sense and adapt to the stiffness of their environments. However, characterization of intracellular stress and elasticity and their relation to substrate rigidity is still lacking. Here, we seek to understand how the interplay of various sources of noise in a non-equilibrium system relates to non-linear responses in living cells.

It is well known that a single polymer shows a nonlinear response to increasing force with a power-law stiffening of the elastic modulus [208]. Stress-dependent stiffness is also present in active bio-polymer networks, as reported by Koenderink *et al.* [192] and Mizuno *et al.* [114], who showed that the mechanical stiffness of an *in-vitro* synthesized cytoskeletal network is altered by the activity of myosin motors. From the average tension in a network of strands due to motor activity, the tension in a single filament can be calculated as a function of its longitudinal extension by use of the worm-like chain model [198, 209]. In the nonlinear elasticity regime, the elastic modulus shows a 1.5 power-law dependence of the differential elastic modulus on tension. A simulation shows that motor-generated forces on the order of 1–10 pN can cause a nearly 100-fold increase in stiffening of the *in-vitro* synthesized cytoskeletal network. The observed changes in mechanical stiffness were interpreted to result from molecular motor-generated dynamic stresses in the network. Nonlinear behavior was also found in the elastic response of biological cells to external stress [59, 200]. It has been speculated whether similar behavior can

occur in the mechanical response of cells to internal motor-generated dynamic stress [23]. However the mechanism by which myosin-generated stress could control intracellular elasticity remains unclear [28, 112, 113, 183, 200].

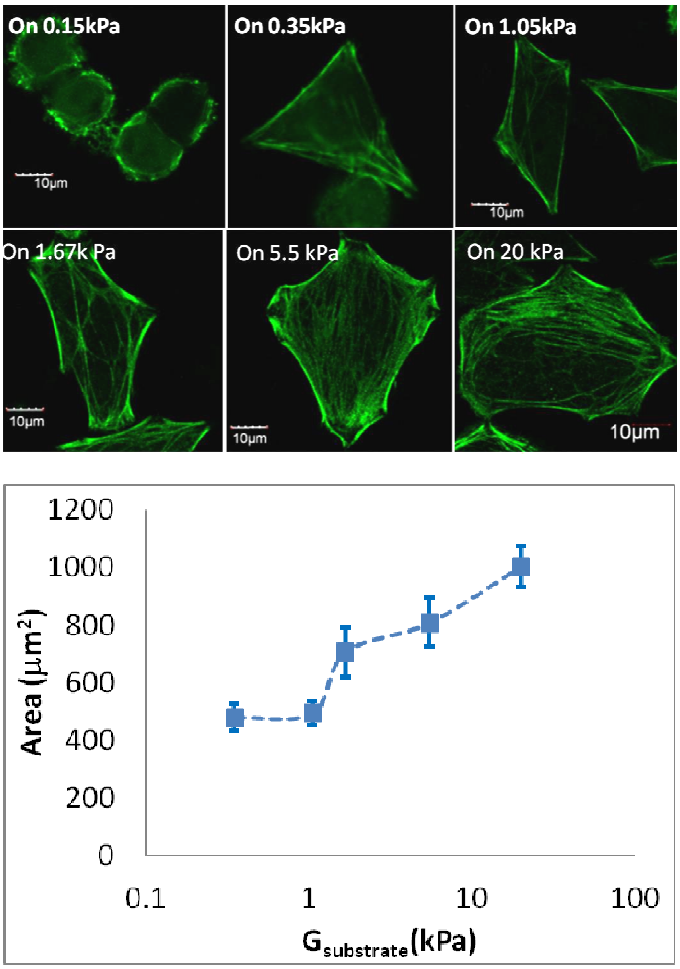

Figure 4.9 Morphology study of HeLa cells on substrates with different stiffness. The means and standard errors are obtained by 10 individual cells for each condition.

We investigate intracellular mechanical properties by two independent methods [114, 192]: (1) an active microrheology method using an internalized micro particle to probe the viscoelasticity of the cell interior, and (2) a passive method based on statistical analysis of fluctuations of the motions of the same particle, as described in the previous section. To observe the myosin

dynamics, we use an engulfed micro-particle as a probe to measure both fluctuating forces and local cellular stiffness in living HeLa cells which have been treated to express myosin-regulatory-light-chains tagged with green fluorescent protein (MRLC-GFP).

HeLa cells expressing MRLC-GFP [78] are grown under standard culture conditions (37°C, 5% CO_2, in a humidified environment). Cells ($6x10^4$ cells/cover-slip) were seeded onto 22 x 22 mm cover-slips coated with collagen I (0.2 mg/ml)-coated polyacrylamide (PA) substrates having varying elastic moduli [80, 81]. The elastic moduli of the polymer substrate is measured by atomic force microscopy as shown in Figure 2.3. Morphology of HeLa cells on substrates with different stiffness is shown in Figure 4.9.

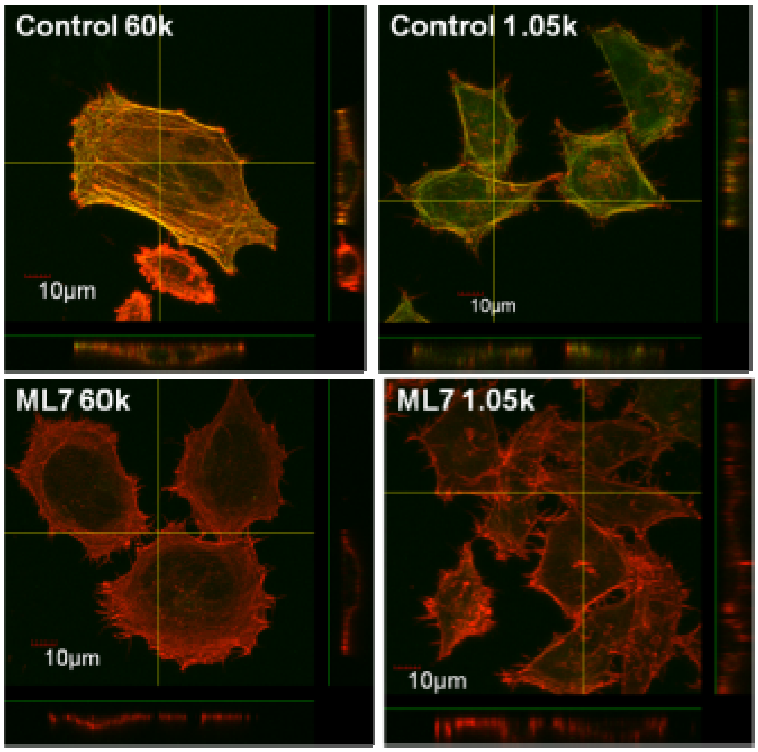

Figure 4.10 Actin filament organization (red) and distribution of myosin regulatory light chain (green) in control cells and in cells treated with 20 µM ML-7, which is a myosin light chain kinase inhibitor.

To explore the internal cell mechanics with respect to the activity of intracellular motors, we treated myosin-inhibitors for 1 hour using (1) ML-7 (20 μM; Sigma, I2764; 1-(5-Iodonaphthalene-1-sulfonyl) -1H -hexahydro- 1,4- diazepine hydrochloride), which is a potent and selective inhibitor of MRLC; (2) Y-27632 (10 μM; Sigma, Y0503; (R)-(+)-trans-4-(1-Aminoethyl)-N- (4-Pyridyl) cyclohexanecarboxamide dihydrochloride), which inhibits the Rho-associated protein kinase (ROCK) and thus inhibits ROCK-mediated myosin light chain phosphorylation; and (3) blebbistatin (20 μM; Sigma, B0560; 1-Phenyl-1,2,3,4-tetrahydro-4-hydroxypyrrolo[2.3-b]-7methylquinolin-4-one), which binds to the myosin ATPase and slows phosphate release.

Cell microrheology is examined using both active [109, 119, 187] and passive [16, 17, 185] approaches to measure intracellular mechanical properties and non-thermal fluctuating forces as described in *Section 4.2*. Figure 4.11 shows the intracellular mechanical properties (*G'* elastic modulus and *G"* viscosity modulus) when cells are cultured on substrates with different stiffness. It is observed that the cells attached to a stiff substrate are significantly more rigid than those attached to a soft substrate. These results are qualitatively consistent with the previous studies of extracellular measurements using atomic force microscopy [35]. In addition, in the frequency range 0.1 to 100 Hz, the mechanical properties of HeLa cells exhibit a relatively solid-like response (i.e., *G' > G"*), similar to measurements of *in-vitro* synthesized active cytoskeletal networks [192].

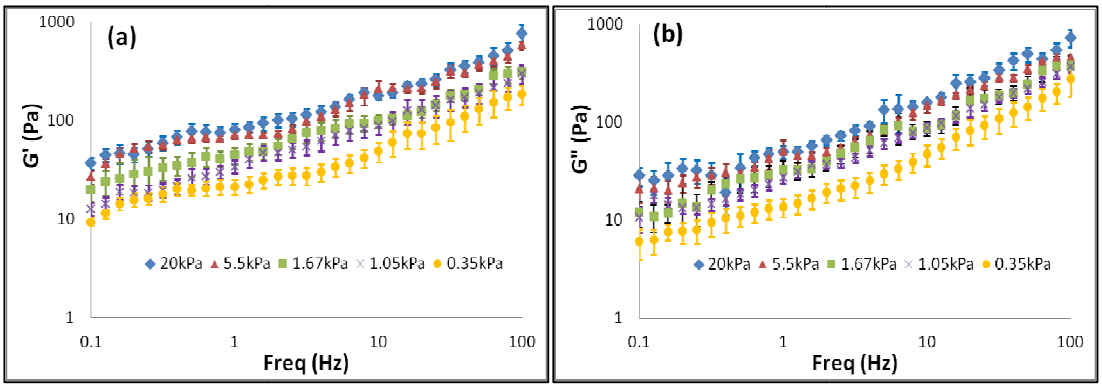

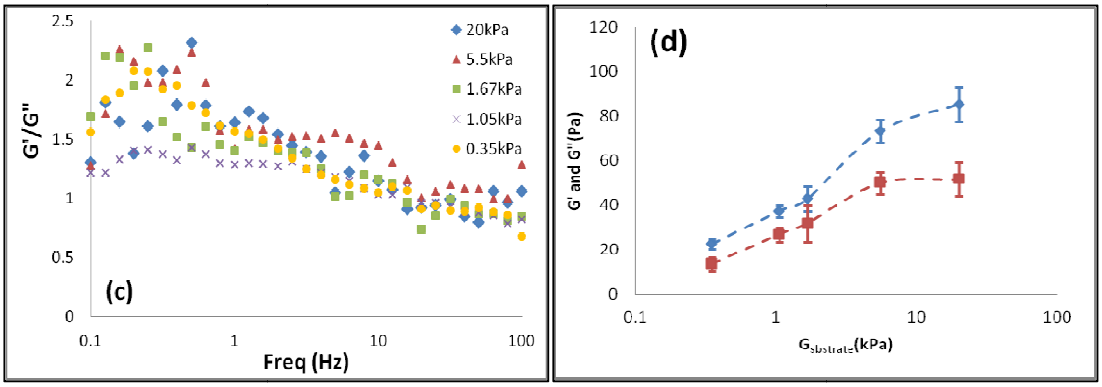

Figure 4.11 Experimental results of intracellular (a) elasticity modulus, *G'*; (b) viscosity modulus, *G"*; and (c) solid-like response behavior, *G'/G"* as a function of frequency. (d) Experimental results of intracellular mechanical properties at 1 Hz. $G_{substrate}$ is the elastic modulus of the substrate. Each data point is the average of 10 measurements for each substrate stiffness. Bars are standard errors of the mean.

To study intracellular dynamic stress, we combine active and passive microrheology to determine non-thermal fluctuations. Figure 4.12 shows the ratio between the power spectrum of total fluctuations (C_{total}) measured by passive microrheology and thermal fluctuations ($C_{thermal}$) estimated by active microrheology. The discrepancy between the PMR and AMR spectra at low frequencies suggests that a stress condition occurs on time scales longer than about 0.1 second. This stress possibly results from the interaction of myosin motor domains with actin filaments. The time scale is consistent with microrheological measurements in F-actin-myosin *in-vitro* solutions [114, 192, 210]. These cells are cultured on surfaces of variable stiffness to modify the local myosin concentration. At lower frequencies, the measurement by PMR (C_{total}) shows a bigger magnitude than the measurement by AMR ($C_{thermal}$) for cells cultured on the stiffer substrate, as shown in Figure 4.12 (control). Those cells have a more of myosin motors than cells cultured on the softer substrate, as shown in Figure 4.9.

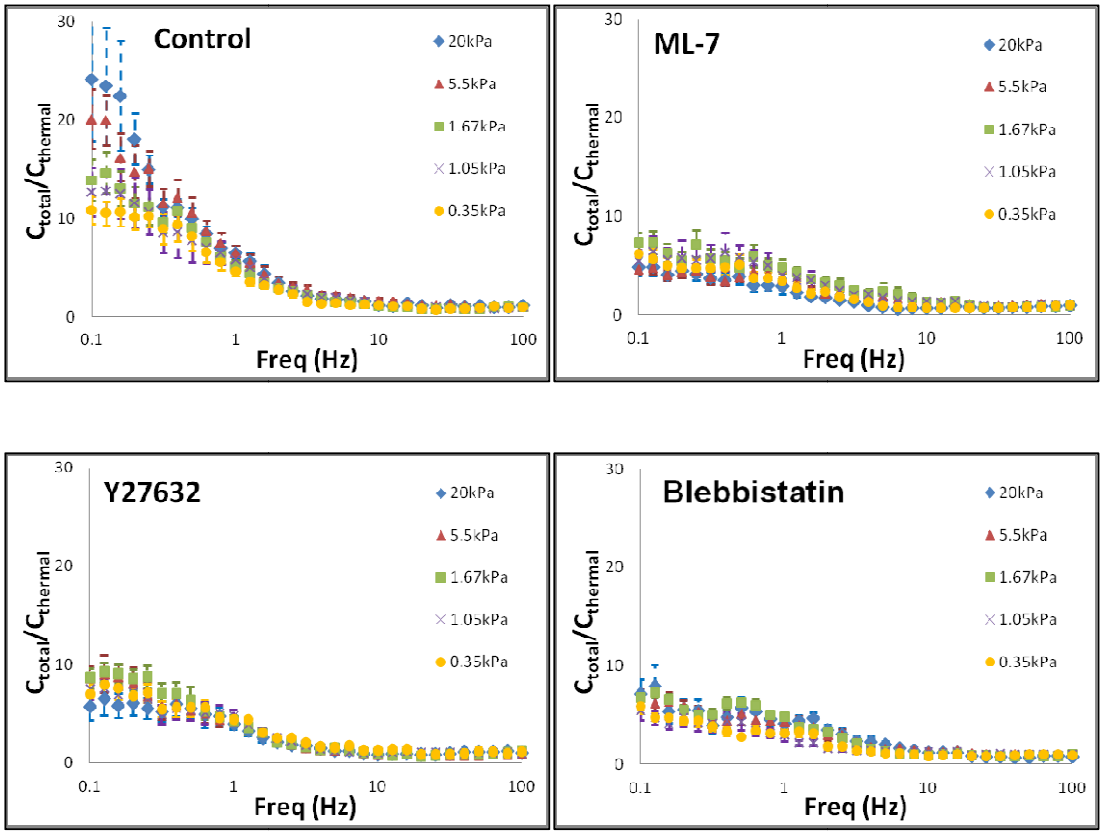

Figure 4.12 Experimental results of $C_{total}/C_{thermal}$ as a function of frequency. Each data point is the average of 10 measurements for each substrate stiffness. Bars are standard errors of the mean.

In additional experiments, we inhibit myosin activity in HeLa cells. To compare control cells with cells treated with myosin inhibitors (ML-7, Y27632, and Blebbistatin), the ratio C_{total} to $C_{thermal}$, "*effective temperature*," is much higher. This result implies myosin motors might create additional non-thermal fluctuations of a probed particle. However, for myosin-inhibited cells, $C_{total}/C_{thermal}$ is reduced but does not reach the equilibrium value ($C_{total}/C_{thermal}$ ~1) at the lower frequencies. It could be that other active processes (such as microtubule dynamics or microtubule motors) may induce intracellular non-thermal forces. Compared with the previous study of non-thermal fluctuations induced by microtubule motor proteins using endosomes as probes [29], our results show that myosin plays a major role in causing living cells to become non-equilibrium systems.

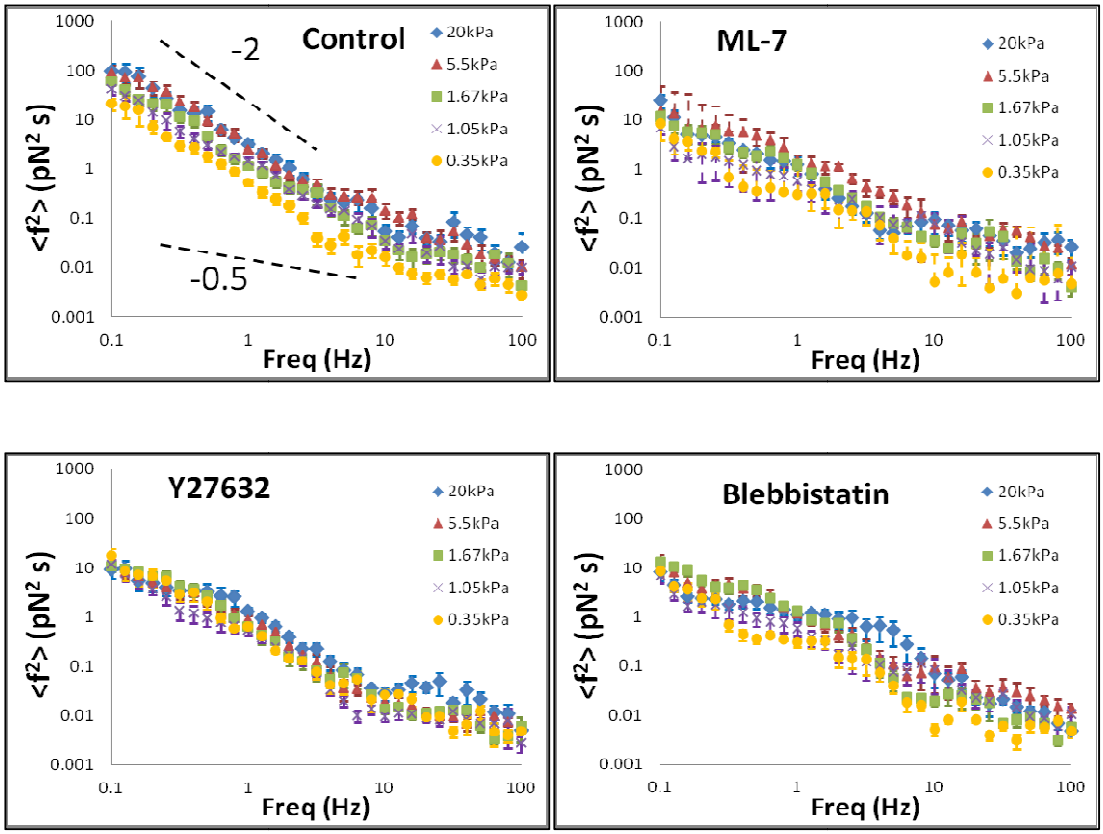

Figure 4.13 Intracellular force spectra (<f^2>) calculated by comparing AMR and PMR. Each data point is the average of 10 measurements for each substrate stiffness. Bars are standard errors of the mean.

The power spectra of the intracellular active dynamic force spectrum (<f^2>) are shown in Figure 4.13. These data are qualitatively consistent with previous measurements of a probed particle attached to a cellular cortex [112, 183] and of a probed particle bound inside a cell [113]. The results imply that molecular motor-generated dynamic forces do not interfere with high-frequency thermal motions either on a cellular cortex or in a cytoskeletal network. Our measurements show that stronger intracellular fluctuating forces are generated in cells cultured on stiffer substrates. The active intracellular forces are shown to follow a power law as a function of frequency with exponent about -1.75 at the lower (0.1~10 Hz) frequencies and about -0.5 at the higher frequencies (10~100Hz) as shown in Figure 4.13 (control). The power-law behavior implies

that the microscopic processes responsible for active stress have a broad distribution of activation rates. Mechanical probing performed with different techniques on different types of eukaryotic cells has shown in most cases a broad spectrum of relaxation times. Compared with previous reports showing $\langle f^2 \rangle \sim \omega^{-2}$, our low-frequency exponent of -1.75 indicates that intracellular motors [113] might be less abundant or less active than motors on the cellular cortex [112, 183], implying that intracellular tension is also smaller than tension on the cellular cortex.

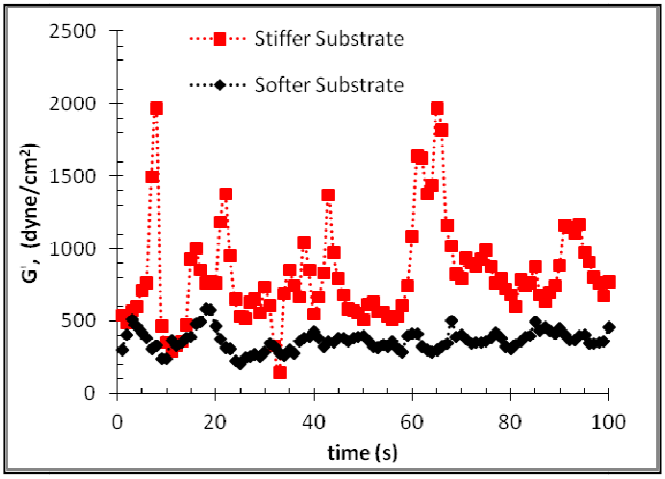

Figure 4.14 Fluctuation of intracellular elastic modulus at 1 Hz as a function of time for living cells, with cells cultured on polyacrylamide (PA) substrates with elastic moduli of 20 kPa (stiffer substrate) and 0.35 kPa (softer substrate).

To further study the relation between intracellular elasticity (G') and intracellular stress (σ), we quantified the ratio of the fluctuations of active stress ($\Delta\sigma$) to the fluctuations of elastic modulus ($\Delta G'$). We define the fluctuations of stress ($\Delta\sigma$) from the intracellular fluctuating force spectrum ($\Delta\sigma = \langle f^2 \rangle^{0.5} / \pi a^2$, where "$a$" is the radius of a probed particle) [113-115] at 1 Hz, and we define the fluctuation of the elastic modulus ($\Delta G'$) as the root-mean-square deviation of G' at 1 Hz averaged over 300 seconds. The results show increasing fluctuations of intracellular-stiffness and intracellular fluctuating stress in response to substrate rigidity as shown in Figures 4.15 and 4.16.

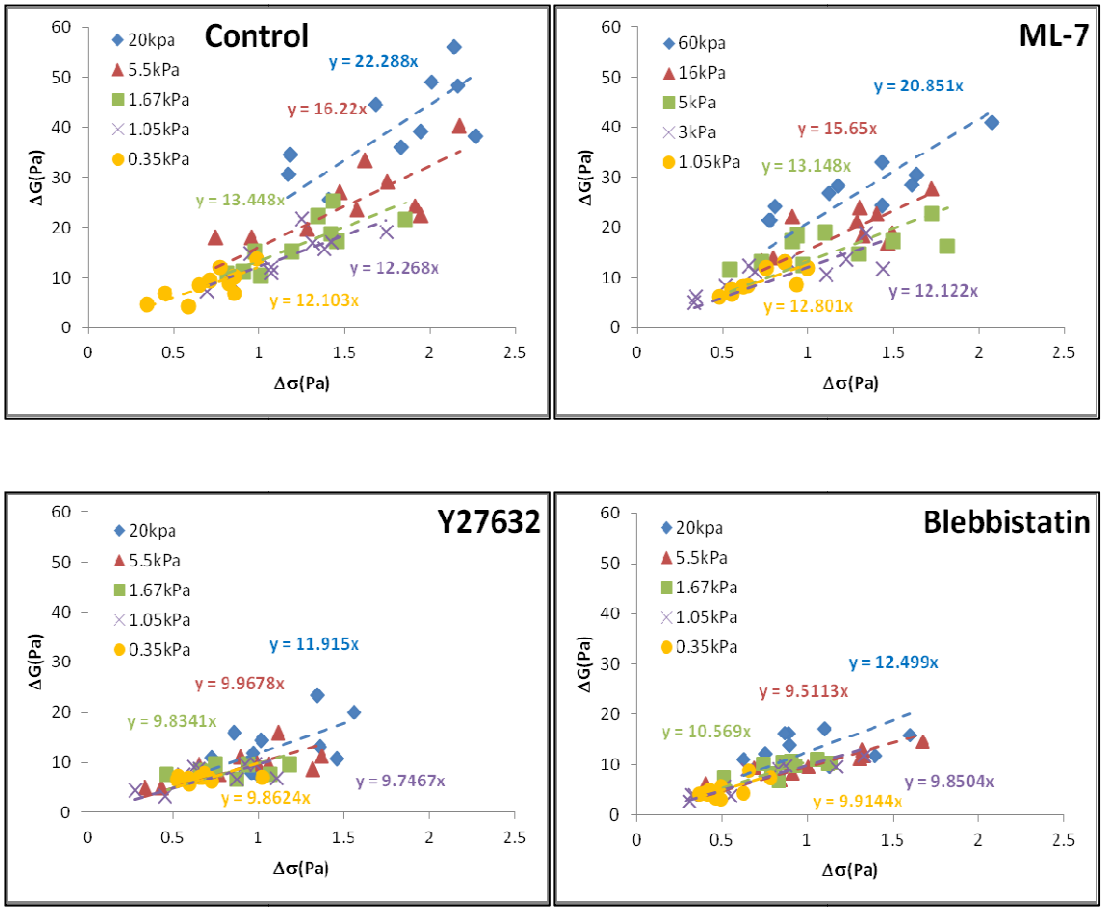

Figure 4.15 For HeLa cells on substrates with different stiffness, under different conditions, experimental magnitudes of fluctuations in the elastic modulus increase with the magnitude of fluctuations in the intracellular stress.

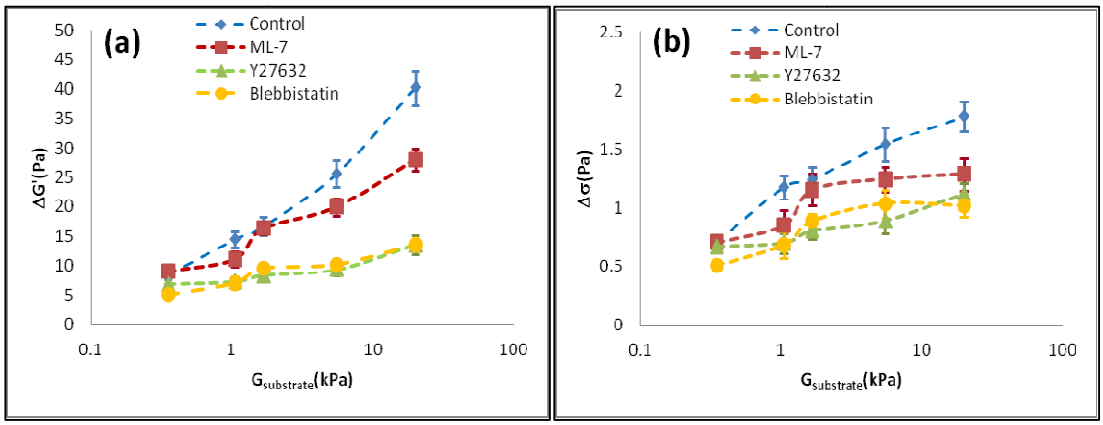

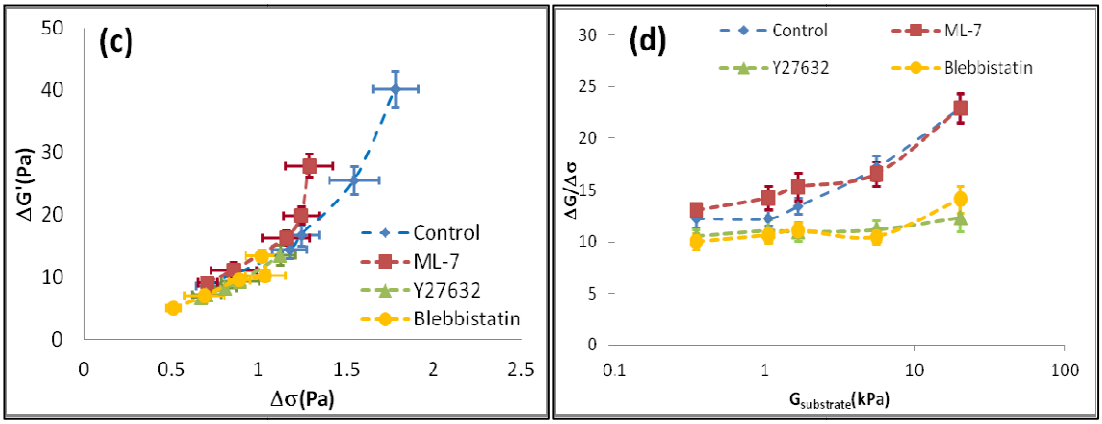

Figure 4.16 Experimental results of (a) the elastic modulus and (b) the dynamic stresses as a function of PA substrate rigidity. (c) Experimental results showing the fluctuation of the elastic modulus, $\Delta G'$, increases with the fluctuation stresses, $\Delta\sigma$. (d) $\Delta G' / \Delta\sigma$ quantifies intracellular stress level when cells are cultured on substrates of different stiffness. $G_{substrate}$ is the elastic modulus of the substrate. Each data point is the average of 10 measurements for each substrate stiffness. Bars are standard errors of the mean.

To determine intracellular stress (σ), we integrate the $\Delta\sigma/\Delta G'$ over all values of intracellular elasticity ($\int \Delta\sigma/\Delta G' \, dG'$), where $\Delta\sigma$ is the fluctuation of intracellular stress and $\Delta G'$ is the fluctuations of intracellular elasticity. First, we use a polynomial fit to the $\Delta\sigma/\Delta G'$ as a function of intracellular elasticity (G') as shown in Figure 4.17(a). In Figure 4.17(b), the relative intracellular stress ($\sigma - \sigma_0$) is calculated by integrating the polynomial function, $\Delta\sigma/\Delta G'$ (G'). σ_0 is the value independent of intracellular elasticity, G', for the integrating polynomial function. In order to determining σ_0, we need to find its physical meaning by looking at how G' varies as a function of σ. Since G' is never zero at any σ, we are looking for the value for the linear modulus G_0' in the absence of intracellular stress, $\sigma = 0$.

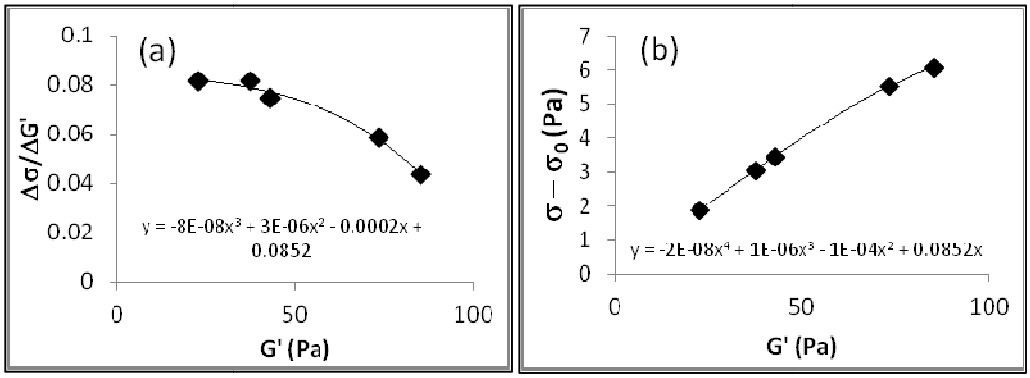

Figure 4.17 (a) Polynomial fitting of $\Delta\sigma/\Delta G'$ as a function of intracellular elasticity, G' and (b) the relative intracellular stress, $\sigma - \sigma_0$, as a function of intracellular elasticity calculated by integrating the polynomial function, $\Delta\sigma/\Delta G'$ (G').

Using the value for the linear modulus G_0' to be 5 Pa, as reported by Kollmannsberger *et al.* [200], Figure 4.18 shows the intracellular elasticity as a function of intracellular stress, $G'(\sigma)$. The G' (σ) as shown in Figure 4.18 can be described a nonlinear relation according to $G'=G_0' + A\,\sigma^P$. The fitted exponent A is 10.18±0.29 and P is 1.2±0.02, which is similar to that of active networks with exponent 1.3 [192].

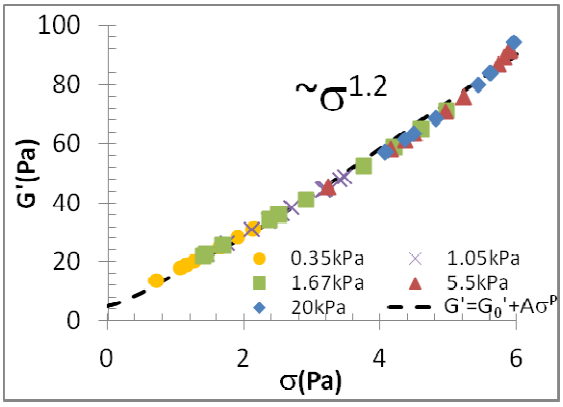

Figure 4.18 The intracellular stiffness as a function of intracellular stress when cells were cultured on substrates of different stiffness. The master curve shows a strong non-linearity of the dependence of cell rigidity on cell stress, with a power of 1.2±0.02.

To study the effect of motor-generated intracellular stresses on intracellular mechanical properties, we treat cells with Y-27632, ML-7 and blebbistatin. Cells treated with Y-27632 and blebbistatin exhibit a decrease in intracellular stress and time-averaged intracellular elastic modulus as shown in Figure 4.19. No significant changes are observed in intracellular stress and time-averaged intracellular elastic modulus of cells treated with ML-7. Figure 4.19 shows that treatments with Y-27632 and blebbistatin inhibit the cell's responses to substrate rigidity, allowing the intracellular stresses to mimic the mechanical properties of the environment. These results are qualitatively consistent with previous studies that cellular traction stress is regulated by ROCK, but not by myosin light chain kinase [211-215].

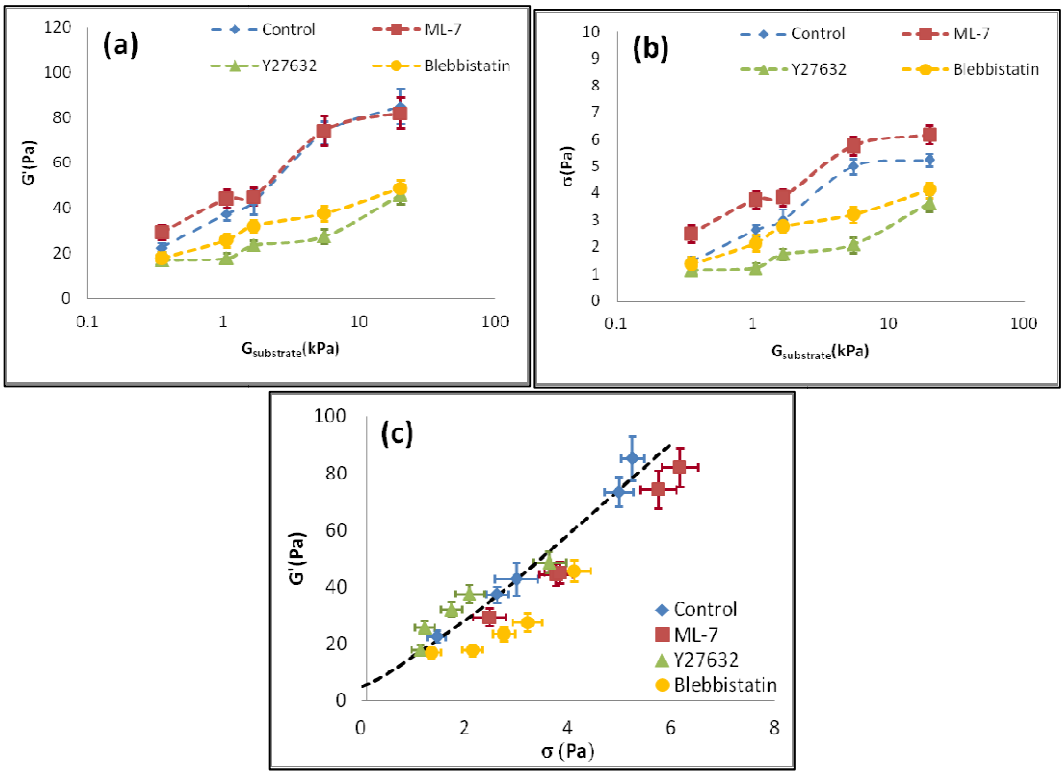

Figure 4.19 Experimental results of (a) the intracellular elastic modulus and (b) the intracellular stress of HeLa cells treated with myosin inhibitors. (c) The nonlinear mechanical responses in intracellular stiffness as a function of intracellular stress when cells are cultured on substrates of different stiffness.

In conclusion, in this section we use microrheology to study intracellular stress in response to substrate rigidity. By combining active and passive microrheology approaches with the same probe inside living cells, our results show that myosin can generate intracellular dynamic stresses, $\Delta\sigma$, at low frequency and myosin activity leads to larger fluctuations in the intracellular-elasticity, $\Delta G'$, locally. We determine intracellular stress by integrating the inverse of intracellular stress level to intracellular elasticity, $\int \Delta\sigma / \Delta G' \, dG'$. We found that the intracellular stress affects nonlinear intracellular elasticity in response to substrate rigidity. It is suggested that the effect of the motors would induce internal tension that brings the network into a nonlinear state.

5. Conclusions and Future Directions

5.1 Summary and Conclusions

This thesis describes several studies of the viscoelasticity of both equilibrium and non-equilibrium systems by using oscillatory optical tweezers based active microrheology. The measurements of micromechanical properties of polymer solutions illustrate that the techniques lead to results consistent with bulk properties when the length scale of inhomogeneity, intrinsic to the polymer network, is much smaller than the size of a probe particle. The results are also in agreement with measurements by a passive approach for equilibrium mechanical systems. We study mechanical properties both of polymer solutions and colloidal-crystal solutions to provide information on the microscopic structures of these materials. In addition, microrheology inside living cells, using an engulfed micro-particle or an endosome as a probe, demonstrates the possibility of investigating intracellular heterogeneity and temporal fluctuations of viscoelasticity. Non-thermal cellular stresses for non-equilibrium mechanical systems in biological cellular environments can also be investigated, from which important biomedical implications can be expected.

In the living cell system, we demonstrated our capability to measure storage and shear moduli (G' and G'') using optical tweezers and to utilize an internal probe as well as an externally attached particle. Whereas extracellular probes attached to the cytoskeleton provide measurements of global cell mechanical properties, intracellular probes provide direct measurements of intracellular mechanical properties. Both external and internal measurements demonstrate power-law relationships with exponents of ~ 0.4, which are consistent with several previous studies that report a soft glassy behavior of cellular materials [16, 111, 187]. Although the internal measurements in this study showed large variations from cell to cell, these variations might be indicative of the intracellular dynamics and inhomogeneity intrinsic to live cells.

To study intracellular stress in response to substrate rigidity, we investigated the relationship between molecular motor-induced fluctuating stress and fluctuations of intracellular elasticity in a non-equilibrium mechanical system. The relationship between fluctuations in cellular stress and fluctuations in cellular elasticity for living cells under different internal tensions reveals a strong non-linearity between cell elasticity and intracellular stress which follows a master curve. It is suggested that motors induce internal tension that brings the network into a non-equilibrium and non-linear state. This consistency emphasizes the close analogy of motor-driven internal stress with external shear stress. These aspects of intracellular stress and stiffness provide a better understanding of fluctuations in the system. The relationship between the different sources of noise in living cells may help reveal the inner workings of the mechanical responses of the highly dynamic cytoskeleton network. From such information we may further understand how a highly adaptive system such as a living cell takes advantage of non-linear responses through evolution.

5.2 Future Directions

In our investigation of HeLa cells, intracellular stress is found to respond to substrate rigidity, and to help cells adapt to their mechanical environment. Further investigation of cell microrheology to study stem cell differentiation would be an important issue. It is well known that adult stem cells can divide to replenish dying cells, regenerate damaged tissue, and are found throughout various systems in the body. For a stem cell to self-renew, it has been suggested that an intrinsically asymmetric cell division occurs, whereby stem cells segregate cell-fate determinants into only one of the two daughter cells by two different mechanisms. During normal embryonic development, the central nervous system often undergoes asymmetric cell division leading to potentially different phenotypic fates [216-221]. Extensive recent work has outlined the importance of the extracellular mechanical environment in stem-cell differentiation [33, 222-227]. Trans-differentiation of human mesenchymal stem cells (hMSCs) has been shown to be substrate dependent [33].

One of the possible future directions is to mimic the intracellular stress and to study the spatiotemporal responses of mitotic cells to artificial extracellular forces. We can use weak and highly localized forces on well-defined physical locations, where either the membrane/cortex or the cytoskeleton is selectively perturbed. In addition, we can study cellular responses to substrate effects by observing three-dimensional live-cell imaging of the dynamics of multiple fluorescent cytoskeleton proteins. Our preliminary results indicate that application of a localized mechanical force to dividing HeLa cells displaces the spindle to an asymmetric position (these cells divide symmetrically under normal conditions of the experiment). Figure 5.1 shows a cell proceeding through anaphase and cytokinesis. We have successfully attached 1.5 μm polystyrene particles to the outside of the cells expressing MRLC-GFP. The particles were coated with monoclonal anti-integrin α_V. Forces (~20 pN) were exerted on the particles using an optical trap, and the cells were imaged with bright-field and fluorescent images. Results show that the mitotic spindle, labeled by MRLC-GFP, appears to move to an asymmetric, post-perturbation position. Figure 5.1

(a) and (b) show a cell prior to the application of an external force. Figures 5.1 (c) and (d) show the effect of an oscillatory force on the particle: the pole moves towards the particle. We observed that in several cases (n = 5) the spindle moved to an asymmetric position, with one pole moving toward the particle when the perturbation was applied during anaphase. In Figures 5.1 (e) and (f) no external force was applied and the pole returned to a symmetric position. In Figures 5.1 (g) and (h), i.e. during cytokinesis, an external force showed no observable effect.

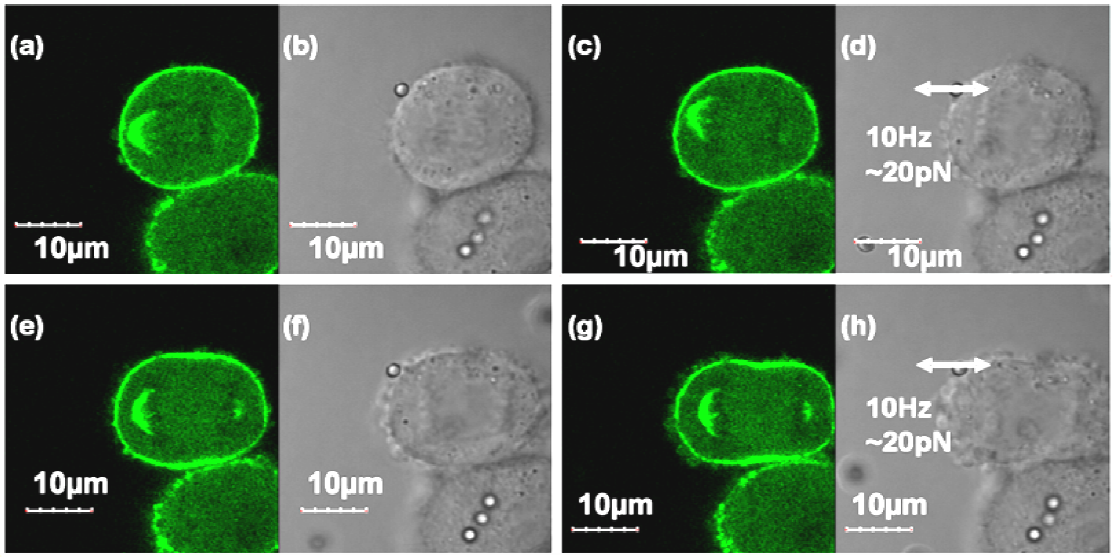

Figure 5.1 Fluorescence microscopy and differential interference contrast images showing the effect of mechanical perturbations of HeLa cells stably expressing MRLC-GFP.

Another possible future direction is to study stem-cell mechanical behaviors in response to substrate rigidity. This investigation might provide useful information to understand how stem cells sense mechanical environments and differentiate into different cell types. In our preliminary studies we studied intracellular microrheology of dental-pulp stem cells. Current research indicates that dental-pulp stem cells may be used to regenerate bone, periodontal ligament, or teeth. Here, dental-pulp stem cells were cultured on stiff and soft polyisoprene (70 kDa) thin films and intracellular mechanical behavior, including stiffness and stress, were measured by an oscillatory optical-tweezers-based microrheometer with an engulfed micro-particle (1 μm diameter

polystyrene). In order to inhibit the differentiation of stem cells, we treated Y-27632 (10 μM), which inhibits the Rho-associated protein kinase (ROCK). Figure 5.2 shows nucleus (blue), actin filament organization (green) and distribution of focal adhesion complex by anti-vinculin (red) in dental-pulp stem cells (control cells and cells treated with 10 μM Y-27632). After 28 days, dental-pulp stem cells cultured on the stiffer substrate generated more osteocalcin proteins than the others. The results of osteocalcin proteins expression in dental-pulp stem cells were took by M. Rafailovich, Stony Brook University. These results imply that culturing cells on stiffer substrates can induce dental-pulp stem cell to differentiate into bone-like cells; however, treatment of Y-27632 might inhibit dental-pulp stem cell differentiation.

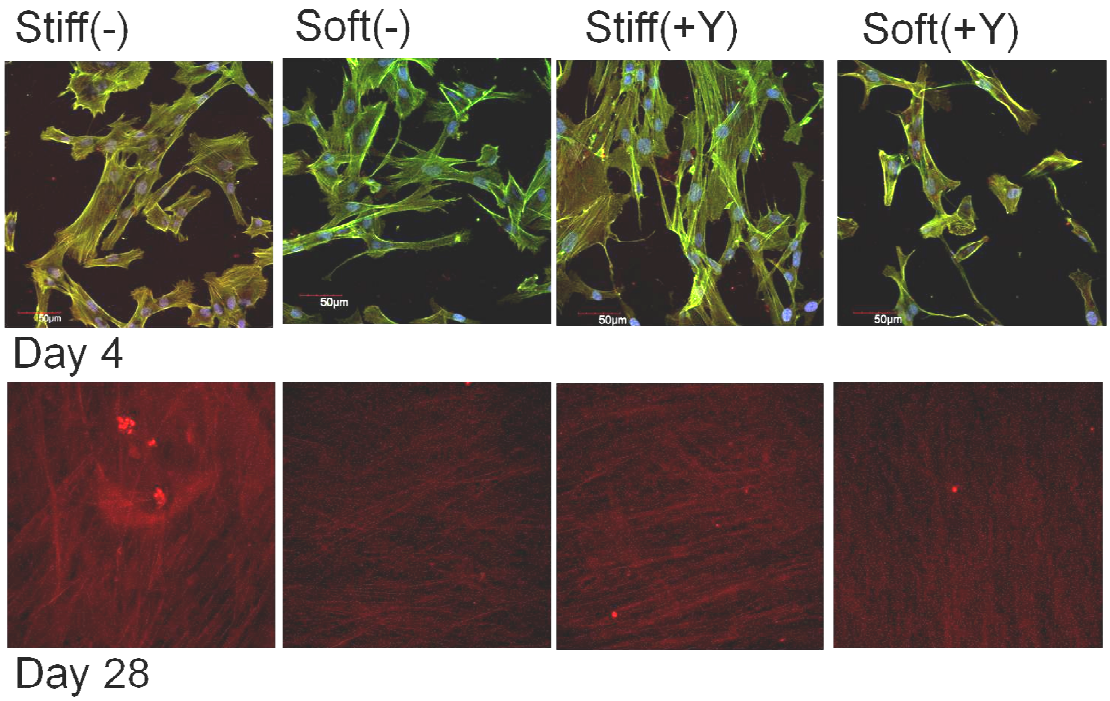

Figure 5.2 (Upper row) Nucleus (blue), actin filament organization (green) and distribution of focal adhesion complex by anti-vinculin (red) in dental-pulp stem cells and in cells treated with 10 μM Y-27632. (Lower row) Distribution of osteocalcin proteins (red) in dental pulp stem cells after 28 days.

Figure 5.3 shows the intracellular elastic modulus (*G'*) when cells were cultured on substrates with different stiffness. The cells attached to a stiff substrate were much more rigid than those attached to a soft substrate and kept increasing their elasticity up to day 7. In addition, cells attached to a stiff substrate can generate stronger intracellular stress (intracellular stress level; $\Delta G'/\Delta\sigma$) than those attached to a soft substrate. However, 10 μM Y-27632 treatment inhibited those cellular mechanical responses. Our preliminary results imply that stem cells can generate stronger intracellular stress that leads the cytoskeletal network to develop a non-linear stiffness state, which helps the stem cells mimic substrate rigidity.

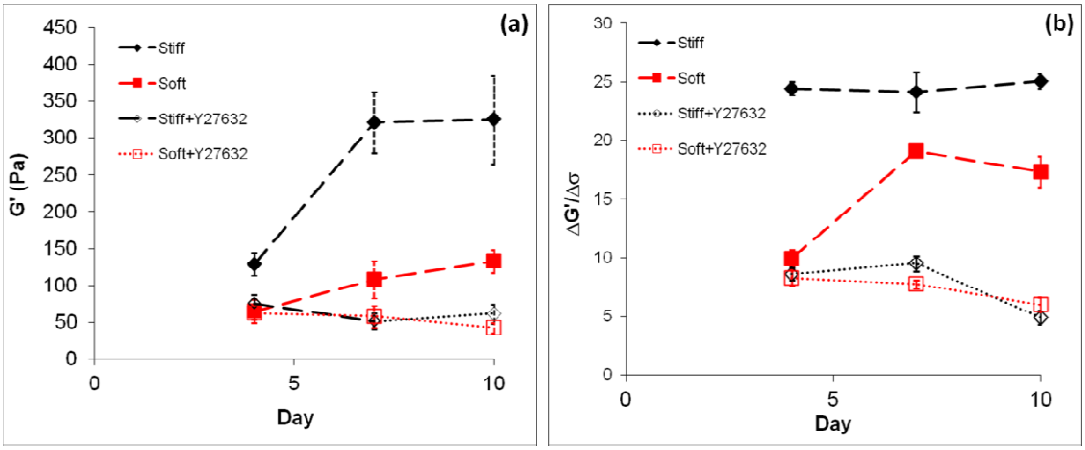

Figure 5.3 Experimental results of intracellular stiffness (*G'*) and intracellular stress level ($\Delta G'/\Delta\sigma$) of Y-27632 treated dental-pulp stem cells cultured on stiff and soft polyisoprene thin-films measured by an oscillatory optical-tweezers-based microrheometer with an engulfed micro-particle (1 μm diameter polystyrene). The means and standard errors are obtained by repeating each condition 5 times with individual cells.

To study and mimic the intracellular stress in response to mechanical properties would help advance our current understanding of how living cells (cancer cells or stem cells) sense and respond to their mechanical environment, leading to new designs in biomaterials, and advancing our understanding of diseases linked to cellular mechanotransduction [21-26].

6. List of References

[1] B. Linder, "Phase transitions and critical phenomena," *Thermodynamics and Introductory Statistical Mechanics*, pp. 119-126, 1983.

[2] G. Forgacs, *et al.*, "Assembly of collagen matrices as a phase transition revealed by structural and rheologic studies," *Biophysical journal*, vol. 84, pp. 1272-1280, 2003.

[3] P.-G. De Gennes, *Scaling concepts in polymer physics*: Cornell university press, 1979.

[4] E. Frey and K. Kroy, "Brownian motion: a paradigm of soft matter and biological physics," *Annalen der Physik*, vol. 14, pp. 20-50, 2005.

[5] P. J. Carreau, *et al.*, *Rheology of polymeric systems: principles and applications*: Hanser Publishers Munich, 1997.

[6] L. E. Nielsen, *Polymer rheology*: M. Dekker, 1977.

[7] M. Elimelech, *et al.*, *Particle deposition & aggregation: measurement, modelling and simulation*: Butterworth-Heinemann, 1998.

[8] C. Largeot, *et al.*, "Relation between the ion size and pore size for an electric double-layer capacitor," *Journal of the American Chemical Society*, vol. 130, pp. 2730-2731, 2008.

[9] R. G. Larson, *The structure and rheology of complex fluids* vol. 702: Oxford university press New York, 1999.

[10] W. W. Graessley, *The entanglement concept in polymer rheology*: Springer, 1974.

[11] H. A. Barnes, *et al.*, *An introduction to rheology* vol. 3: Elsevier, 1989.

[12] A. S. Popel and P. C. Johnson, "Microcirculation and hemorheology," *Annual review of fluid mechanics*, vol. 37, p. 43, 2005.

[13] S. Chien, *et al.*, "Comparative hemorheology--hematological implications of species differences in blood viscosity," *Biorheology*, vol. 8, pp. 35-57, 1971.

[14] T. M. Squires and T. G. Mason, "Fluid mechanics of microrheology," *Annual Review of Fluid Mechanics*, vol. 42, p. 413, 2009.

[15] D. Wirtz, "Particle-tracking microrheology of living cells: principles and applications," *Annu. Rev. Biophys.*, vol. 38, pp. 301-326, 2009.

[16] B. D. Hoffman, *et al.*, "The consensus mechanics of cultured mammalian cells," *PNAS*, vol. 103, pp. 10259–10264, 2006.

[17] B. D. Hoffman and J. C. Crocker, "Cell mechanics: dissecting the physical responses of cells to force," *Annu. Rev. Biomed. Eng*, vol. 11, pp. 259–288, 2009.

[18] I. Titushkin and M. Cho, "Modulation of cellular mechanics during osteogenic differentiation of human mesenchymal stem cells," *Biophysical journal*, vol. 93, pp. 3693-3702, 2007.

[19] R. Ananthakrishnan, *et al.*, "Modelling the structural response of an eukaryotic cell in the optical stretcher " *Current Science,* vol. 88, pp. 1434-1440, 10 May 2005.

[20] K. A. Kilian, *et al.*, "Geometric cues for directing the differentiation of mesenchymal stem cells," *Proceedings of the National Academy of Sciences,* vol. 107, pp. 4872-4877, 2010.

[21] Y. Wang, *et al.*, "Visualizing the mechanical activation of Src," *Nature,* vol. 434, pp. 1040-1045, 21 April 2005.

[22] S. Chien, "Mechanotransduction and endothelial cell homeostasis: the wisdom of the cell," *Am J Physiol Heart Circ Physiol* vol. 292, pp. H1209-H1224, 2007.

[23] C. S. Chen, "Mechanotransduction – a field pulling together?," *Journal of Cell Science,* vol. 121, pp. 3285-3291, 2008.

[24] N. Wang, *et al.*, "Mechanotransduction at a distance: mechanically coupling the extracellular matrix with the nucleus," *Nature Review,* vol. 10, pp. 75-82, 2009.

[25] K. K. Parker and D. E. Ingber, "Extracellular matrix, mechanotransduction and structural hierarchies in heart tissue engineering," *Phil. Trans. R. Soc. B,* vol. 2114, pp. 1-13, 2007.

[26] J. C. d. Alamo, *et al.*, "Anisotropic rheology and directional mechanotransduction in vascular endothelial cells," *PNAS,* vol. 105, pp. 15411–15416, 2008.

[27] G. Danuser and C. M. Waterman-Storer, "Quantitative fluorescent speckle microscopy of cytoskeleton dynamics," *Annu. Rev. Biophys. Biomol. Struct.,* vol. 35, pp. 361-87, 2006.

[28] C. M. Hale, *et al.*, "Resolving the role of actoymyosin contractility in cell microrheology," *PLoS One,* vol. 4, p. e7054 (11 pages), 2009.

[29] D. Robert, *et al.*, "In vivo determination of fluctuating forces during endosome trafficking using a combination of active and passive microrheology," *Plos One,* vol. 5, p. e10046, 2010.

[30] P. Kollmannsberger and B. Fabry, "Linear and nonlinear rheology of living cells," *Annu. Rev. Mater. Res.* , vol. 41, pp. 75-97, 2011.

[31] Y. Aratyn-Schaus, *et al.*, "Dynamic and structural signatures of lamellar actomyosin force generation," *Molecular Biology of the Cell,* vol. 22, pp. 1330-1339, 2011.

[32] N. Wang, *et al.*, "Mechanotransduction across the cell surface and through the cytoskeleton," *Science,* vol. 260, pp. 1124-1127, 1993.

[33] A. J. Engler, *et al.*, "Matrix elasticity directs stem cell lineage specification," *Cell,* vol. 126, pp. 677-689, 2006.

[34] N. Wang, *et al.*, "Cell prestress. I. Stiffness and prestress are closely associated in adherent contractile cells," *American Journal of Physiology - Cell Physiolog,* vol. 282, pp. C606-C616, 2002.

[35] F. J. Byfield, *et al.*, "Absence of filamin a prevents cells from responding to stiffness gradients on gels coated with collagen but not fibronectin," *Biophysical Journal,* vol. 96, pp. 5095-5102, 2009.

[36] L. Trichet, *et al.*, "Evidence of a large-scale mechanosensing mechanism for cellular adaptation to substrate stiffness," *PNAS*, vol. 109, pp. 6933-6938, 2012.

[37] S. J. Han, *et al.*, "Decoupling substrate stiffness, spread area, and micropost density: a close spatial relationship between traction forces and focal adhesions," *Biophys J.*, vol. 103, pp. 640-648, 2012.

[38] S.-Y. Tee, *et al.*, "Cell shape and substrate rigidity both regulate cell stiffness " *Biophys J*, vol. 100, pp. L25–L27, 2011.

[39] T. Mason, *et al.*, "Rheology of complex fluids measured by dynamic light scattering," *Journal of Molecular Structure*, vol. 383, pp. 81-90, 1996.

[40] F. Gittes, *et al.*, "Microscopic viscoelasticity: shear moduli of soft materials determined from thermal fluctuations," *Physical Review Letters*, vol. 79, p. 3286, 1997.

[41] T. Mason, *et al.*, "Particle tracking microrheology of complex fluids," *Physical Review Letters*, vol. 79, p. 3282, 1997.

[42] B. Schnurr, *et al.*, "Dynamical intermediates in the collapse of semiflexible polymers in poor solvents," *EPL (Europhysics Letters)*, vol. 51, p. 279, 2000.

[43] L. Hough and H. Ou-Yang, "A new probe for mechanical testing of nanostructures in soft materials," *Journal of Nanoparticle Research*, vol. 1, pp. 495-499, 1999.

[44] D. Mizuno, *et al.*, "Nonequilibrium mechanics of active cytoskeletal networks," *Science*, vol. 315, pp. 370-373, 2007.

[45] M.-T. Wei, *et al.*, "A comparative study of living cell micromechanical properties by oscillatory optical tweezers," *Optics express*, vol. 16, pp. 8594-8603, 2008.

[46] C.-C. Chiang, *et al.*, "Optical tweezers based active microrheology of sodium polystyrene sulfonate (NaPSS)," *Optics Express*, vol. 19, pp. 8847-8854, 2011.

[47] D. J. McGrail, *et al.*, "Differential mechanical response of mesenchymal stem cells and fibroblasts to tumor-secreted soluble factors," *PLoS One*, vol. 7, p. e33248, 2012.

[48] P. Panorchan, *et al.*, "Microrheology and ROCK signaling of human endothelial cells embedded in a 3D matrix," *Biophysical Journal*, vol. 91, pp. 3499–3507, 2006.

[49] T. G. Mason, *et al.*, "Particle tracking microrheology of complex fluids," *Physical Review Letters*, vol. 79, pp. 3282–3285, 1997.

[50] A. R. Bausch, *et al.*, "Local measurements of viscoelastic parameters of adherent cell surfaces by magnetic bead microrheometry," *Biophysical Journal*, vol. 75, pp. 2038–2049, 1998.

[51] J. Guck, *et al.*, "Optical deformability as an inherent cell marker for testing malignant transformation and metastatic competence," *Biophysical journal*, vol. 88, pp. 3689-3698, 2005.

[52] J. Guck, *et al.*, "Optical deformability of soft biological dielectrics," *Physical review letters*, vol. 84, p. 5451, 2000.

[53] D.-H. Kim, *et al.*, "Microengineered platforms for cell mechanobiology," *Annual review of biomedical engineering*, vol. 11, pp. 203-233, 2009.

[54] D. N. Robinson, *et al.*, "Quantitation of the distribution and flux of myosin-II during cytokinesis," *BMC Cell Biol.*, vol. 3, p. 4, 2002.

[55] J. P. Evans and D. N. Robinson, "The spatial and mechanical challenges of female meiosis," *Molecular Reproduction and Development*, vol. 78, pp. 769–777, 2011.

[56] C. C. Poirier, *et al.*, "Deconvolution of the cellular force-generating subsystems that govern cytokinesis furrow ingression," *Plos One*, vol. 8, p. e1002467, 2012.

[57] A. Surcela, *et al.*, "Cytokinesis through biochemical–mechanical feedback loops," *Seminars in Cell & Developmental Biology*, vol. 21, pp. 866-873, 2010.

[58] D. N. Robinson and J. A. Spudich, "Towards a molecular understanding of cytokinesis," *Trends Cell Biol.*, vol. 10, pp. 228-237., 2000.

[59] P. Fernández, *et al.*, "A master relation defines the nonlinear viscoelasticity of single fibroblasts," *Biophys J.*, vol. 90, pp. 3796-3805., 2006.

[60] J. Guck, *et al.*, "The optical Stretcher: a novel laser tool to micromanipulate cells," *Biophysical Journal*, vol. 81, pp. 767-784, 2001.

[61] P. B. Bareil, *et al.*, "Local stress distribution on the surface of a spherical cell in an optical stretcher," *Optics Express*, vol. 14, pp. 12503-12509, 2006.

[62] P. B. Bareil, *et al.*, "Calculation of spherical red blood cell deformation in a dual-beam optical stretcher," *Optics Express*, vol. 15, pp. 16029-16034, 2007.

[63] P. B. Bareil, *et al.*, "Calculation of spherical red blood cell eformation in a dual-beam optical stretcher," *Optics Express*, vol. 15, pp. 16029-16034, 2007.

[64] G.-B. Liao, *et al.*, "One-dimensional jumping optical tweezers for optical stretching of bi-concave human red blood cells," *Optics Express*, vol. 16, pp. 1996-2004, 2008.

[65] S. Rancourt-Grenier, *et al.*, "Dynamic deformation of a soft particle in dual-trap optical tweezers," in *SPIE Optics Photonics*, San Diego, USA, 2010, p. 77621H.

[66] Y. Q. Chen, *et al.*, "Effect of N-ethylmaleimide, chymotrypsin, and H2O2 on the viscoelasticity of human erythrocytes: Experimental measurement and theoretical analysis," *Journal of biophotonics*, 2013.

[67] S. Rancourt-Grenier, *et al.*, "Dynamic deformation of red blood cell in dual-trap optical tweezers," *Optics Express*, vol. 18, pp. 10462-10472, 2010.

[68] T. Hugel, *et al.*, "Elasticity of single polyelectrolyte chains and their desorption from solid supports studied by AFM based single molecule force spectroscopy," *Macromolecules*, vol. 34, pp. 1039-1047, 2001.

[69] B. Rajwa, *et al.*, "AFM/CLSM data visualization and comparison using an open-source toolkit," *Microsc Res Tech,* vol. 64, pp. 176-84, 2004.

[70] M. Puig-de-Morales-Marinkovic, *et al.*, "Viscoelasticity of the human red blood cell," *Am J Physiol Cell Physiol,* vol. 293, pp. C597–C605, 2007.

[71] B. Fabry, *et al.*, "Time scale and other invariants of integrative mechanical behavior in living cells," *Physical Review E,* vol. 68, p. 041914, 2003.

[72] A. Ashkin, *et al.*, "Observation of a single-beam gradient force optical trap for dielectric particles," *Optics Letters,* vol. 11, pp. 288-290, 1986.

[73] A. Ashkin, *et al.*, "Optical trapping and manipulation of single cells using infrared laser beams," *Nature,* vol. 330, pp. 769-771, 1987.

[74] S.-L. Liu, *et al.*, "Optical forced oscillation for the study of lectin-glycoprotein interaction at the cellular membrane of a Chinese hamster ovary cell," *Optics Express,* vol. 15, pp. 2713-2723, 2007.

[75] L. Hough and H. Ou-Yang, "Viscoelasticity of aqueous telechelic poly (ethylene oxide) solutions: Relaxation and structure," *Physical Review E,* vol. 73, p. 031802, 2006.

[76] M. Valentine, *et al.*, "Forces on a colloidal particle in a polymer solution: a study using optical tweezers," *Journal of Physics: Condensed Matter,* vol. 8, p. 9477, 1996.

[77] Y. Arakawa, *et al.*, "F11L-mediated inhibition of RhoA-mDia signaling stimulates microtubule dynamics during vaccinia virus infection," *Cell Host Microbe,* vol. 1, pp. 213-26, 2007.

[78] K. Kamijo, *et al.*, "Dissecting the role of Rho-mediated signaling in contractile ring formation," *Mol. Biol. Cell,* vol. 17, pp. 43-55, 2006.

[79] T. Kobayashi and T. Murayama, "Cell cycle-dependent microtubule-based dynamic transport of cytoplasmic dynein in mammalian cells," *PLoS One,* vol. 4, p. e7827, 2009.

[80] T. Yeung, *et al.*, "Effects of substrate stiffness on cell morphology, cytoskeletal structure, and adhesion," *Cell Motility and the Cytoskeleton* vol. 60, pp. 24-34, 2005.

[81] K. R. Johnson, *et al.*, "Demystifying the effects of a three-dimensional microenvironment in tissue morphogenesis," *Methods Cell Biol.* , vol. 83, pp. 547–583, 2007.

[82] J. L. Hutter and J. Bechhoefer, "Calibration of atomic-force microscope tips," *Rev. Sci. Instrum.,* vol. 64, pp. 1868-1873, 1993.

[83] A. Ashkin, "Acceleration and trapping of particles by radiation pressure," *Physical Review Letters,* vol. 24, pp. 156-159, 1970.

[84] A. Ashkin, "Optical trapping and manipulation of neutral particles using lasers," *PNAS,* vol. 94, pp. 4853-4860, 1997.

[85] k. Svoboda, *et al.*, "Direct observation of Kinesin stepping by optical trapping interferometry," *Nature,* vol. 365, pp. 721-727, 1993.

[86] C.-H. Lien, *et al.*, "Probing the dynamic differential stiffness of dsDNA interacting with RecA in the enthalpic regime," *Optics Express*, vol. 17, pp. 20376-20385, 2009.

[87] A. Ashkin and J. M. Dziedzic, "Optical trapping and manipulation of single cell using infrared laser beams," *Nature*, vol. 330, pp. 769-771, 1987.

[88] K. Svoboda, *et al.*, "Conformation and elasticity of the isolated red blood cell membrane skeleton," *Biophysical Journal*, vol. 63, pp. 784-793, 1992.

[89] M.-T. Wei, *et al.*, "The interaction of lipopolysaccharide with membrane receptors on macrophages pretreated with extract of Reishi polysaccharides measured by optical tweezers," *Optics Express*, vol. 15, pp. 11020-11032, 2007.

[90] A. L. Stout, "Detection and characterization of individual intermolecular bonds using optical tweezers," *Biophysical Journal*, vol. 80, pp. 2976-2986, 2001.

[91] J.-C. Meiners and S. R. Quake, "Direct measurement of hydrodynamic cross correlations between two particles in an external potential," *Physical Review Letters*, vol. 82, pp. 2211-2214, 1999.

[92] L. A. Hough and H. D. Ou-Yang, "Correlated motions of two hydrodynamically coupled particles confined in separate quadratic potential wells," *Physical Review E*, vol. 65, p. 021906 (7 pages), 2002.

[93] S. Henderson, *et al.*, "Propagation of hydrodynamic interactions in colloidal suspensions," *Physical Review Letters*, vol. 88, p. 088302 (4 pages), 2002.

[94] H. D. Ou-Yang and M.-T. Wei, "Complex fluids: probing mechanical properties of biological systems with optical tweezers," *Annu. Rev. Phys. Chem.* , vol. 61, pp. 421-440, 2010.

[95] A. Yao, *et al.*, "Microrheology with optical tweezers," *Lab on a chip*, vol. 9, pp. 2568–2575, 2009.

[96] D. Preece, *et al.*, "Optical tweezers: wideband microrheology," *J. Opt.*, vol. 13, p. 044022 (6 pages), 2011.

[97] A. Pertsinidis and X. S. Ling, "Equilibrium configurations and energetics of point defects in two-dimensional colloidal crystals," *Physical Review Letters*, vol. 87, p. 098303 (4 pages), 2001.

[98] J. C. Crocker and D. G. Grier, "Microscopic measurement of the pair interaction potential of charge-stabilized colloid," *Physical Review Letters*, vol. 73, pp. 352-355, 1994.

[99] E. n. Andablo-Reyes, *et al.*, "Microrheology from rotational diffusion of colloidal particles," *Physical Review Letters*, vol. 94, p. 106001 (4 pages), 2005.

[100] L. G. Wilson, *et al.*, "Microrheology and the fluctuation theorem in dense colloids," *EPL*, vol. 93, p. 58007, 2011.

[101] N. Murazawa, *et al.*, "Rheology measurement at liquid-crystal water interface using laser tweezers," *Japanese Journal of Applied Physics*, vol. 45, pp. 977–982, 2006.

[102] G. M. Koenig, *et al.*, "Single nanoparticle tracking reveals influence of chemical functionality of nanoparticles on local ordering of liquid crystals and nanoparticle diffusion coefficients," *Nano Lett.*, vol. 9, pp. 2794-2801, 2009.

[103] D. Mizuno, *et al.*, "Electrophoretic microrheology of a dilute lamellar phase: Relaxation mechanisms in frequencydependent mobility of nanometer-sized particles between soft membranes," *Physical Review E,* vol. 70, p. 011509, 2004.

[104] L. A. Hough, *et al.*, "Viscoelasticity of single wall carbon nanotube suspensions," *Physical Review Letters,* vol. 93, p. 168102 (4 pages), 2004.

[105] E. Helfer, *et al.*, "Viscoelastic properties of actin-coated membranes," *Physical Review E,* vol. 63, p. 021904 (13 pages), 2001.

[106] E. Helfer, *et al.*, "Microrheology of biopolymer-membrane complexes," *Physical Review Letters,* vol. 85, pp. 457–460, 2000.

[107] E. Helfer, *et al.*, "Buckling of actin-coated membranes under application of a local force," *Physical Review Letters,* vol. 87, p. 088103 (4 pages), 2001.

[108] M. Yanai, *et al.*, "Intracellular elasticity and viscosity in the body, leading, and trailing regions of locomoting neutrophils " *Am J Physiol Cell Physiol* vol. 277, pp. C432-C440, 1999.

[109] M.-T. Wei, *et al.*, "A comparative study of living cell micromechanical properties by oscillatory optical tweezer," *Optics Express,* vol. 16, pp. 8594-8603, 2008.

[110] H. C. Yalcin, *et al.*, "Influence of cytoskeletal structure and mechanics on epithelial cell injury during cyclic airway reopening," *Am J Physiol Lung Cell Mol Physiol,* vol. 297, pp. L881–L891, 2009.

[111] M. Balland, *et al.*, "Power laws in microrheology experiments on living cells: Comparative analysis and modeling," *Physical Review E,* vol. 74, pp. 021911-1-17, 2006.

[112] F. Gallet, *et al.*, "Power spectrum of out-of-equilibrium forces in living cells: amplitude and frequency dependence," *Soft matter,* vol. 5, pp. 2947–2953, 2009.

[113] C. Wilhelm, "Out-of-equilibrium microrheology inside living cells," *Physical Review Letters,* vol. 101, p. 028101 (4 pages), 2008.

[114] D. Mizuno, *et al.*, "Nonequilibrium mechanics of active cytoskeletal networks," *Science,* vol. 315, pp. 370-373, 2007.

[115] D. Mizuno, *et al.*, "Active and passive microrheology in equilibrium and nonequilibrium systems," *Macromolecules,* vol. 41, pp. 7194-7202, 2008.

[116] M. R. K. Mofrad, "Rheology of the cytoskeleton," *Annu. Rev. Fluid Mech,* vol. 41, pp. 433–453, 2009.

[117] V. Pelletier, *et al.*, "Microrheology of microtubule solutions and actin-microtubule composite networks," *Physical Review Letters,* vol. 102, p. 188303 (4 pages), 2009.

[118] X. Zhu, *et al.*, "Viscoelasticity of entangled λ-phage DNA solutions," *The Journal of Chemical Physics,* vol. 129, p. 185103 (6 pages), 2008.

[119] L. A. Hough and H. D. Ou-Yang, "Viscoelasticity of aqueous telechelic poly(ethylene oxide) solutions: Relaxation and structure," *Physical Review E,* vol. 73, p. 031802 (8 pages), 2006.

[120] H. Lee, *et al.*, "Stochastic optical active rheology," *Appl. Phys. Lett.*, vol. 101, p. 031902, 2012.

[121] O. Latinovic, *et al.*, "Structural and micromechanical characterization of type I collagen gels," *Journal of Biomechanics,* vol. 43, pp. 500-506, 2010.

[122] M. Shayegan and N. R. Forde, "Microrheological characterization of collagen systems: From molecular solutions to fibrillar gels " *PLoS ONE,* vol. 8, p. e70590, 2013.

[123] S. He´non, *et al.*, "A new determination of the shear modulus of the human erythrocyte membrane using optical tweezers," *Biophysical Journal,* vol. 76, pp. 1145-1151, 1999.

[124] C. T. Lim, *et al.*, "Large deformation of living cells using laser traps," *Acta Materialia,* vol. 52, pp. 1837-1845, 2004.

[125] M. Daoa, *et al.*, "Mechanics of the human red blood cell deformed by optical tweezers," *Journal of the Mechanics and Physics of Solids,* vol. 51, pp. 2259-2280, 2003.

[126] E. V. Lyubin, *et al.*, "Cellular viscoelasticity probed by active rheology in optical tweezers," *J. Biomed. Opt.* , vol. 17, p. 101510, 2012.

[127] J.-C. Meiners and S. R. Quake, "Femtonewton force spectroscopy of single extended DNA molecules," *Physical Review Letters,* vol. 84, pp. 5014-5017, 2000.

[128] W. H. Wright, *et al.*, "Radiation trapping forces on microspheres with optical tweezers," *Applied Physics Letters,* vol. 63, pp. 715-717, 1993.

[129] L. P. Ghislain, *et al.*, "Measurement of small forces using an optical trap," *Reiew of Scientific Instruments,* vol. 65, pp. 2762-2768, 1994.

[130] A. Ashkin, "Forces of a single-beam gradient laser trap on a dielectric sphere in the ray optics regime," *Biophysical Journal,* vol. 61, pp. 569-582, 1992.

[131] A. Mazolli, *et al.*, "Theory of trapping forces in optical tweezers," *Proc. R. Soc. Lond. A,* vol. 459, pp. 3021-3041, 2003.

[132] A. C. Richardson, *et al.*, "Non-harmonic potential of a single beam optical trap," *Optics Express,* vol. 16, pp. 15709-15717, 2008.

[133] F. Merenda, *et al.*, "Escape trajectories of single-beam optically trapped micro-particles in a transverse fluid flow," *Optics Express,* vol. 14, pp. 1685-1699, 2006.

[134] W. J. Greenleaf, *et al.*, "Passive all-optical force clamp for high-resolution laser trapping," *Physical Review Letters,* vol. 95, p. 208102 (4 pgaes), 2005.

[135] A. A. R. Neves, *et al.*, "Electromagnetic forces for an arbitrary optical trapping of a spherical dielectric," *Optics Express,* vol. 14, pp. 13101-13106, 2006.

[136] M. Jahnel, *et al.*, "Measuring the complete force field of an optical trap," *Opt. Lett.*, vol. 36, pp. 1260-1262, 2011.

[137] L. Ling, *et al.*, "Perturbation between two traps in dual-trap optical tweezers," *J. Appl. Phys.* , vol. 109, p. 083116, 2011.

[138] C.-C. Huang, *et al.*, "Optical tweezers as sub-pico-newton force transducers," *Optics Communications*, vol. 195, pp. 41-48, 2001.

[139] A. Rohrbach, *et al.*, "Three-dimensional tracking of small spheres in focused laser beams influence of the detection angular aperture," *Optics Letters*, vol. 28, pp. 411-413, 2003.

[140] A. Rohrbach, *et al.*, "Trapping and tracking a local probe with a photonic force microscope," *Reiew of Scientific Instruments*, vol. 75, pp. 2197-2210, 2004.

[141] A. Rohrbach, "Stiffness of optical traps: quantitative agreement between experiment and electromagnetic theory," *Physical Review Letters*, vol. 95, p. 168102, 2005.

[142] M.-T. Wei, *et al.*, "Three-dimensional optical force field on a Chinese hamster ovary cell in a fiber-optical dual-beam trap," *Optics Express*, vol. 14, pp. 3056-3064 2006.

[143] M.-T. Wei and A. Chiou, "Three-dimensional tracking of Brownian motion of a particle trapped in optical tweezers with a pair of orthogonal tracking beams and the determination of the associated optical force constants " *Optics Express*, vol. 13, pp. 5798-5806, 2005.

[144] L. P. Ghislain and W. W. Webb, "Scanning-force microscope based on an optical trap," *Optics Letters*, vol. 18, pp. 1678-1680, 1993.

[145] M. T. Valentine, *et al.*, "Forces on a colloidal particle in a polymer solution: a study using optical tweezers," *J. Phys.: Condens. Matter*, vol. 8, pp. 9477–9482, 1996.

[146] L. A. Hough and H. D. Ou-Yang, "A new probe for mechanical testing of nanostructures in soft materials," *Journal of Nanoparticle Research* vol. 1, pp. 495-499, 1999.

[147] M.-T. Wei, *et al.*, "Transverse force profiles of individual dielectric particles in an optical trap," in *SPIE Optics Photonics*, San Diego, USA, 2012.

[148] O. Latinovic, *Micromechanics and Structure of Soft and Biological Materials: An Optical Tweezers Study*: Verlag Dr. Muller Publishing, 2010.

[149] W. H. Wright, *et al.*, "Parametric study of the forces on microspheres held by optical tweezers," *Applied Optics*, vol. 33, pp. 1735-1748, 1999.

[150] J. P. Barton, *et al.*, "Theoretical determination of net radiation force and torque for a spherical particle illuminated by a focused laser beam," *J. Appl. Phys.*, vol. 66, pp. 4594-4602, 1989.

[151] P. Zema´nek, *et al.*, "Optical trapping of Rayleigh particles using a Gaussian standing wave," *Optics Communications*, vol. 151, pp. 273-285, 1998.

[152] D. Ganic, *et al.*, "Exact radiation trapping force calculation based on vectorial diffraction theory," *Optics Express*, vol. 12, pp. 2670-2675, 2004.

[153] N. B. Viana, *et al.*, "Absolute calibration of optical tweezers," *Applied Physics Letters,* vol. 88, p. 131110, 2006.

[154] K. Dholakia and P. Zemánek, "Colloquium: Gripped by light: optical binding," *Reviews of Modern Physics,* vol. 82, pp. 1767–1791, 2010.

[155] M. M. Burns, *et al.*, "Optical matter: crystallization and binding in intense optical fields," *Science,* vol. 249, pp. 749-754, 1990.

[156] M. M. Burns, *et al.*, "Optical binding," *Physical Review Letters,* vol. 63, pp. 1233-1236, 1989.

[157] M. Guillon, *et al.*, "Longitudinal optical binding of high optical contrast microdroplets in air," *Phys. Rev. Lett.* , vol. 96, p. 143902, 2006.

[158] T. M. Grzegorczyk, *et al.*, "Stable optical trapping based on optical binding forces," *Phys. Rev. Lett,* vol. 96, p. 113903, 2006.

[159] D. Haefner, *et al.*, "Conservative and nonconservative torques in optical binding," *Phys Rev Lett.*, vol. 103, p. 173602, 2009.

[160] S. Tatarkova, *et al.*, "One-dimensional optically bound arrays of microscopic particles," *Phys Rev Lett.* , vol. 89, p. 283901, 2002.

[161] R. Gómez-Medina and J. J. Sáenz, "Unusually strong optical interactions between particles in quasi-one-dimensional geometries," *Physical Review Letters,* vol. 93, p. 243602, 2004.

[162] J. M. Taylor, *et al.*, "Emergent properties in optically bound matter," *Optics Express,* vol. 16, pp. 6921-6929, 2008.

[163] M.-T. Wei, *et al.*, "Measurement of optical binding force between two colloidal particles," in *SPIE Optics Photonics*, San Diego, USA, 2009, p. 74001E.

[164] B. Richards and E. Wolf, "Electromagnetic diffraction in optical systems, II Structure of the image field in an optical system," *Proc. R. Soc. Lond. A.*, vol. 253, pp. 358-379, 1959.

[165] P. Török, *et al.*, "Electromagnetic diffraction of light focused through a planar interface between materials of mismatched refractive indices: structure of the electromagnetic field. I," *JOSA A,* vol. 12, pp. 2136-2144, 1997.

[166] J. Ng, *et al.*, "Theory of optical trapping by an optical vortex beam," *Physical Review Letters,* vol. 104, p. 103601, 2010.

[167] A. A. R. Neves, *et al.*, "Axial optical trapping efficiency through a dielectric interface," *Physical Review E,* vol. 76, p. 061917, 2007.

[168] L. Novotny and B. Hecht, *Principles of Nano-Optics*: Cambridge University Press, 2006.

[169] J. Ng, *et al.*, "Photonic clusters formed by dielectric microspheres: Numerical simulations," *Physical Review B,* vol. 72, pp. 085130-1-11, 2005.

[170] Y. Zhao, *et al.*, "Spin-to-orbital angular momentum conversion in a strongly focused optical beam," *Physical Review Letters,* vol. 99, p. 073901, 2007.

[171] H. Fujiwara, *et al.*, "Observation of the discrete transition of optically trapped particle position in the vicinity of an interface," *Applied Physics Letters*, vol. 84, pp. 13-15, 2004.

[172] R. R. Brau, *et al.*, "Passive and active microrheology with optical tweezers," *J. Opt. A: Pure Appl. Opt.* , vol. 9, pp. S103–S112, 2007.

[173] J. D. Ferry, *Viscoelastic properties of polymers* New York: Wiley, 1970.

[174] B. R. Dasgupta, *et al.*, "Microrheology of polyethylene oxide using diffusing wave spectroscopy and single scattering," *Phys. Rev. E*, vol. 65, p. 051505 (10 Pages), 2002.

[175] Y. Huang and M. M. Santore, "Dynamics in adsorbed layers of associative polymers in the Limit of strong backbone-surface attractions," *Langmuir*, vol. 18, pp. 2158-2165, 2002.

[176] F. Gittes and F. C. MacKintosh, "Dynamic shear modulus of a semiflexible polymer network," *Physical Review E*, vol. 58, pp. R1241-R1244, 1998.

[177] B. Schnurr, *et al.*, "Determining microscopic viscoelasticity in flexible and semiflexible polymer networks from thermal fluctuations," *Macromolecules*, vol. 30, pp. 7781–7792, 1997.

[178] T. G. Mason and D. A. Weitz, "Optical measurements of frequency-dependent linear viscoelastic moduli of complex fluids," *Physical Review Letters*, vol. 74, pp. 1250-1253, 1995.

[179] M. S. Green and A. V. Tobolsky, "A new approach to the theory of relaxing polymeric media," *J. Chem. Phys.* , vol. 14, p. 1724109, 1946.

[180] T. Annable, *et al.*, "The rheology of solutions of associating polymers: Comparison of experimental behavior with transient network theory " *J. Rheol.*, vol. 37, pp. 695-727, 1993.

[181] Q. T. Pham, *et al.*, "Polymeric and colloidal modes of relaxation in latex dispersions containing associative triblock copolymers " *J. Rheol.*, vol. 43, pp. 1599-1616, 1999.

[182] J. F. Joanny, "Acoustic shear waves in colloidal crystals," *Journal of Colloid and Interface Science*, vol. 71, pp. 622-624, 1979.

[183] D. Mizuno, *et al.*, "High-resolution probing of cellular force transmission," *Physical Review Letters*, vol. 102, p. 168102 (4 pages), 2009.

[184] A. J. Levine and T. C. Lubensky, "One- and two-particle microrheology," *Physical Review Letters*, vol. 85, pp. 1774-1777, 2000.

[185] J. C. Crocker, *et al.*, "Two-point microrheology of inhomogeneous soft materials," *Physical Review Letters*, vol. 85, pp. 888-891, 2000.

[186] A. I. Bishop, *et al.*, "Optical microrheology using rotating laser-trapped particles," *Physical Review Letters*, vol. 92, p. 198104 (4 pages), 2004.

[187] B. Fabry, *et al.*, "Scaling the microrheology of living cells," *Physical Review Letters*, vol. 87, p. 148102 (4 pages), 2001.

[188] A. Hoffmann, *et al.*, "Optical tweezers for confocal microscopy," *Applied Physics B Lasers and Optics*, vol. 71, pp. 747-753, 2000.

[189] D. Choquet, *et al.*, "Extracellular matrix rigidity causes strengthening of integrin–cytoskeleton linkages," *Cell*, vol. 88, pp. 39-48, 1997.

[190] V. M. Laurent, *et al.*, "Assessment of mechanical properties of adherent living cells by bead micromanipulation: comparison of magnetic twisting cytometry vs optical tweezers," *Journal of Biomechanical Engineering*, vol. 204, pp. 408-421, 2002.

[191] X. Trepat, *et al.*, "Viscoelasticity of human alveolar epithelial cells subjected to stretch," *Am J Physiol Lung Cell Mol Physiol*, vol. 287, pp. L1025–L1034, 2004.

[192] G. H. Koenderink, *et al.*, "An active biopolymer network controlled by molecular motors," *PNAS*, vol. 106, pp. 15192-15197, 2009.

[193] M. S. e. Silva, *et al.*, "Active multistage coarsening of actin networks driven by myosin motors," *PNAS*, vol. 108, pp. 9408-9413, 2011.

[194] K. John, *et al.*, "Nonlinear elasticity of cross-linked networks," *Phys Rev E*, vol. 87, p. 042721, 2013.

[195] A.-C. Reymann, *et al.*, "Actin network architecture can determine myosin motor activity," *Science*, vol. 336, pp. 1310-1314, 2012.

[196] B. Stuhrmann, *et al.*, "Nonequilibrium fluctuations of a remodeling in vitro cytoskeleton," *Phys Rev E*, vol. 86, , p. 020901(R) [5 pages] 2012.

[197] A. W. C. Lau, *et al.*, "Microrheology, stress fluctuations, and active behavior of living cells," *Physical Review Letters*, vol. 91, p. 198101 (4 pages), 2003.

[198] F. C. MacKintosh and A. J. Levine, "Nonequilibrium mechanics and dynamics of motor-activated gels," *Phys Rev Lett*, vol. 100, p. 018104, 2008.

[199] C. P. Brangwynne, *et al.*, "Nonequilibrium microtubule fluctuations in a model cytoskeleton," *Phys. Rev. Lett.*, vol. 100, p. 118104, 2008.

[200] P. Kollmannsberger, *et al.*, "Nonlinear viscoelasticity of adherent cells is controlled by cytoskeletal tension," *Soft Matter*, vol. 7, pp. 3127-3132, 2011.

[201] N. Y. Yao, *et al.*, "Stress-enhanced gelation: A dynamic nonlinearity of elasticity," *Physical Review Letters*, vol. 110, p. 018103, 2013.

[202] L. Bruno, *et al.*, "Mechanical properties of organelles driven by microtubule-dependent molecular motors in living cells," *Plos One*, vol. 6, p. e18332, 2011.

[203] M.-T. Wei and H. D. Ou-Yang, "Thermal and non-thermal intracellular mechanical fluctuations of living cells," in *SPIE Optics Photonics*, San Diego, USA, 2010, p. 77621L.

[204] M.-T. Wei, *et al.*, "Intracellular microrheology in the presence of myosin-generated forces in living cells," *Submitted*, 2014.

[205] C. S. Chen, *et al.*, "Cell shape provides global control of focal adhesion assembly," *Biochemical and Biophysical Research Communications*, vol. 307, pp. 355-361, 2003.

[206] C. Grashoff, *et al.*, "Measuring mechanical tension across vinculin reveals regulation of focal adhesion dynamics," *Nature*, vol. 466, pp. 263–266, 2010.

[207] C. S. Chen, *et al.*, "Mechanotransduction at cell-matrix and cell-cell contacts," *Annual Review of Biomedical Engineering*, vol. 6, pp. 275-302, 2004.

[208] M. L. Gardel, *et al.*, "Elastic behavior of cross-linked and bundled actin networks," *Science*, vol. 34, pp. 1301-1305, 2004.

[209] J. F. Marko and E. D. Siggia, "Stretching DNA," *Macromolecules*, vol. 28, pp. 8759-8770, 1995.

[210] C. Bustamante, *et al.*, "The nonequilibrium thermodynamics of small systems," *Physics Today* vol. 58, pp. 43-48 2005.

[211] G. Totsukawa, *et al.*, "Distinct roles of ROCK (Rho-kinase) and MLCK in spatial regulation of MLC phosphorylation for assembly of stress fibers and focal adhesions in 3T3 fibroblasts," *J Cell Biol.*, vol. 150, pp. 797-806, 2000.

[212] K. Katoh, *et al.*, "Stress fiber organization regulated by MLCK and Rho-kinase in cultured human fibroblasts," *American Journal of Physiology-Cell Physiology*, vol. 280, pp. C1669-C1679, 2001.

[213] E. Kniazeva and A. J. Putnam, "Endothelial cell traction and ECM density influence both capillary morphogenesis and maintenance in 3-D," *American Journal of Physiology-Cell Physiology*, vol. 297, pp. C179-C187, 2009.

[214] R. Rosenthal, *et al.*, "Effects of ML-7 and Y-27632 on carbachol- and endothelin-1-induced contraction of bovine trabecular meshwork," *Experimental Eye Research*, vol. 80, pp. 837-845, 2005.

[215] K. Tanner, *et al.*, "Dissecting regional variations in stress fiber mechanics in living cells with laser nanosurgery," *Biophysical Journal*, vol. 99, pp. 2775-2783, 2010.

[216] B. A. Reynolds, *et al.*, "A multipotent EGF-responsive striatal embryonic progenitor cell produces neurons and astrocytes," *Journal of Neuroscience*, vol. 12, pp. 4565-4574, 1992.

[217] S. J. Morrison and J. Kimble, "Asymmetric and symmetric stem-cell divisions in development and cancer," *Nature*, vol. 441, pp. 1068-1074, 2006.

[218] S. C. Noctor, *et al.*, "Cortical neurons arise in symmetric and asymmetric division zones and migrate through specific phases," *Nature Neuroscience*, vol. 7, pp. 136-144, 2004.

[219] M. Gotz and W. B. Huttner, "The cell biology of neurogenesis," *Nature Reviews Molecular Cell Biology*, vol. 6, pp. 777-788, 2005.

[220] N. Fuse, *et al.*, "Heterotrimeric G proteins regulate daughter cell size asymmetry in Drosophila neuroblast divisions," *Current Biology*, vol. 13, pp. 947-954, 2003.

[221] J. Betschinger and J. A. Knoblich, "Dare to be different: asymmetric cell division in Drosophila, C-elegans and vertebrates," *Current Biology*, vol. 14, pp. R674-R685, 2004.

[222] E. J. Arnsdorf, *et al.*, "Mechanically induced osteogenic differentiation - the role of RhoA, ROCKII and cytoskeletal dynamics," *Journal of Cell Science*, vol. 122, pp. 546-553, 2009.

[223] F. Guilak, *et al.*, "Control of stem cell fate by physical interactions with the extracellular matrix," *Cell Stem Cell*, vol. 5, pp. 17-26, 2009.

[224] I. Levental, *et al.*, "Soft biological materials and their impact on cell function," *Soft Matter*, vol. 3, pp. 299-306, 2007.

[225] E. A. Klein, *et al.*, "Cell-cycle control by physiological matrix elasticity and In vivo tissue stiffening," *Current Biology*, vol. 19, pp. 1511-1518, 2009.

[226] A. J. Engler, *et al.*, "Substrate compliance alters human mesenchymal stem cell morphology," *Molecular Biology of the Cell*, vol. 15, p. 1652, 2004.

[227] A. Engler, *et al.*, "Substrate compliance versus ligand density in cell on gel responses," *Biophysical Journal*, vol. 86, pp. 617-628, 2004.

Vita

Ming-Tzo Wei is a Ph.D. student in Bioengineering Program at Lehigh University. He received his BS degree in physics from National Dong Hwa University in 2004, and MS degree in Biophotonics from National Yang-Ming University in 2006. His research interest is in biophysics and biophotonics. His main research topics include colloidal interactions in optical field and electrical field, electrokinetics, non-equilibrium microrheology, and cell mechanics.

Education

Ph. D, Bioengineering, Lehigh University

GPA= 3.32 out of 4.00

M. Sc., Institute of Biophotonics Engineering, National Yang-Ming University, Taiwan

GPA= 4.00 out of 4.00, August 2006

Thesis: The influence of extract of Reishi polysaccharides on macrophage measured by optical tweezers

B.Sc. the Department of Physics, National Dong Hwa University, Taiwan

GPA= 3.68 out of 4.50, Jane 2004

Fields of specialty

optics, photonics, biophotonics, biophysics, cell mechanics, nonequilibrium rheology, soft matter, polymers, colloids, cytoskeleton, cell division, stem cells, dielectrophoresis, electrophoresis, optical microscopy, optical trapping, fluorescence imaging, confocal microscopy, fluorescence correlation spectroscopy, optical spectroscopy, Raman spectroscopy, atomic force microscopy, computer software (Labview, Matlab, and COMSOL)

Professional Activities

Referee for *Optics Express, Journal of Biophotonics* and *Optics Communications*

Member of *Biophysical Society*, *American Physical Society (APS)*, *International Society for Optics and Photonics (SPIE)*, and *Biomedical Engineering Society (BMES)*

Awards

- 2013 Lehigh Valley Section of Society of Plastics Engineers, *Excellence in Polymer Science & Engineering Award*
- 2013 Best Poster, *International Workshop on Stem Cell Differentiation: The Influence of Biomaterials and Biomechanics*, Shanghai, China
- Student Travel Award for 2013 Graduate Research Seminar/International Polymer Colloids Group, Shanghai, China
- 2006 Graduate Academic Excellence, Yang-Ming University
- Excellence Award for 2006 Annual Thesis Competition, Yang-Ming University
- Best Master Thesis in 2006, Optical Engineering Society of Republic of China
- 2004 Graduate Academic Excellence, National Dong Hwa University
- 4 outstanding academic achievement awards in 8 semesters, National Dong Hwa University
- Best campus club award while president of the harmonica club, National Dong Hwa University
- 2002 and 2003 *Quartet Harmonica Awards*, Taiwan

Related Publications

Books

1. **Ming-Tzo Wei**, O. Latinovic, L.A. Hough, Y.Q. Chen, H.D. Ou-Yang and A. Chiou, "Studying microrheology of soft and living materials using optical trapping," in *Handbook of Photonics for Biomedical Engineering*, D. Kim, A. Ho, and M. Somekh (Eds.), Springer-Verlag, Berlin, 2014, in press.

Journal papers

1. Y.Q. Chen, C.Y. Kuo, **Ming-Tzo Wei**, K. Wu, P.T. Su, C.S. Huang and A. Chiou, "Intracellular viscoelasticity of HeLa cells during cell division studied by video particle-tracking microrheology," *J. Biomed. Opt.* (2014) 19, 011008.
2. J. Wang, **Ming-Tzo Wei**, J. A. Cohen and H.D. Ou-Yang, "Mapping AC electroosmotic flow at the dielectrophoresis crossover frequency of a colloidal probe," *Electrophoresis* (2013) 34, 1915-1921.
3. H. Park, **Ming-Tzo Wei** and H.D. Ou-Yang, "Dielectrophoresis force spectroscopy for colloidal clusters," *Electrophoresis* (2012) 33, 2491-2497.
4. Y.Q. Chen, P.L. Chou, C.Y. Cheng, C.C. Chiang, **Ming-Tzo Wei**, C.T. Chuang, Y.L.S. Chen and A. Chiou, "Microrheology of human synovial fluid of arthritis patients studied by diffusing wave spectroscopy," *J. Biophotonics* (2012) 5, 777-784.
5. C.C. Chiang, **Ming-Tzo Wei**, Y.Q. Chen, P.W. Yen, Y.C. Huang, J.Y. Chen, O. Lavastre, H. Guillaume, D. Guillaume and A. Chiou, “Optical tweezers based active microrheology of sodium polystyrene sulfonate (NaPSS),” *Opt. Express* (2011) 19, 8847-8854.
6. I.H. Jaafar, C.E. LeBlon, **Ming-Tzo Wei,** H.D. Ou-Yang, J.P. Coulter and S.S. Jedlicka, “Improving fluorescence imaging of biological cells on biomedical polymers,” *Acta Biomaterialia* (2011) 7, 1588-1598.

7. H.D. Ou-Yang and **Ming-Tzo Wei**, "Complex fluids: probing mechanical properties of biological systems with optical tweezers," *Annu. Rev. Phys. Chem.* (2010) 61, 421-440. **(Cited >15 times)**
8. S. Rancourt-Grenier, **Ming-Tzo Wei**, J.J. Bai, A. Chiou, P.P. Bareil, P.L. Duval and Y. Sheng, "Dynamic deformation of red blood cell in dual-trap optical tweezers," *Opt. Express* (2010) 18, 10462-10472. **(Cited >15 times)**
9. H.C. Yalcin, K.M. Hallow, J. Wang, **Ming-Tzo Wei**, H.D. Ou-Yang and S.N. Ghadiali, "Influence of cytoskeletal structure and mechanics on epithelial cell injury during cyclic airway reopening," *Am. J. Physiol. Lung Cell Mol. Physiol.* (2009) 297, L881-L891.
10. C.H. Lien, **Ming-Tzo Wei**, C.D. Lee, T.Y. Tseng, C. Wang, T.F. Wang, H.D. Ou-Yang, C.H. Lin and A. Chiou, "The RecA-dsDNA dynamics interactions monitored by the mechanical properties of a dsDNA with oscillatory optical tweezers," *Opt. Express* (2009) 17, 20376–20385.
11. **Ming-Tzo Wei**, J. Junio and H.D. Ou-Yang, "Direct measurements of the frequency dependent dielectrophoresis force," *Biomicrofluidics* (2009) 3, 012003. **(Cited >20 times)**
12. **Ming-Tzo Wei**, A. Lengel, H.C. Yalcin, J. Wang, M. Hallow, S. N. Ghadiali, A. Chiou and H.D. Ou-Yang, "A comparative study of living cell micromechanical properties by oscillatory optical tweezers," *Opt. Express* (2008) 16, 8694-8603. **(Cited >40 times)**

Conference proceedings

1. **Ming-Tzo Wei**, J. Ng, C.T. Chan, A. Chiou and H.D. Ou-Yang, "Transverse force profiles of individual dielectric particles in an optical trap," *SPIE Optics Photonics*, San Diego, USA, 2012. (SPIE Proc. 8458).
2. Y.Q. Chen, C.Y. Cheng, C.C. Chiang, **Ming-Tzo Wei**, Y.C. Huang, O. Lavastre, H. Guillaume, D. Guillaume and A. Chiou, "Microrheology of sodium polystyrene sulfonate (NaPSS) solutions with different polymer concentrations and molecular weights studied by diffusing wave spectroscopy," *SPIE Photonics Asia,* Beijing, China, 2010. (SPIE Proc. 7848).

3. **Ming-Tzo Wei** and H.D. Ou-Yang, "Thermal and non-thermal intracellular mechanical fluctuations of living cells," *SPIE Optics Photonics*, San Diego, USA, 2010. (SPIE Proc. 7762).
4. S. Rancourt-Grenier, **Ming-Tzo Wei**, J.J. Bai, A. Chiou, P. Bareil, P.L. Duval and Y. Sheng, "Dynamic deformation of a soft particle in dual-trap optical tweezers," *SPIE Optics Photonics*, San Diego, USA, 2010. (SPIE Proc. 7762, 2010).
5. **Ming-Tzo Wei**, J. Ng, C.T. Chan and H.D. Ou-Yang, "Measurement of optical binding force between two colloidal particles," *SPIE Optics Photonics*, San Diego, USA, 2009. (SPIE Proc. 7400)
6. P.W. Yen, P. T. Su, L.J. Hung, **Ming-Tzo Wei**, W.J. Syu and A. Chiou, "The interaction of Escherichia coli with its surrounding three dimensional substrate measured by oscillatory optical tweezers," *SPIE Optics Photonics*, San Diego, USA, 2009. (SPIE Proc. 7400)

In preparation

1. **Ming-Tzo Wei**, J. Ng, C.T. Chan and H.D. Ou-Yang, "Multiple-scattering optical binding force between two colloidal particles." (in preparation)
2. **Ming-Tzo Wei**, W. Nie, C.T. Curley, S.S. Jedlicka and H.D. Ou-Yang, "Intracellular microrheology in the presence of myosin-generated forces." (in preparation)
3. **Ming-Tzo Wei**, M. Liao, K. Reddy and H.D. Ou-Yang, " Low frequency electrophoresis of an optically trapped colloidal particle." (in preparation)
4. J. Wang**, Ming-Tzo Wei** and H.D. Ou-Yang, "Low-frequency dielectrophoretic response of a single particle in aqueous suspensions." (in preparation).
5. W. Nie, **Ming-Tzo Wei**, H.D. Ou-Yang, S. Jedlicka and D. Vavylonis, " Dynamic of myosin II organization into contractile networks and fibers at the medial cell cortex." (Submitted to *Cytoskeleton*)
6. Y.Q. Chen, P.T. Su, Y.H. Chen , **Ming-Tzo Wei**, C.H. Huang, K. Osterday, J.C. Alamo, W.J. Syu and A. Chiou, "The effect of Enterohemorrhagic E. coli infection on the cell mechanics of host cells." (Submitted to *PlosOne*)

Conference talks and posters

1. **Ming-Tzo Wei** and H.D. Ou-Yang, "Nonlinear intracellular elasticity controlled by myosin-generated fluctuating stress," *APS March Meeting*, Denver, CO, USA, 2014.
2. W. Nie, **Ming-Tzo Wei**, H.D. Ou-Yang, S. Jedlicka and D. Vavylonis, "Dynamics of myosin II organization into cortical contractile networks and fibers," *APS March Meeting*, Denver, CO, USA, 2014.
3. **Ming-Tzo Wei** and H.D. Ou-Yang, "Microrheology of a non-equilibrium system produced by molecular motor-generated forces in living cells," *SPIE Optics Photonics*, San Diego, CA, USA, 2013.
4. **Ming-Tzo Wei** and H.D. Ou-Yang, "The influence of myosin-generated force to the intracellular microrheology in living cells," *APS March Meeting*, Baltimore, MD, USA, 2013.
5. K. Reddy, **Ming-Tzo Wei**, J.A. Cohen and H.D. Ou-Yang, "Drag coefficient of an electrophoretic colloidal particle," *APS March Meeting*, Baltimore, MD, USA, 2013.
6. **Ming-Tzo Wei** and H.D. Ou-Yang "Intracellular microrheology in the presence of myosin-generated forces in living cells," *Biophysical Society Annual Meeting*, Philadelphia, PA, 2013. (Poster)
7. W. Nie, **Ming-Tzo Wei**, H.D. Ou-Yang, S. Jedlicka and D. Vavylonis, "Dynamics of non-muscle myosin II organization into stress fibers and contractile networks," *Biophysical Society Annual Meeting*, Philadelphia, PA, 2013. (Poster)
8. J.A. Cohen, **Ming-Tzo Wei** and H.D. Ou-Yang, "Too much charge weakens electrostatic interactions between charged liposomes in low ionic-strength solutions," *Biophysical Society Annual Meeting*, Philadelphia, PA, 2013. (Poster)

9. **Ming-Tzo Wei**, S. Jedlicka, D. Vavylonis and H.D. Ou-Yang, “Microrheology of a non-equilibrium system produced by molecular motor-generated forces in living cells,” *BMES 2012 Annual Meeting*, Atlanta, GA, 2012.
10. **Ming-Tzo Wei** and H. D. Ou-Yang, “Non-equilibrium intracellular microrheology in living cells,” *SPIE Optics Photonics*, San Diego, CA, USA, 2012.
11. J.A. Cohen, **Ming-Tzo Wei** and H.D. Ou-Yang, “Shear modulus and viscosity of deionized suspensions of charged liposomes,” *Biophysical Society Annual Meeting*, San Diego, CA, 2012. (Poster)
12. W. Nie, **Ming-Tzo Wei**, I. Biaggio, H.D. Ou-Yang, S. Jedlicka and D. Vavylonis, “Stress fiber organization and dynamics in cells adhered to substrates of varying stiffness,” *Biophysical Society Annual Meeting*, San Diego, CA, 2012. (Poster)
13. C. T. Curley, K. Fanale, **Ming-Tzo Wei**, D. Ou-Yang, D. Vavylonis and S. S. Jedlicka, “Characterizing the effect of substrate stiffness on neural stem cell differentiation,” *Institute of Biological Engineering 17th Annual Conference*, Indianapolis, IN, USA, 2012. (Poster)
14. **Ming-Tzo Wei**, J. Ng, C.T. Chan and H.D. Ou-Yang, “Lateral optical binding forces between two colloidal Mie particles,” *APS March Meeting*, Boston, MA, USA, 2012.
15. **Ming-Tzo Wei**, D. Vavylonis and H.D. Ou-Yang, “Extracellular mechanical perturbations on cytoskeletal dynamics of mitotic HeLa cells,” *BMES 2011 Annual Meeting*, Hartford, CT, USA, 2011. (Poster)
16. **Ming-Tzo Wei**, J. Ng, C.T. Chan and H.D. Ou-Yang, “Experimental and theoretical study of optical binding forces between two colloidal particles,” *SPIE Optics Photonics*, San Diego, CA, USA, 2011.
17. **Ming-Tzo Wei** and H.D. Ou-Yang, “Non-equilibrium microrheology of living cells,” *APS March Meeting*, Dallas, TX, USA, 2011.

18. **Ming-Tzo Wei**, D. Vavylonis and H.D. Ou-Yang, “Myosin cortical assembly and spindle oscillations during HeLa cell division,” *Biophysical Society Annual Meeting*, Baltimore, MD, USA, 2011. (Poster)

19. J. Wang, **Ming-Tzo Wei** H.D. Ou-yang, “Mapping the induced-charge electro-osmosis (ACEO) by optical tweezers DEP force spectroscopy,” *APCE 2010*, Hong Kong, 2010.

20. Y.Q. Chen, C.Y. Cheng, C.C. Chiang, **Ming-Tzo Wei**, Y.C. Huang, O. Lavastre, H. Guillaume, D. Guillaume and A. Chiou, “Microrheology of sodium polystyrene sulfonate (NaPSS) solutions with different polymer concentrations and molecular weights studied by diffusing wave spectroscopy,” *SPIE Photonics Asia*, Beijing, China, 2010.

21. C.C. Chiang, Y.Q. Chen, P.W. Yen, **Ming-Tzo Wei**, Y.C. Huang, J.Y. Chen, O. Lavastre, H. Guillaume, D. Guillaume and A. Chiou, “Optical tweezers based active microrheology of polysodium styrene sulfonate (NaPSS),” *Optics Within Life Sciences*, Quebec, Canada, 2010.

22. S.H. Wu, **Ming-Tzo Wei**, A. Chiou, P.K. Wei and X. Cheng, “Surface plasmon resonance for dynamic analysis of cell secreting behavior,” *BMES 2010 Annual Meeting*, Austin, TX, USA, 2010.

23. **Ming-Tzo Wei** and H.D. Ou-Yang, "Thermal and non-thermal intracellular mechanical fluctuations of living cells," *SPIE Optics Photonics*, San Diego, CA, USA, 2010.

24. S. Rancourt-Grenier, **Ming-Tzo Wei**, J.J. Bai, A. Chiou, P. Bareil, P.L. Duval and Y. Sheng, "Dynamic deformation of a soft particle in dual-trap optical tweezers," *SPIE Optics Photonics*, San Diego, CA, USA, 2010.

25. **Ming-Tzo Wei** and H.D. Ou-Yang, “Intracellular mechanical properties of living cells,” *APS March Meeting*, Portland, OR, USA, 2010.

26. H. Park, **Ming-Tzo Wei** and H.D. Ou-Yang, and D. Pine, “Dielectrophoresis force of PMMA colloidal clusters,” *APS March Meeting*, Portland, OR, USA, 2010.

27. P.W. Yen, P.T. Su, L.J. Hung, **Ming-Tzo Wei**, W.J. Syu and A. Chiou, “The interaction of Escherichia coli with its surrounding three dimensional substrate measured by oscillatory optical tweezers,” *Optics and Photonics Taiwan*, Taiwan, 2009.

28. C.H. Ho, Y.T. Wu, **Ming-Tzo Wei** and A. Chiou, “The effect of oxidative stress on human erythrocytes deformability studied by jumping optical tweezers,” *Optics and Photonics Taiwan*, Taiwan, 2009.

29. **Ming-Tzo Wei**, J. Ng, C.T. Chan and H.D. Ou-Yang, “Measurement of optical binding force between two colloidal particles,” *SPIE Optics Photonics*, San Diego, CA, USA, 2009.

30. P.W. Yen, P.T. Su, L.J. Hung, **Ming-Tzo Wei**, W.J. Syu, and A. Chiou, “The interaction of Escherichia coli with its surrounding three dimensional substrate measured by oscillatory optical tweezers,” *SPIE Optics Photonics*, San Diego, CA, USA, 2009.

31. **Ming-Tzo Wei** and H.D. Ou-Yang, “Mechanical anisotropy of viscoelasticity in biological cells,” *APS March Meeting*, Pittsburgh, PA, USA, 2009.

32. J. Wang, **Ming-Tzo Wei**, J. Junio and H.D. Ou-Yang, “DEP force spectroscopy,” *APS March Meeting*, Pittsburgh, PA, USA, 2009.

33. C.Y. Lin, H.Y. Lin, **Ming-Tzo Wei** and H.D. Ou-Yang, “Optical trapping of colloidal nanoparticles by a weakly focused laser beam,” *APS March Meeting*, Pittsburgh, PA, USA, 2009.

34. H.D. Ou-Yang and **Ming-Tzo Wei**, “Optical binding force acting on two optically trapped particles,” *APS March Meeting*, Pittsburgh, PA, USA, 2009.